AN EXPERIMENTAL INVESTIGATION OF THE CHARACTERISTICS OF RF SURFACE WAVE GENERATED PLASMAS

Thesis for the Degree of M. S.
MICHIGAN STATE UNIVERSITY

RONALD EDWARD FRITZ

1979

[redacted]

OVERDUE FINES ARE 25¢ PER DAY
PER ITEM

Return to book drop to remove
this checkout from your record.

MSU

[redacted]

ABSTRACT

AN EXPERIMENTAL INVESTIGATION OF THE CHARACTERISTICS
OF RF SURFACE WAVE GENERATED PLASMAS

By

Ronald Edward Fritz

This thesis summarizes the results of a systematic investigation of the experimental properties of two rf surface wave plasma sources. The objective was to provide information required for the engineering design of the rf plasma sources.

The plasma was generated by surface waves from a low power (0-80W) coaxial cavity and a high power (0-600W) variable length microwave cavity. Two low power oscillators were available: one with a TWT amplifier (1.7 to 3.8 GHz), the other with a transistor amplifier (850 MHz). A high power magnetron oscillator at 2.45 GHz was also used.

The experimental parameters measured were the power absorbed per unit length of the plasma (P/L), approximate electron density (n_e), power match (M), and light output from the plasma.

For the parameters that were varied it was found that (1) P/L and n_e were relatively constant over a range of pressures from 100 mT to 10 T, (2) P/L and n_e increased with absorbed rf power, (3) power density and n_e were inversely porportional to the cross sectional area of the tube, (4) P/L and n_e increased with excitation frequency, (5) high P/L was characteristic of gases with high loss mechanisms, and (6) n_e could be varied by adjusting the cavity geometry.

AN EXPERIMENTAL INVESTIGATION OF THE CHARACTERISTICS OF RF SURFACE WAVE GENERATED PLASMAS

By

Ronald Edward Fritz

A THESIS

Submitted to
Michigan State University
in partial fulfillment of the requirements
for the degree of

MASTER OF SCIENCE

Department of Electrical Engineering and Systems Science

1979

...whatever you do, do it all for the glory of God. 1 Cor. 10:31

ACKNOWLEDGMENTS

The author wishes to express his sincere appreciation to Dr. J. Asmussen for his continuous guidance and encouragement in all of the phases of this work.

The author thanks his wife, Glenda, and daughter, Trisha, for all their understanding and encouragement, especially over the past two years.

This research was supported in part by the Division of Engineering Research of Michigan State University.

TABLE OF CONTENTS

LIST OF TABLES

LIST OF FIGURES

Figure		Page

Figure		Page

Figure Page

ABBREVIATIONS AND SYMBOLS

rf	radio frequency
EM	electromagnetic
P/L or P_a/L_p	absorbed power per unit length of plasma
ω	radian frequency of excitation source
ω_p	radian frequency of the plasma
k	wave number = $2\pi/\lambda$
λ	wave length
a	plasma tube radius
n_e or n	plasma electron density, measured in particles/cm^3
e	charge on the electron
m	mass of the electron
ε_o	permittivity of free space
CW	continuous wave
M	power match, defined as P_a/P_i, given in %
P_a	absorbed power = $P_i - P_r$
P_i	power incident on plasma-cavity system
P_r	power reflected from the plasma-cavity system
L or L_p	plasma length
p	pressure, measured in microns or torr
ν_e	effective electron-neutral collision frequency

CHAPTER I

INTRODUCTION

The ability to create and sustain long plasma columns by coupling radio frequency (rf) energy onto surface waves on the plasma has been observed for a number of years. The observation of long rf excited plasma columns has been mentioned in papers without relating their behavior to surface waves, and relatively little work has been performed with the objective of designing the rf surface wave plasma source to meet the needs of applications, such as in laser technology, plasma chemistry, and light sources. The objective of the experiments discussed in this thesis is to provide information required for the engineering design of these rf plasma sources.

The format to be followed is a brief review of microwave discharges and plasma behavior, a description of the experimental set-up and procedures used during this study, followed by the results of the experiments, and analysis of the results with conclusions.

Chapter 2 is a review of microwave (MW) discharges and plasma behavior begining with MW discharges in general, and devices used for their production. The objective of many of the experiments was to produce plasma sources which could absorb large amounts of the rf power in the frequency range of hundreds of MHz to several GHz, and, in some cases, to produce large plasma volumes. Most of the efficient devices were equipped with tuning mechanisms to match the plasma-cavity system impedance to the transmission line impedance. This is followed by a review of some of the earlier observations of rf surface wave generated plasmas. These observations were characterized by plasma extending outside the discharge cavity or coupling structure, and are now described as surface wave generated plasmas. A surface wave is launched from the coupling structure onto the plasma tube and propagates along the tube, ionizing the experimental gas and sustaining the plasma. Significant characteristics of these surface waves are discussed, and the Gould-Trivelpiece surface mode dispersion diagram can be used to determine group and phase speeds of the surface waves. When standing surface waves can be observed on the plasma tube, the normalized dispersion diagram can be used to determine the plasma density.

Chapter 3 describes in detail the experimental systems used for the experiments reported in later chapters. The rf surface wave couplers are a low power (0-50W) coaxial cavity and a high power (0-1200W) cylindrical cavity. The geometry (cavity length and probe position, and gap in the coaxial cavity) of each cavity is variable, allowing most of the incident energy to be coupled into the plasma-cavity system. The coaxial cavity was operated from frequencies of 850 MHz to 3.8 GHz, while the cylindrical cavity was operated at a frequency of 2.45 GHz. The external microwave circuits for each system are shown and discussed.

The chapter continues with a discussion of the vacuum systems and the gases used. The cylindrical quartz tubes could be evacuated to 1 to 10 microns before introducing the experimental gases. Pressures for the discharges ranged from about 50 microns to 10 or 20 torr, and were measured with a thermocouple vacuum gauge and a mercury manometer.

The radiation problems associated with long surface wave generated plasmas are generally not appreciated. Since microwave radiation (including that radiated from the plasma) may be hazardous, protective screens were used to shield the operator during experiments, and the rf power levels around the apparatus were monitored. Sketches of the screening are presented and described, along with the monitoring system.

Relative electron densities could be determined from photodiode measurements of the light output from the plasma column. These measurements were used to determine how the electron density changed as the cavity and other experimental parameters were varied, with the pressure held constant.

The optical spectrum of an rf Ar discharge was also examined with a spectroscope to determine the wave lengths of the observed lines. Lines of the same wave lengths as those emitted by Ar^+ lasers were observed, suggesting that this type of plasma source may be used to create an Ar^+ laser. A diagram of the experimental set-up is discussed.

Chapter 3 concludes with a general description of experimental techniques, with the objective of aiding other experimenters in duplicating and extending this research.

The results of many, but not all, of the experiments are presented in Chapter 4. Early experimentation with the coaxial system showed the absorbed power per unit length of plasma (P/L) to be a function of (1) gas pressure, (2) absorbed power, (3) plasma or tube diameter, (4) excitation frequency and source type, (5) ionization energy of the experimental gas, and (6) cavity geometry. Excitation frequency and source type were not varied for experiments performed with the cylindrical cavity, and cavity geometry was varied only for tuning purposes. Values of absorbed power per unit length of plasma (P/L) were approximately .5 W/cm for Ar, slightly lower for the heavier inert gases, and of the order of 3 to

6 W/cm for He, He-Ne, and O_2, depending on rf power levels, gas pressure, etc. In Chapter 5, it is shown that this result is to be expected. For a steady state discharge the absorbed power is equal to the power lost from the plasma. The loss terms for He, He-Ne and O_2 are larger than those for Ar, Kr, and Xe.

Measurement of the plasma density using standing surface waves indicated values of the order of 10^{10} to 10^{12} cm^{-3} for plasmas in a region about 30 cm from the cylindrical cavity, at an absorbed rf power of approximately 200 W. The actual value depended on the position along the plasma tube. Similar measurements with two coaxial cavities showed plasma density to be of the order of 10^{12} cm^{-3} in the region between the cavities, which were about 20 cm apart. The absorbed power was about 80 W.

The spectrum of an rf Ar discharge at 200 microns and 200 W of absorbed power was filled with many distinct lines superposed on a continuous background. This background was eliminated by isolating the discharge tube from the vacuum pump, so that there was no significant flow of gas through the tube.

Results of P/L vs. absorbed power experiments suggested using two coaxial cavities to excite a surface wave plasma. It was found that the absorbed power per unit length of plasma was about 30% lower for the doubly excited surface wave plasma. Since P/L was shown by other experiments to be proportional to the plasma electron density, this indicates that the plasma density may be lower for the doubly excited surface wave plasma.

The last section of Chapter 4 lists a number of experiments that could be performed to further the understanding of the physics of the surface wave couplers, and for making these sources more efficient in applications.

Chapter 5 is a summary and analysis of the experimental results, based on the dispersion diagram described in Chapter 2, and on the power absorption and loss characteristics of steady state microwave discharges. An equation is given showing the loss mechanisms in the steady state discharge, and equating the power lost to the power absorbed in the plasma. This equation is used to account for (1) a flat region observed in P/L vs. pressure curves, (2) the increase in P/L with absorbed power, (3) an apparent minimum in P/L, below which the surface wave generated plasma does not exist, (4) the dependence of P/L on gas type, and (5) the effect of tube size on P/L. The normalized dispersion diagram is used to explain the frequency dependence of P/L and an approximate determination of plasma density in the discharge using the visually observed standing waves on the plasma column. Finally, measurement of the wave lengths of an rf Ar discharge shows lines that have been observed in Ar ion lasers. The lines are the result of electrons reaching higher energy levels through multiple collisions with neutral atoms.

This thesis is concluded by discussing briefly the implications and applications of surface wave generated plasmas. This information will be useful in the engineering design of these rf surface wave plasma sources. The applications will require the proper choice of excitation frequency, tube diameter, absorbed power levels and coupling structure.

CHAPTER II

REVIEW OF MICROWAVE DISCHARGES AND PLASMA BEHAVIOR

2.1 Introduction

This section begins with a review of the work done over the past 14 years on continuous wave cylindrically bounded microwave discharges, with no external magnetic field. Numerous papers have been published on results obtained with microwave cavities and specialized structures. The results of some of these are described.

Following the general review, methods of continuous wave radio frequency surface wave excitation are reviewed, including results that have been published within the past year. Most of the work on radio frequency surface wave generated plasmas has been published by two groups: one led by J. Asmussen, the other by M. Moisan. Developments will be discussed in the order in which they appeared in the literature, along with papers by other groups.

This review will lead into a discussion of general principles of plasma surface waves, with a derivation of an ω-k diagram for the Gould-Trivelpiece surface wave modes of a plasma bounded by a cylindrical dielectric and a cylindrical metal waveguide.

Lastly, a general description of the behavior of the radio frequency surface waves is presented and explained using a normalized ω-k diagram. The use of standing surface waves along the tube for plasma density determination is discussed.

2.2 A Review of Microwave Discharges

Though plasmas have been investigated for many years, most of the studies have been confined to direct-current (dc) discharges. With the development of microwave technology, inexpensive sources of microwave power became available, opening the investigations to radio frequency (rf) studies.

This review begins with the work of Fehsenfeld, et al., in 1965 (1). Using a magnetron-powered medical diathermy unit, they obtained a maximum of 125 watts of microwave power at a frequency of 2.45 GHz. This power was fed into five different microwave cavities (individually) to produce discharges, without an external magnetic field. The cavities were modified rectangular waveguides or coaxial and cylindrical cavities. Tuning mechanisms were added as the experimenters realized that coupling power into the discharges was affected by gas pressure, gas type and the plasma itself. A table of operating characteristics is presented, comparing the cavities, using He and H_2. The type of cavity with the best overall performance was described as a foreshortened quarter-wave coaxial structure, approximately five inches long. The resonant frequency of the cavity was adjusted by means of a tuning stub and the coupling adjusted by a coaxial coupling slider. The adjustments allowed for a wide operating range, and minimal reflected power from the cavity. There was no gap in this cavity.

Results from Table II of their paper showed that He discharges could be sustained for pressures ranging from 1 mtorr to over 700 torr, with less than 1 per cent reflected power in the range from 0.1 torr to 100 torr. The cavities needed to retuned after breakdown of the gas.

In most cases, the discharges were confined to the cavities. When ejection of the plasma outside the cavities occurred, household aluminum foil was used to shield the operator from microwave radiation.

The authors suggested that these microwave discharges could be used as light sources, for production of free radicals for plasma chemistry experiments, and as excitation sources for gaseous electronics studies.

In 1970 Dorman and McTaggart (2) described the absorption of microwave power by plasmas, using He, Ar, H_2, N_2, O_2, CO_2, C_4H_{10}, and Cl_2. They used a tetrode vacuum tube power generator driven by a triode oscillator at a frequency of 900 MHz. More than 1 kilowatt of power was available. Maximum applied power was 520 watts with about 96% (500 watts) absorbed. The cavity is described simply as a waveguide resonator, rectangular or cylindrical is not indicated.

Their experimental curves show that the absorbed power passes through a maximum at a pressure which is characteristic of each gas, in a range from 1 to 80 torr. Other results are stated: 1) for a given incident power, all the gases used, except Cl_2, absorbed approximately the same amount of power when the pressure reached the optimum value; 2) as the incident power was increased more power was absorbed at any given pressure, and the pressure at which the discharge extinguished rose; 3) static systems showed no significant differences from systems in which the gas was flowing at rates up to 500 cm^3/min; 4) addition of up to 2% water vapor to O_2, N_2, and H_2 showed no significant differences in the power absorption curves; 5) temperature measurements with a thermocouple on the surface of the discharge tube showed that temperature rose with increasing pressure, reaching a maximum at a pressure about 40% higher than that for maximum power absorption. Temperature at optimum pressure for power absorption ranged from 160 C to 173 C; power absorption for air showed little difference for tube diameters of 3.4, 1.8, and 0.8 cm.

In the theoretical discussion the absorbed power was shown to be the product of the electron concentration, plasma volume, effective electric field, electron charge and electron drift velocity, and was independent of the flow rate of the gas. Double probe measurements showed that for pressures of 0.1 to 1 torr, the plasmas were in a near resonant state, with respect to electron concentration. Except for nitrogen, the pressures at which maximum power absorption occurred for diatomic molecules followed in the order of bond energies.

Experiments at 2450 MHz with hydrogen showed that pressures characterized by maximum power absorption increased from 10 to 70 torr over the values obtained at 900 MHz.

Abstracts for a paper by Lee and Asmussen (3) and another by Fredericks and Asmussen (4) appeared in the Bulletin of the American Physical Society in 1970. In the first paper, plasma column impedance vs. density and vs. incident power is plotted on a Smith chart. The figures show that the plasma can be resonantly sustained only in a discrete set of states corresponding to the different resonant states of the linear impedance and that a point of stable operation for a resonantly sustained plasma is always on the capacitive side of a resonance curve.

The second paper (4) describes experiments done with a cylindrical cavity and a re-entrant cavity. For input powers of 2 to 20 watts, an rf plasma with average densities above the critical density could be sustained, and the plasma density could be increased by a factor greater

than four by varying the cavity dimensions while the plasma was resonantly sustained.

The cavities used in the experiments to be described in this thesis are similar to the ones used in the Fredericks and Asmussen paper, reference (4).

Maksimov (5) has measured relative and absolute spectral line intensities and ionization rates in a steady state He microwave discharge. The cavity used was a resonant chamber of the Nikol'skii type, which is somewhat of a curved section of waveguide joined along a broad side to a flat section of waveguide to form a resonant chamber. A quartz tube was inserted at one end. A diagram is given in the first reference of the paper, no dimensions are given. The power source is a magnetron operating at a frequency of 3 GHz, available power is not indicated. The maximum power level shown on a graph is 90 watts. Operating pressures for the He discharge are 3 to 30 torr.

Intensities of the 4713 A and 5016 A lines were measured as functions of applied microwave power. Results showed the intensities in the 4713 A line to be linear with applied power up to 90 watts; in the 5016 A line, linear to approximately 50 watts, then the rate of rise decreased. Pressures ranged form 2.6 to 9.6 torr, the rate of increase in spectral intensity was greater for the lower pressures. The intensity of the 4713 A line increased linearly with the power density (watts/cm^3) of the plasma, and also with the electron density. The ionization rate in the plasma was approximately linear with the electron density, the slope was greater for 4.8 torr than for 16 torr. Linearity of line intensity with power density was stated as the result of: (1) excitation being principally direct, as opposed to stepwise ionization processes, (2) electron density being proportional to discharge power, (3) average electron energy being constant. Agreement between experiment and theory became less than satisfactory for pressures greater than 12 torr, indicating that the discrepancy is associated with deviation from a Maxwellian electron velocity distribution function as the pressure increases.

Investigation of the ionization rate dependence on average electron density showed that direct ionization is predominant in helium even at pressures greater than 10 torr. Charge balance in the plasma is maintained by diffusive decay.

Concerning the energy balance in a microwave plasma, Maksimov found that the fraction of power expended in ionization decreased with an increase in pressure, together with a decrease in the average electron energy. It was also stated that this fraction is higher for a microwave discharge than for a dc discharge, due to much higher average electron energies in the microwave discharge.

Maksimov concluded by saying that electron energies are higher for microwave discharges than dc discharges and that at a helium pressure of about 5 torr the electron velocity distribution function in nearly Maxwellian. As the pressure increases the MW plasma becomes more deficient in fast electrons; but a pure Dryuvesteyn distribution is not achieved.

Bossisio, et al, (6) described a large volume microwave plasma generator (LMP is their abbreviation), which used a slow wave structure to produce plasma volumes well in excess of 1000 cm^3. About 90% of the applied 2.5 kilowatts of microwave power was absorbed, at a frequency of 2.45 GHz. An important feature of the open slow wave structure and plasma was that field coupling could be adjusted in such a way that the microwave power density was dissipated uniformly along the entire length of the plasma reactor, resulting in a high percentage of power absorption. This plasma reactor was sandwiched between two slow wave structures that were excited in opposite directions, permitting larger reactor diameters, and hence large plasma volumes.

A plot of absorbed microwave power vs. pressure for flowing argon plasmas showed absorbed power to be nearly constant at roughly 90% of the incident power, up to a given pressure, where it begins to fall off. The "fall-off" pressure increased as the incident power increased, being crudely linear. This result was estimated from figure 9 of reference (6).

Some of the observed qualitative aspects of the discharges were given:

> At low pressures both cavity and LMP plasmas appeared uniformly luminous; they filled the entire reactor vessel, and even extended several centimeters beyond the confines of the cavity or slow wave applicator, particularly in the case of inert gas plasmas. As pressure was increased, inhomogeneities began to appear: the plasma tended to extinguish in the low-field regions of the reactor until, at pressures close to extinction, only a small fraction of the reactor volume was occupied by a dense plasma. In the case of argon, "streamers" were usually observed.

A plot of per cent dissociation of oxygen gas vs. absorbed power was nearly linear up to approximately 1.2 kilowatts and appeared to become saturated by 2.0 kilowatts (their figure 13).

In dissociation experiments with diatomic gases, the LMP was found to be approximately twice as efficient as a cavity used by Mearns and Morris (reference 22 of their paper) under otherwise similar experimental conditions (figures 12, 15, and 16 of the paper).

In comparing the LMP with cavity resonators the authors stressed the advantage of a larger volume for processing the gas.

The theoretical discussion showed the microwave electric field strength to be proportional to the square root of the incident microwave power.

A radiation shield was used to "protect personnel against stray microwave radiation from the slow wave structure, or ultraviolet radiation from the plasma." This shield was basically a double-walled plastic box opening into a metal cabinet at the bottom. Except for gas entrance and exit ports, the slow wave structure and reactor tube were completely enclosed. The ½ inch space between the walls of the box was filled with water. Microwave radiation levels at the outside surface of the shield were less than 1 mW/cm^2, when the LMP was operated at 2.5 kilowatts.

Overheating of the reactor tube was no problem. The large tubes provided large surface areas for forced-air convective cooling, so that high power discharges could be maintained almost indefinitely.

Finally, three applications of the LMP as listed by the authors were: use in organic reactions, modification of polymers by plasmas, and light sources, including possible excitation of an Ar laser and a He-Ne laser.

During the period from 1970 to 1978, Asmussen and collaborators published a number of papers dealing with discharges in microwave cavities. They investigated the behavior of microwave discharges in rf coupling structures, including cylindrical cavities. Their work attempted to explain the dependence of plasma density on rf power levels, cavity length and probe geometry, gas pressure and flow rates. Several structures were built which allowed the coupling of large amounts of rf energy into the plasma. Surface waves (to be discussed in the following section) were observed as part of this work.

In 1970 a paper from Lee, Colestock and Asmussen (7) appeared, describing the discharge in a plasma tube inserted into a ridge waveguide excited at 3.03 GHz. Plasmas over 23 cm in length were observed (8). In 1971 Fredericks and Asmussen (9) described a short gap coaxial or re-entrant type of cavity operating in the TEM mode. Only discharges confined to the gap region were discussed in the paper, although plasmas extending outside the cavity were observed. These plasmas were recognized as being due to surface wave propagation in the discharge (8).

Using the same coaxial cavity, Fredericks and Asmussen (10) describe retuning and hysteresis effects of an rf plasma. The plasma was dc sustained and "perturbed" by rf power coupled into the cavity. After the plasma had been excited, the authors utilized the capability of changing cavity length to retune the plasma to obtain greater densities. The primary method of controlling the plasma density in a cavity of fixed length was by variation of the current to the filament of the dc discharge in the sealed tube containing Hg plasma. Increase of incident rf power had only a minor effect in increasing the plasma density. However, the plasma density could be increased dramatically by changing the cavity length L_s without increasing the incident rf power. Experimental curves of luminosity (plasma density) vs. cavity length showed hysteresis effects--cavity length varying from 1.7 to

2.2 centimeters. The retuning and hysteresis effects were explained using power absorbed and power loss curves, showing how rf power is coupled into the dc sustained plasma depending on the intersection of the two curves. Rf powers absorbed were of the order of 5 watts or less.

In a simple cylindrical cavity of adjustable length the same authors showed that a high density plasma can be resonantly sustained by the rf field of a 3.03 GHz klystron (11). Densities over ten critical densities ($f_e = 10$ f) were obtained by retuning the cavity at input powers of about 20 watts. Without the dc input mentioned in the previous experiments, the plasma density would be entirely dependent on input rf power and coupling geometry, i.e., cavity length and probe position.

Still another microwave plasma cavity was used and described by Asmussen, et. al., in January 1974 (12). The plasma tube and cylindrical cavity were concentric, cavity length was variable and excitation frequency was 2.45 GHz (magnetron). By adjusting the cavity length and coupling probe, microwave plasmas were sustained in flowing and nonflowing argon from pressures of several microns to over one atmosphere. High plasma densities were possible for this method of operation. Energy coupling and rf plasma stability were explained by a set of power absorbed curves and a power loss curve, and expressions were given for power absorption and loss. Stability results when the variation of power absorbed versus density curve has a negative slope and the physical explanation for this was presented. Plasma density was varied by length tuning the cavity, with high densities (10 critical densities) being possible.

Other results obtained with this cylindrical cavity were presented at the 1974 RF Plasma Heating Conference (13). Lossy plasma-cavity eigenfrequencies were computed as functions of plasma density, effective collision frequency and cavity length. In addition, a variable, high density plasma with densities in excess of 1000 critical densities could be sustained. Adjustment of cavity length and coupling allowed microwave plasmas to be sustained in flowing and nonflowing argon gaseous environments from pressures of several microns to over one atmosphere.

Experimental characteristics of a discharge in this cylindrical cavity are described in greater detail by Mallavarpu, Asmussen and Hawley (14) (1978) for a wide range of pressures and flow rates for Argon gas, with variable power levels. Results are explained qualitatively using linear, lossy, cold plasma theory, which is restricted to small signal linear phenomena and gases with a zero flow rate. Despite these restrictions the theory explains pressure dependence of the rf absorbed power by attributing plasma losses to electron-neutral particle collisions. Coupling of EM energy to surface waves was demonstrated and qualitatively explained using cavity eigenlength versus $(\omega_e/\omega)^{\frac{1}{2}}$ and (ν_e/ω) curves obtained from the above theory. Surface wave coupling was used to produce long plasma columns (about 4 ft). A smaller cylindrical cavity was also described in this paper; it produced long plasma columns using surface waves, with P/L around .6 W/cm, for Argon. Using a length dependent mode (TE 011) and the length independent region of the TE* 112 mode, the absorbed power characteristics for flowing Ar were shown to be different from those of the nonflowing gas. Absorbed power increased directly as a function of flow rate for low flow rates and reached a saturation value at higher flows. This result was explained by the shielding effect of the plasma layer adjacent to the quartz tube. The pressure dependence of absorbed power was relatively uniform for different power levels, exceptions being found in the lower region of the pressure range (below 10 torr). By optimizing the length, discharge pressure and gas flow rate an impedence match between the external microwave system and the cavity could be achieved, with more than 90% of the incident power being coupled into the plasma.

In comparing microwave discharges with other types of electrical excitation, studies indicate that microwave discharges produce a higher degree of ionization and dissociation in chemical species, can sustain plasma at higher pressures, and the carrier gas remains moderately cool, even with a significant degree of ionization.

In general, microwave generated plasmas can be created and sustained in cavities where moderate (10 - 100W) to large amounts (several kW) of rf power can be coupled into a confined gas at low pressures. This differs from dc discharges where energy is coupled into the discharge gas through electrodes in the gas tube, with ionization being produced by steady currents rather than oscillating fields. When the microwave cavity was designed with a tuning mechanism, absorbed powers as high as approximately 95% of the incident power were observed. In addition, the cavity could be retuned as plasma conditions changed, to keep coupling efficiency high. Large plasma volumes can be obtained, without the contamination of sputtering electrodes as in the dc discharge. Applications range from plasma chemistry experiments to microwave pumping of lasers.

2.3 Observations of RF Surface Wave Generated Plasmas

Fehsenfeld, Evenson and Broida in a 1965 paper (1) observed rf surface waves in plasmas in several microwave cavities operating at 2450 MHz, indicating that the discharges extended outside the cavities for several centimeters, though they did not relate the phenomena to space charge waves.

Vandenplas (15) in 1968, described a surface wave plasma extending outside a waveguide, with the plasma length being proportional to the input power. In 1969, Messiaen and Vandenplas (16) described a discharge ejected 8 cm outside an ordinary S band waveguide without magnetic field.

Surface wave plasmas were observed in nearly all the investigations of Asmussen and his collaborators. However, their objective was to couple large amounts of microwave energy into the discharges. Consequently, the plasma was generally confined to a small region in the pyrex or quartz tubes used and observations of the surface wave generated plasmas were not reported in the early papers. As previously mentioned, in the ridged-waveguide used by Lee, Colestock and Asmussen (7), plasmas about 23 cm long were observed to extend outside the waveguide (8).

A photograph of a surface wave generated plasma is shown in a 1974 paper by Asmussen, et al., (12). The flowing argon discharge extended several inches above and below the microwave cavity, indicating the presence of surface wave modes. In the paper delivered to the 1974 Rf Plasma Heating Conference (13), they reported that adjustment of the cavity eigenlength for an intersection between electromagnetic and cold plasma resonances resulted in the plasma being "ejected from the cavity sometimes filling the entire length of the 4 ft. quartz tube." Figure 5 of the 1978 paper (14) is actually a photograph of this mode of operation:

a 4 foot tube completely filled with an argon discharge.

Moisan, Beaudry, Leprince and co-workers have published results of a number of studies of bounded rf surface wave plasmas. In 1974, Moisan, Beaudry and Leprince (17) described a modification of a short gap cavity similar to the one described by Asmussen and Fredericks in 1970. With a short gap coaxial cavity and capacitive coupling (rather than the inductive coupling of the short gap cavity of Asmussen and Fredericks) they produced a 25 mm diameter, 1.80 m long plasma with 80 watts of rf power at a frequency of 500 MHz. The plasma density was approximately 10^{10} to 10^{11} electrons per cm^3. Plasma length was a maximum between 0.01 and 1 torr. Plasma density and luminosity decreased nearly linearly as the detector was moved away from the gap.

In 1975 the same authors described a modified version of the "surfatron" discussed above (18). Their plasma exhibited low electron density fluctuations and absorbed nearly 100% of the incident power. Absorbed power, plasma length and density were maximum when the coupler was near, but not adjacent to, the plasma tube. Excitation frequency could be changed with only minor effects in the absorbed power. Plasma frequency decreased slightly with increasing frequency, as did plasma length. A result of significance to this thesis is the determination of plasma length as a function of absorbed power, at several values of the Ar gas pressure. Their straight line through the data points (which is not a good fit) corresponds to a P_a/L_p of .54 watts/cm. Detailed curves explaining the variation of density with tube diameter, rf power gas type, and excitation frequency were not given. Up to 80 watts, plasma length is directly proportional to absorbed power, while at higher powers, plasma length varies as $P_a{}^{0.7}$. Several practical applications of the discharges were also listed.

In another paper, Moisan, et al., (19) described the short gap cavity and a waveguide structure to produce surface wave plasmas, along with electron density and power absorption measurements, with application to a chemical HF laser. In 1977 Moisan and Ricard (20) published density measurements of metastable atoms in an Ar surface wave plasma, with maximum density (7×10^{11} cm^{-3}) at about .15 torr. These densities are higher than those obtained with a positive column operating under similar conditions.

Finally, the same authors with collaborators (21) considered the problem of attenuation of surface waves, showing that the attenuation of the surface wave in a plasma is collisional in nature over most of the investigated pressure range, 10 microns to 150 microns, and frequencies of 360 MHz to 650 MHz. Though not specifically discussed, Figure 2 of the paper shows standing wave variations in the rf electric field intensity, measured as a function of axial position along the plasma tube. In the same figure, interferometer measurements exhibit the same type of pattern, with the wave length varying from 20 cm to 38 cm.

This brief review has shown that while surface waves on dc columns have been understood for a number of years, rf and microwave surface wave generated plasmas are relatively new. The plasmas observed are rf sustained and can be made to extend outside the coupling structures. Experimenters have measured power absorption, plasma density, light intensity of emitted wave lengths and proposed applications for this new type of discharge. As already mentioned in the introduction to this work, the purpose of the work presented herein is to extend these studies to gain an understanding of the behavior of these surface wave generated plasmas as variations are made in external parameters (cavity geometry, coupling structure, diameter of plasma tube, input power, excitation frequency) and in internal parameters (gas pressure and gas type).

2.4 Plasma Surface Wave Modes

When dealing with plasma surface wave modes, two different physical situations are possible. The first to be investigated was that of an electromagnetic wave propagating along the surface of a cylindrical plasma column. The plasma is created and maintained by a dc source and only perturbed by alternating (rf) fields. The rf electric fields, energy propagation and space charge waves are all concentrated at and travel along the plasma surface, hence, the name surface wave. See Figure 2.1.

The other physical situation is that of a discharge created and sustained by electromagnetic waves propagating along the gas-dielectric tube interface. As the wave propagates along the tube, it ionizes the gas and sustains the discharge, without the presence of dc currents. Historically, this surface wave generated plasma evolved by two different methods. One was for the experimenters to increase the rf energy that was applied to a dc discharge, while decreasing the dc current. The other was to start an rf discharge in a plasma cylinder and increase the power supplied to the plasma-cavity system. When coupling geometry is appropriate for the propagation of surface waves, the plasma extends outside the cavity. In fact, with the proper coupling geometry, surface modes are difficult to suppress. Without the proper geometry, they are difficult to obtain.

While this thesis is concerned with surface wave generated plasmas, a summary of the basic theory of surface waves on the plasma column will be presented below as in Krall & Trivelpiece (22).

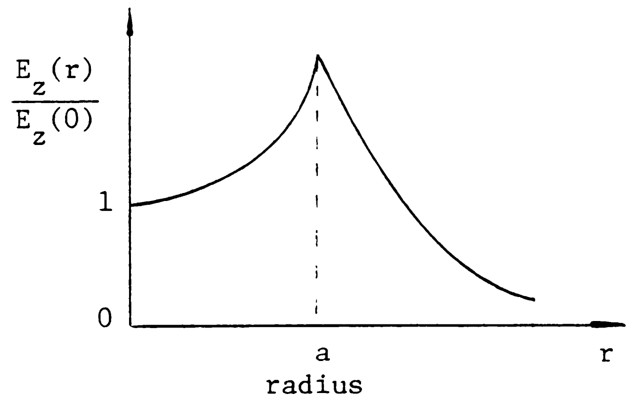

(a) Electric Field for the Azimuthally Symmetric Surface Wave Mode as a Function of Radius for an Unmagnetized Plasma Column in Free Space

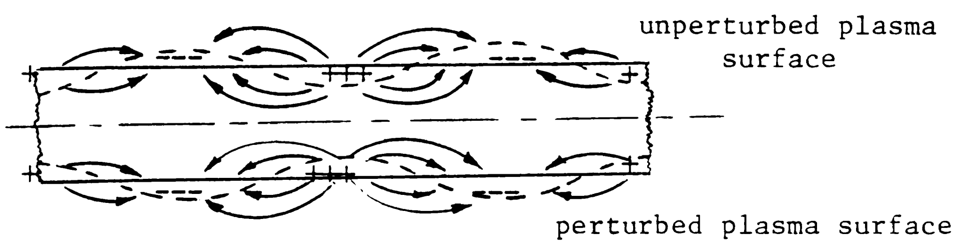

(b) Electric Field for the Azimuthally Symmetric Surface Wave Mode on an Unmagnetized Plasma Column in Free Space

Figure 2.1 Electric Field for the Azimuthally Symmetric Surface Wave Mode Reproduced from (22).

The discussion presented by Krall and Trivelpiece is taken from a 1959 paper by Trivelpiece and Gould (23), considering only the sections that deal with an unmagnetized plasma column. (Trivelpiece and Gould also consider magnetized plasmas.) In such a column the dielectric tensor reduces to the scalar dielectric constant

$$\varepsilon = \varepsilon_o(1 - \omega_p^2/\omega^2)$$

The plasmas has a radius a, and is in a conducting cylinder of radius b. The space between the plasma column and conducting cylinder is taken to be a vacuum. Maxwell's equations in each region within the cylinder lead to the following wave equations:

$$\{\nabla_T^2 + (\varepsilon\omega^2/c^2 - k^2)\}\binom{E_{1z}}{B_{1z}} = 0 \qquad 0 < r < a$$

$$\{\nabla_T^2 + (\ \omega^2/c^2 - k^2)\}\binom{E_{1z}}{B_{1z}} = 0 \qquad a < r < b$$

where $\nabla_T^2 = \frac{1}{r}\frac{\partial}{\partial r} r \frac{\partial}{\partial r} + \frac{1}{r^2}\frac{\partial^2}{\partial \theta^2}$ in cylindrical coordinates.

All of the transverse field components are derivable from E_{1z} and B_{1z} in this cylindrical system.

The waves associated with the differential equation for the (electric) E field are called E modes, and those associated with the (magnetic induction) B field are B modes. Though the differential equations are the same, they have different eigenmodes because the boundary conditions are different at the plasma and vacuum boundaries.

The solution for azimuthally symmetric slow wave E modes is

$$E_{1z} = \begin{cases} A \dfrac{I_o(\tau r)}{I_o(\tau a)} e^{j(kz-\omega t)} & \text{for } 0 < r < a \\[2ex] A \dfrac{I_o(\tau_o r)K_o(\tau_o b) - I_o(\tau_o b)K_o(\tau_o r)}{I_o(\tau_o a)K_o(\tau_o b) - I_o(\tau_o b)K_o(\tau_o a)} e^{j(kz-\omega t)}, & \text{for } a < r < b \end{cases}$$

where τ and τ_o are defined by the relations

$$\tau_o^2 = k^2 - \omega^2/c^2$$

$$\tau^2 = k^2 - \omega^2/c^2 + \omega_p^2/c^2$$

and I_o and K_o are modified Bessel's functions of the first and second kind, respectively. With this solution, E_{1z} is finite on the axis, continuous at r = a and zero at r = b. Continuity of the tangential magnetic field ($B_{1\theta}$) leads to the dispersion relation for waves,

$$\varepsilon \frac{1}{\tau a} \frac{I_o'(\tau a)}{I_o(\tau a)} = \frac{1}{\tau a} \frac{I_o'(\tau_o a)K_o(\tau_o b) - I_o(\tau_o b)K_o'(\tau_o a)}{I_o(\tau_o a)K_o(\tau_o b) - I_o(\tau_o b)K_o(\tau_o a)}$$

with the prime denoting a derivative with respect to the argument of the Bessel function.

This dispersion relation is shown graphically in Figure 2.2, for various values of $\omega_p a/c$. c/ω_p is the reactive skin depth of the plasma, denoted here by δ. When a/δ is very small, the fields penetrate into the plasma, and for low frequencies, are nondispersive slow waves (phase speed is less than c). As the ratio increases, which means that the skin depth decreases, the fields penetrate less into the plasma, becoming concentrated at the plasma column surface outside the plasma and extending from the plasma itself. The waves propagate with higher phase speeds, approaching c for a very large ratio of a/δ. The mode becomes like the TEM wave on a coaxial line, with each component of the field being largest at the plasma-vacuum boundary and decreasing away from the boundary. Figure 2.2 is reproduced from (22).

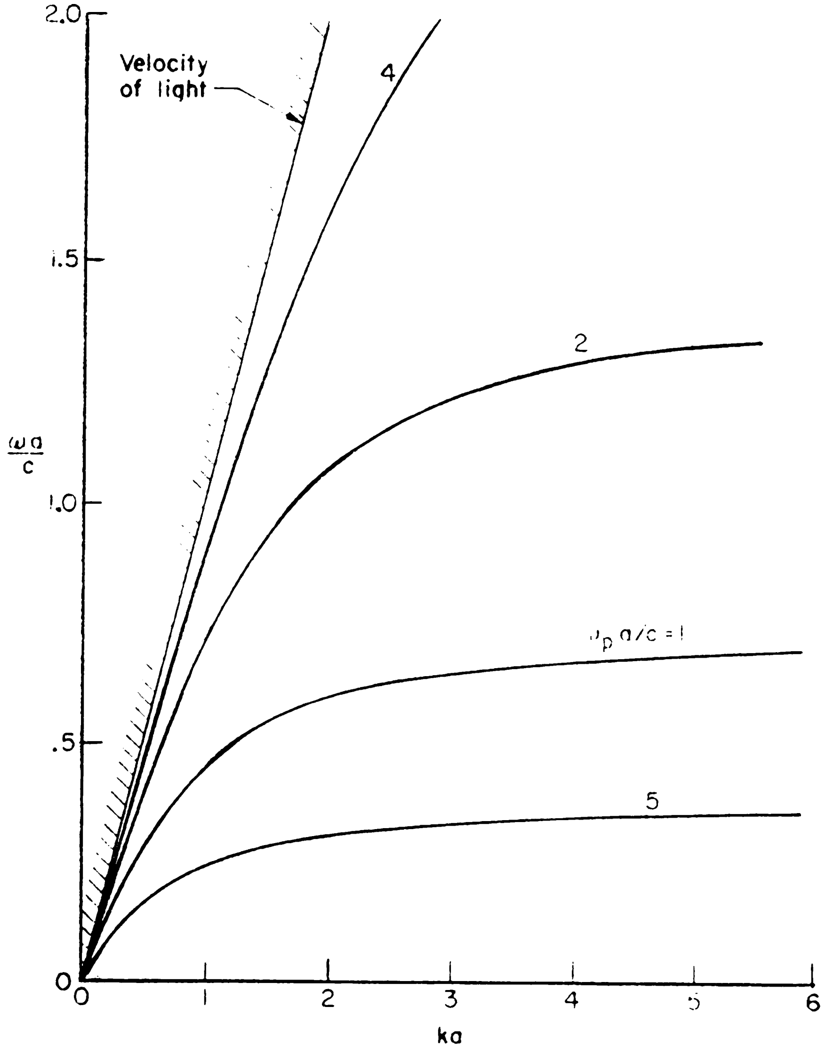

Figure 2.2 Frequency vs. Wave Number Diagram for Surface Wave on an Unmagnetized Plasma Column of Radius a

2.5 Dispersion Diagrams and Standing Surface Waves

Whenever wave propagation in some medium is considered, the description of the wave behavior is facilitated by a dispersion diagram, which is a plot of the dispersion relation. The most common use of the diagram is to obtain the phase and group speeds of the propagating waves.

The dispersion diagram to be used here is a normalized curve for the Gould-Trivelpiece surface mode. Specific points on the graph will be discussed, along with the probable region of the curve which is applicable to the propagation of ionizing surface waves. The section will be concluded by describing how to use the curve to calculate the approximate electron density in the discharge when a standing wave pattern can be observed in the plasma tube.

The normalized dispersion diagram is shown in Figure 2.3. Phase and group speeds for the wave for points A and C will be discussed. ω refers to the excitation frequency of the source, ω_p is the plasma electron frequency, k is the propagation constant of the surface wave, equal to $2\pi/\lambda$, and a is the plasma radius.

First consider point A on the curve. In this region, the phase speed, ω/k, and the group speed, $d\omega/dk$ (which indicates the speed at which energy travels along the tube), are nearly equal. For this point a given phase of the wave and ionizing energy will travel along the plasma column at close to the speed of light, since the curve is close to the light line. As the energy propagates along the tube, it ionizes the gas, creating and sustaining the plasma.

At point C on the curve, the phase and group speeds are considerably different. Note that the phase speed, ω/k, is lower than at point A,

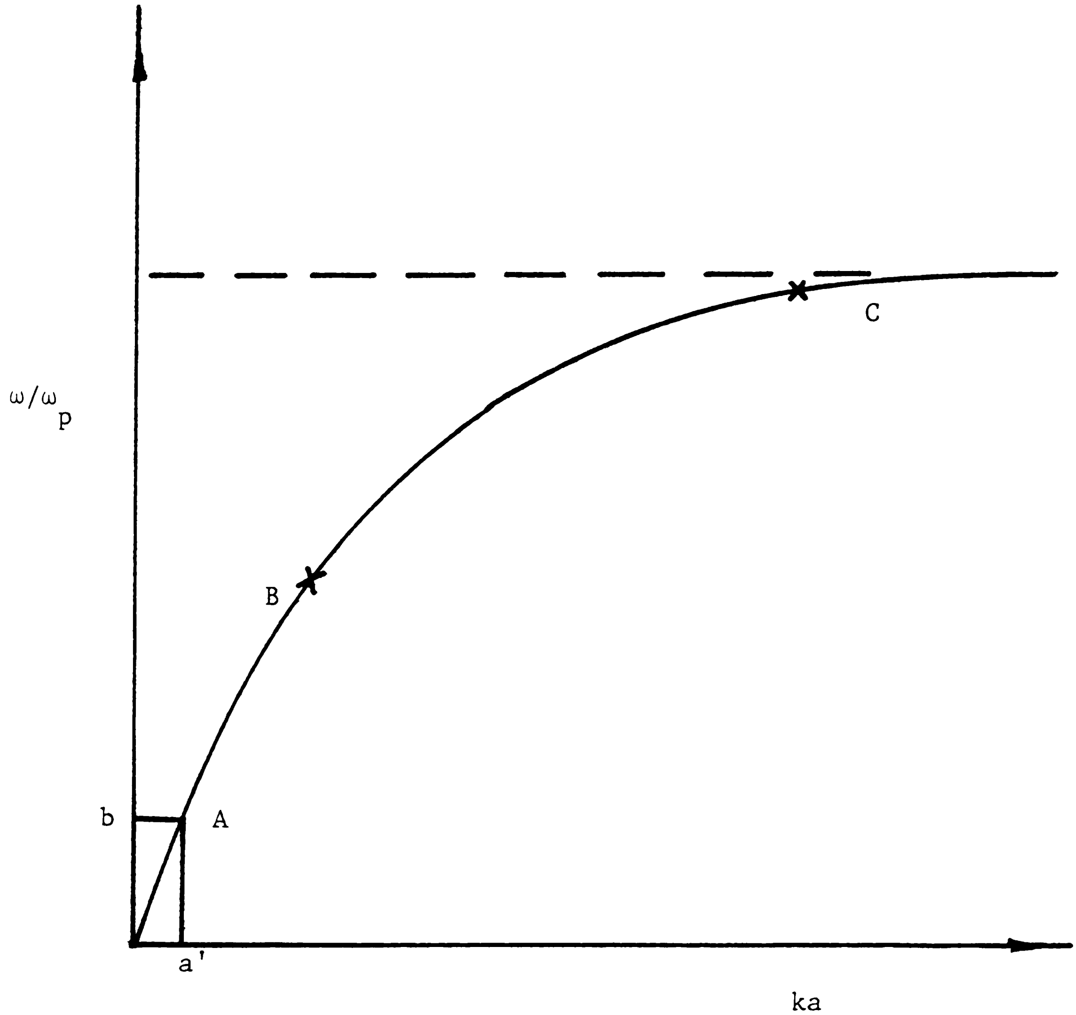

Figure 2.3 Normalized Dispersion Diagram for the Gould-Trivelpiece Mode

and decreases as one moves in the direction of increasing ka, since ω/ω_p remains nearly constant. The group speed (the slope of the curve) has decreased nearly to zero, meaning that in this region of the curve, or for slightly larger k, electromagnetic energy travels very slowly, if at all, along the plasma tube. Since the energy does not travel along the tube, the gas will not be ionized and there will be no discharge due to the surface wave. For initial breakdown of the gas, the relevant point on the curve would be near point B, moving down on the curve as the ionization increases the plasma density.

An ordinary dispersion diagram, with ω vs. k, would allow only the determination of the phase and group speeds of the wave. The normalization of the curve, ω/ω_p vs. ka, allows the plasma electron density to be determined, when the standing wavelength can be measured. For the standing wave pattern along the plasma tube, bright and dark regions appear, and the distance between any two adjacent bright or dark regions is equal to one half of the wavelength (this will vary along the length of the tube). Doubling this distance gives the wave length, λ. The wave number, k is given by $2\pi/\lambda$, and the tube radius, a, would be known. The product of the two gives a point on the horizontal axis, such as point a'. The ratio of ω/ω_p is then found at point b. Since the excitation frequency of the source is known, the reciprocal of the value at point b multiplied by the excitation frequency gives the plasma frequency. The plasma electron density is then determined from the equation

$$\omega_p = (ne^2/m\varepsilon_o)^{1/2} .$$

As given here, n is in particles per m^3.

The value of the plasma density as determined by this method is subject to some uncertainty, since the determination of the wavelength involves a small region of the plasma, rather than simply a point. If the wavelengths are measured at a number of places along the plasma tube, the variation of electron density as a function of position along the tube can be determined.

Now suppose, for example, that a small plasma tube is used and the observed wavelength is large. Thus k is small and the value of ka will be small, yielding a low value for ω/ω_p. This means that ω_p is large in a relative sense, thus the electron density is large. If a change in the plasma-cavity system results in a shorter wavelength, the operating point moves up on the curve, with a larger value of ω/ω_p, indicating that the electron density, n, has decreased. The benefit of this method is that the approximate density and changes in density can be determined without special apparatus and without concern for gas pressure or other internal factors in the discharge. The values obtained are approximations, correct to a factor of perhaps 3 or 4, though this method has not been compared to other methods for determining plasma density. This approach was mentioned by Trivelpiece and Gould (23).

CHAPTER III

EXPERIMENTAL SET-UP

3.1 Introduction

This chapter discusses: (1) the two types of cavities used in this research to couple rf energy into the surface wave, (2) the coupling structures within the cavities, (3) the microwave circuits and measurement systems, (4) the vacuum systems for both cavities, (5) protective screening, and (6) a photodiode circuit to measure relative plasma densities.

The last section of the chapter comments on general techniques and experimental methods used to obtain the reported results. These comments are included so that an investigator wishing to duplicate or extend the experimental results could more easily simulate the conditions under which the results were obtained.

3.2 RF Surface Wave Couplers

Detailed figures and photographs of the cavities used for surface wave excitation are described in this section, first for the coaxial cavity, then for the cylindrical cavity.

The outside view of the coaxial cavity in Figure 3.1 shows the screened viewing windows, which were used for observation of the coupling geometry inside the cavity, and the viewing holes for determination of plasma length when the discharge terminates within the cavity. The inner conductor of the cavity has similarly spaced holes so that the

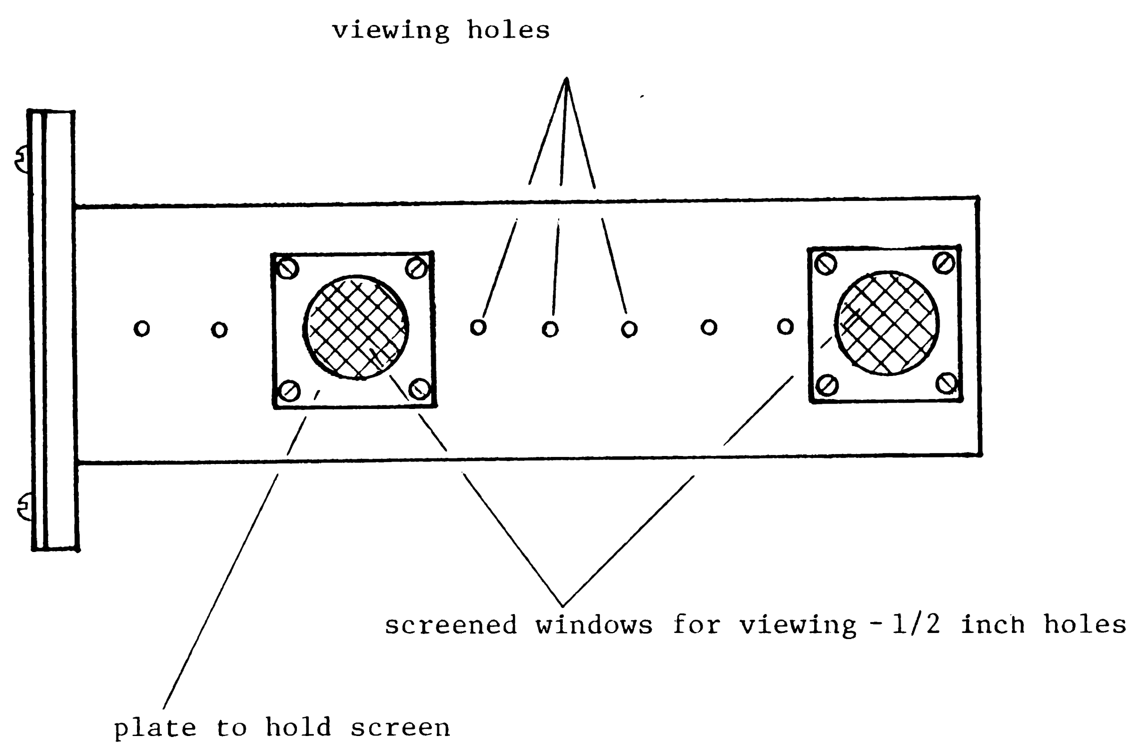

Figure 3.1 Outside View of the Coaxial Cavity

quartz tube can be seen when the windows of both parts are aligned. This cavity is a modification of that used by Fredericks and Asmussen (9).

Figure 3.2 is a longitudinal cross section of the coaxial cavity with adjusting mechanisms included. The gap between the center conductor and end plate of the cavity can be continuously adjusted by simply rotating the threaded center conductor. The gap length, L_g, is measured by a mark on the part of the center conductor where it exits the endplate at the rear of the cavity. Two of these cavities were built.

The inductive coupling loop, shown above the gap in Figure 3.2 is formed by the inner conductor (wire) of a section of microcoaxial cable curved around to form a loop approximately 6 mm in diameter, and soldered to the outer layer of the cable. This is reinforced by winding a thin wire around the loop and filling in any gaps with solder.

Other types of coupling loops were also used, including rectangular loops. An alternative type of loop consisted of a commercially prepared antenna loop, about 1 mm thick and 6 mm in diameter, that was soldered onto the microcoaxial cable as shown in Figure 3.3.

The section of coaxial cable passed through the sliding short, the end plate of the cavity and an adjusting plate, all of which are labeled in Figure 3.2. The holes were slightly larger than the cable to allow for easy movement of the loop. Thus the loop could be moved longitudinally and also rotated. Longitudinal adjustment of the loop was accomplished by passing the loop cable through a small plate attached to an adjusting screw as shown in Figure 3.2. A setscrew in this plate prevented the loop from rotating by itself.

A sliding short was used to vary the cavity length. Details of the sliding short and finger stock are shown in Figure 3.4. The finger stock

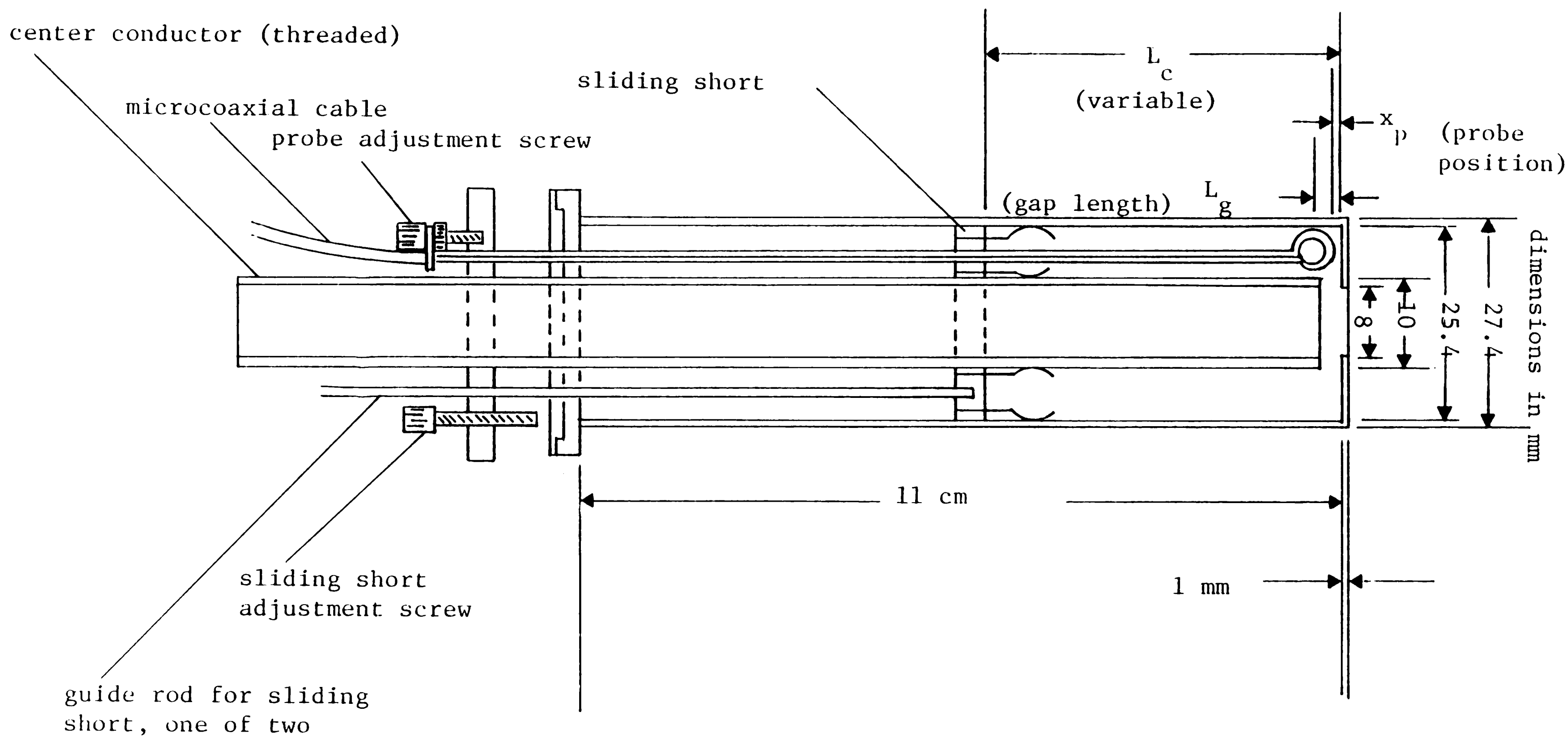

Figure 3.2 Cross Section of the Coaxial Cavity

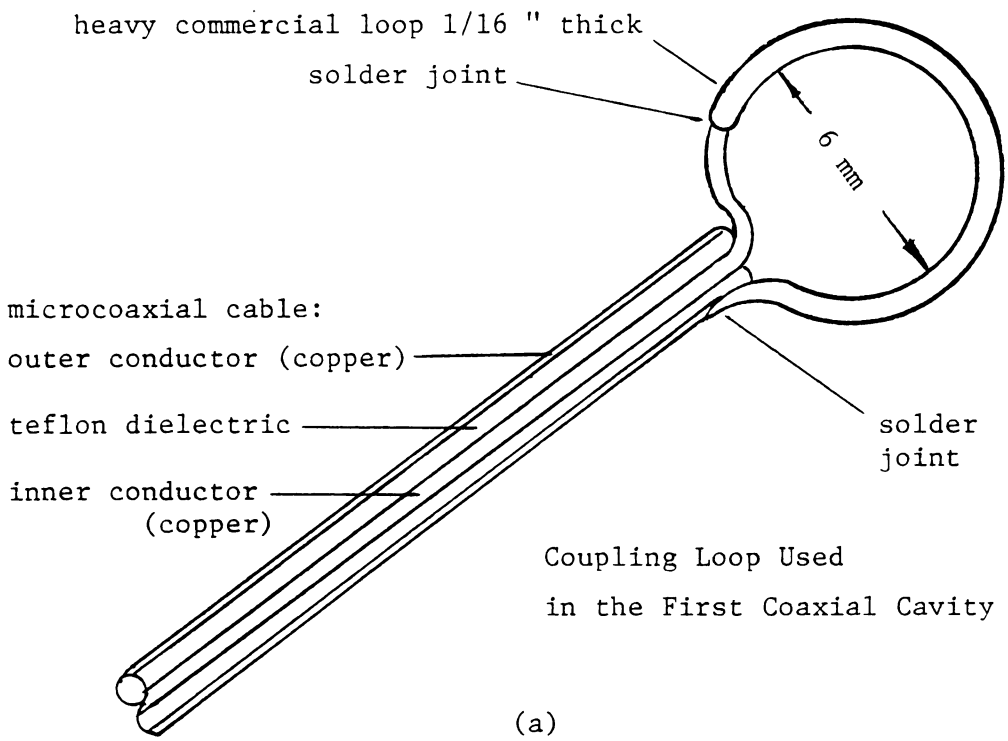

Coupling Loop Used
in the First Coaxial Cavity

(a)

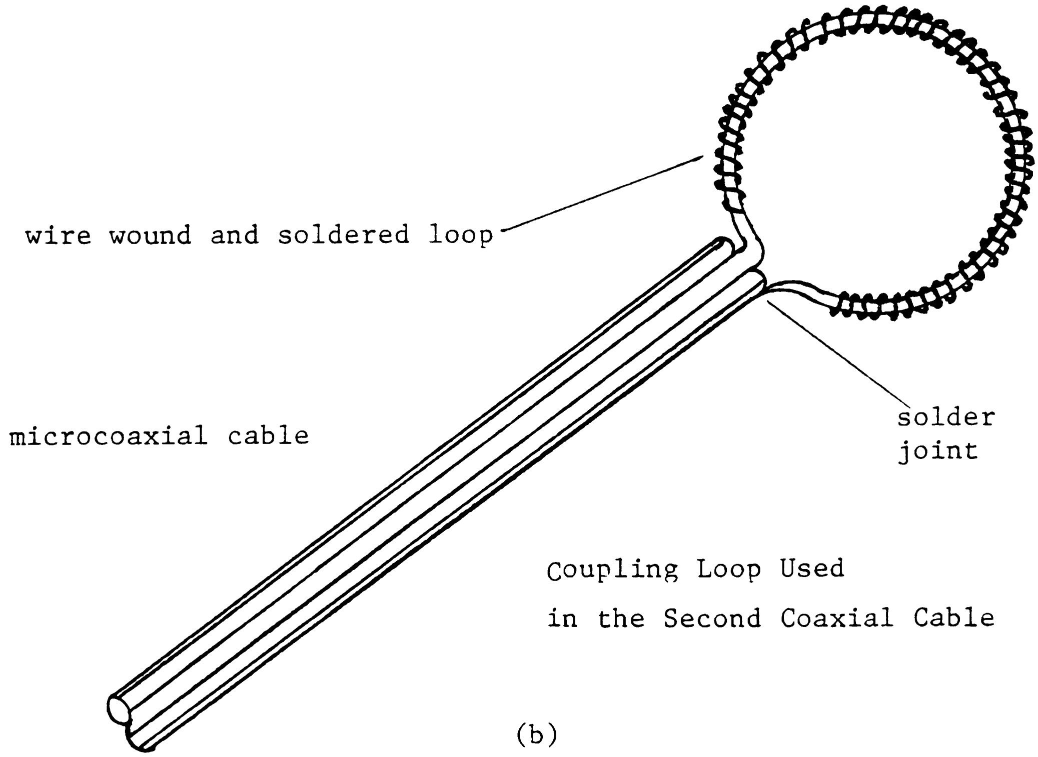

Coupling Loop Used
in the Second Coaxial Cable

(b)

Figure 3.3 Coupling Probes Used in the Coaxial Cavities

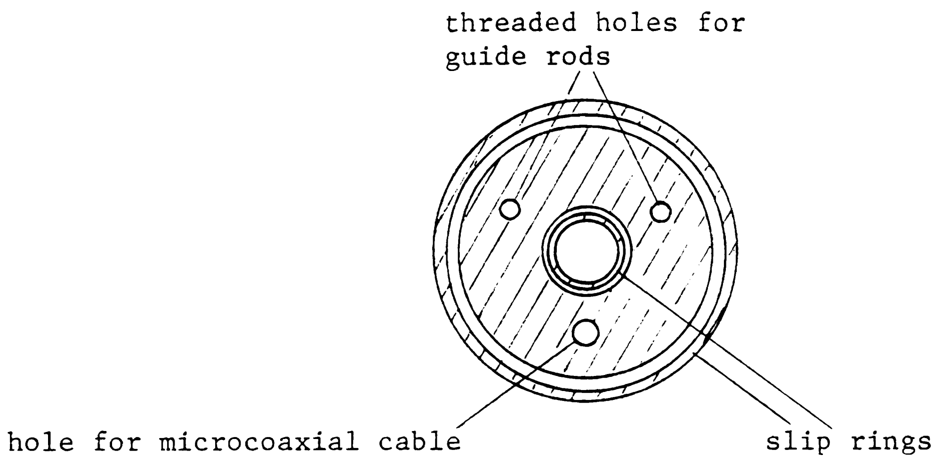

(a) Axial View

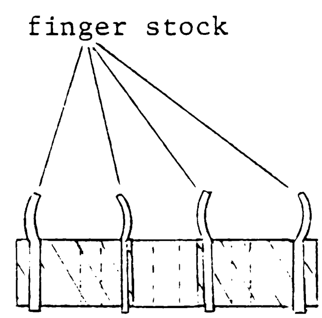

(b) Side View

Figure 3.4 Detail of Sliding Short for the Coaxial Cavity kept the short parallel to the ends of the cavity and, since it was silver coated, provided good electrical contact between the short and the walls of the cavity. Two "rings" of finger stock were used, one for contact with the outer wall of the cavity and one for the center conductor. The finger stock was held in place by tightly fitting slip rings. The short was moved by means of 1 1/2 mm rods that screwed into the bottom of the short and passed out the rear end plate of the cavity to the adjusting plate, where they were fastened by set screws. This adjusting plate could be continuously moved by a screw that passed through the plate and rested against the end plate of the cavity. Turning the screw moved the plate away from the cavity, pulling the guide rods, which in turn, pulled the short and lengthened the cavity. The cavity was shortened by turning the screw backwards and pushing the adjustment plate inward by hand. Thus, all cavity parameters--gap, probe position and orientation, and cavity length--are continuously variable.

The cavity and inner conductor are made of brass, adjustment screws are steel, and the short adjustment plate is aluminum. The microcoaxial cable is copper with a teflon dielectric.

The high power, cylindrical brass cavity is shown in Figure 3.5. This cavity is similar to the one used by Mallavarpu and Asmussen (14). The cavity length is adjustable by moving the sliding short, connected to a brass plate on the outside of the cavity by three steel guide rods, which keep the short parallel to the end plates of the cavity. A threaded rod with a knob passes through the outside plate. This rod is used to adjust the position of the sliding short. Electrical contact is made from the short to the side wall of the cavity by CFM 300 finger stock.

The coupling probe can be moved by loosening a ring clamp and sliding

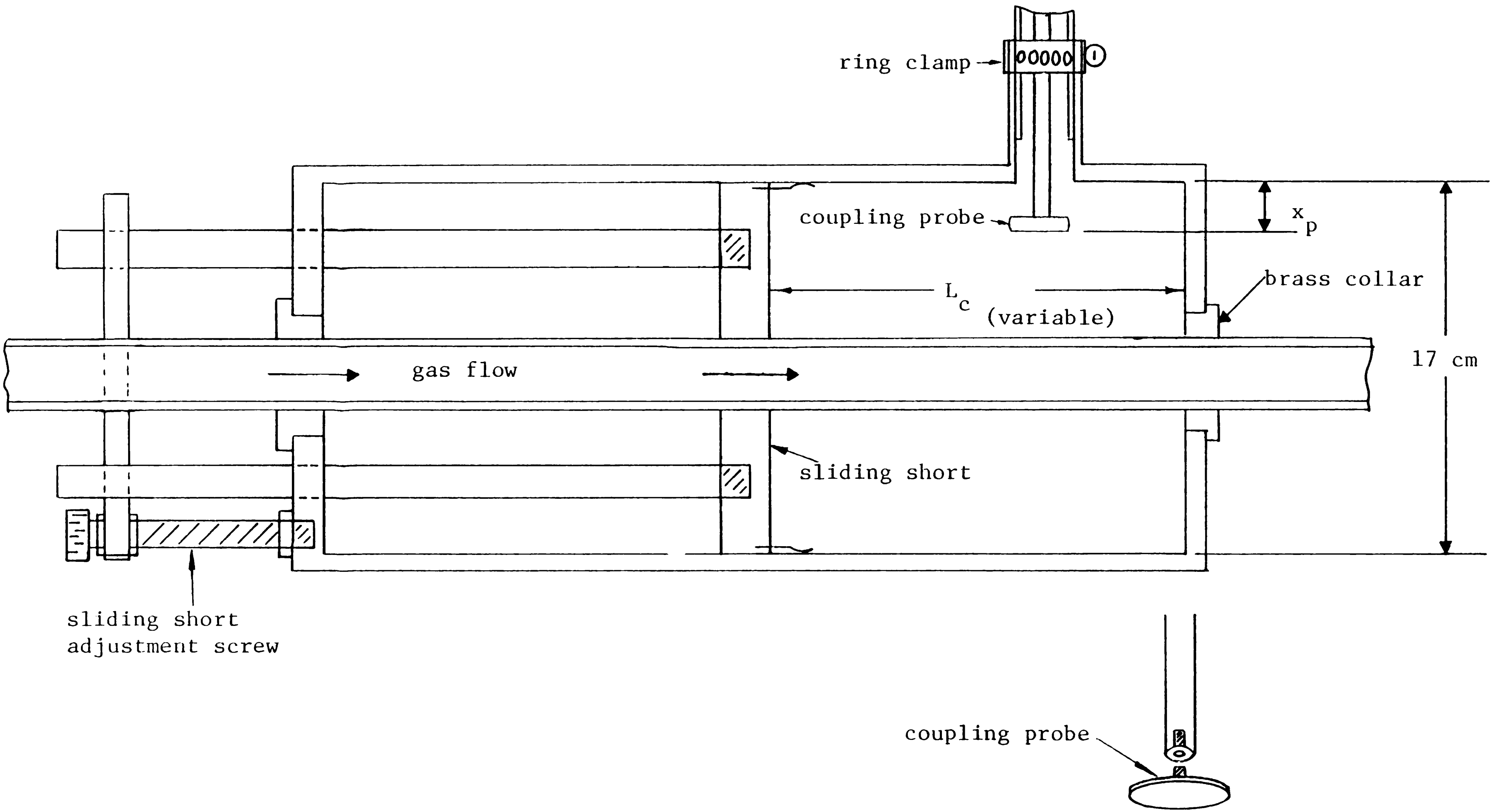

Figure 3.5 Cross Section of the Cylindrical Cavity

the probe housing in or out of the cavity.

The quartz tube could be moved off axis, vertically and/or horizontally, when the collars in the end plates of the cavity are larger than the tube outer diameter. These brass collars are used to minimize cavity perturbation due to openings in cavity end plates and to support the quartz tube. A set of different sized collars allows different tube sizes to be placed into the cavity. The collars are held in place by screws and washers.

The cavity has water cooling tubes soldered around the outside and to the bottom of the sliding short.

The coupling probe shown in Figure 3.5 consists of a brass disc that screws into a brass rod which forms the inner conductor of a coaxial structure. This coaxial structure originates at a waveguide to coaxial transition. This capacitive probe is moved by loosening the ring clamp and moving the coaxial structure by hand. The purpose of the ring clamp is to prevent rf radiation from leaking at the fitting.

3.3 External Microwave Circuits

The external microwave circuit is an important part of the whole experimental system. This circuit is the means by which energy is transmitted from the source to the plasma-cavity system and includes instrumentation. The external microwave circuits of the coaxial and cylindrical cavities will be described.

Three different experimental circuits used for the coaxial cavity are shown in Figures 3.6, 3.7 and 3.8. The one that is used depends on what experimental conditions are desired. Figures 3.6 and 3.7 show the

the rf systems that were used to investigate surface wave discharge characteristics as a function of excitation frequency.

In the system shown in Figure 3.6, the oscillator operated at a fixed frequency of 850 MHz. Its output was amplified by a Hughes TWT amplifier to a maximum of approximately 25 watts. A 2-4 GHz circulator was checked and found to be suitable for use at 850 MHz. The circulator was used to isolate the load from the power source. Reflected power was directed through a 30 dB attenuator into a matched load. The incident power passed through a 2-4 GHz directional coupler, that was calibrated at 850 MHz, to the 2 mm microcoaxial cable input to the cavity. Incident and reflected power were measured by Hewlett-Packard power meters. The absorbed power was determined from the difference between the incident and reflected powers. The frequency meter inserted between the 20 dB attenuator and reflected power meter was used to determine the excitation frequency.

The system shown in Figure 3.7 is similar in design and purpose to the circuit just described. In this case, the Hewlett-Packard continuous-wave (CW) oscillator is variable from about 1.7 to 3.8 GHz. The output passes through a variable attenuator (used to control incident power to the cavity) to a TWT amplifier with an output of about 20 watts. The 2-4 GHz isolator prevents reflected power from entering the amplifier. The rest of the circuit is the same as the one in Figure 3.6.

These two circuits were used for low power, variable frequency operation, where maximum incident power to the cavity was about 25 watts and excitation frequency ranged from 850 MHz to 3.8 GHz.

Figure 3.8 is a schematic of the high power (0-1200 watts) circuit. The magnetron operated at full output into an impedance matched power

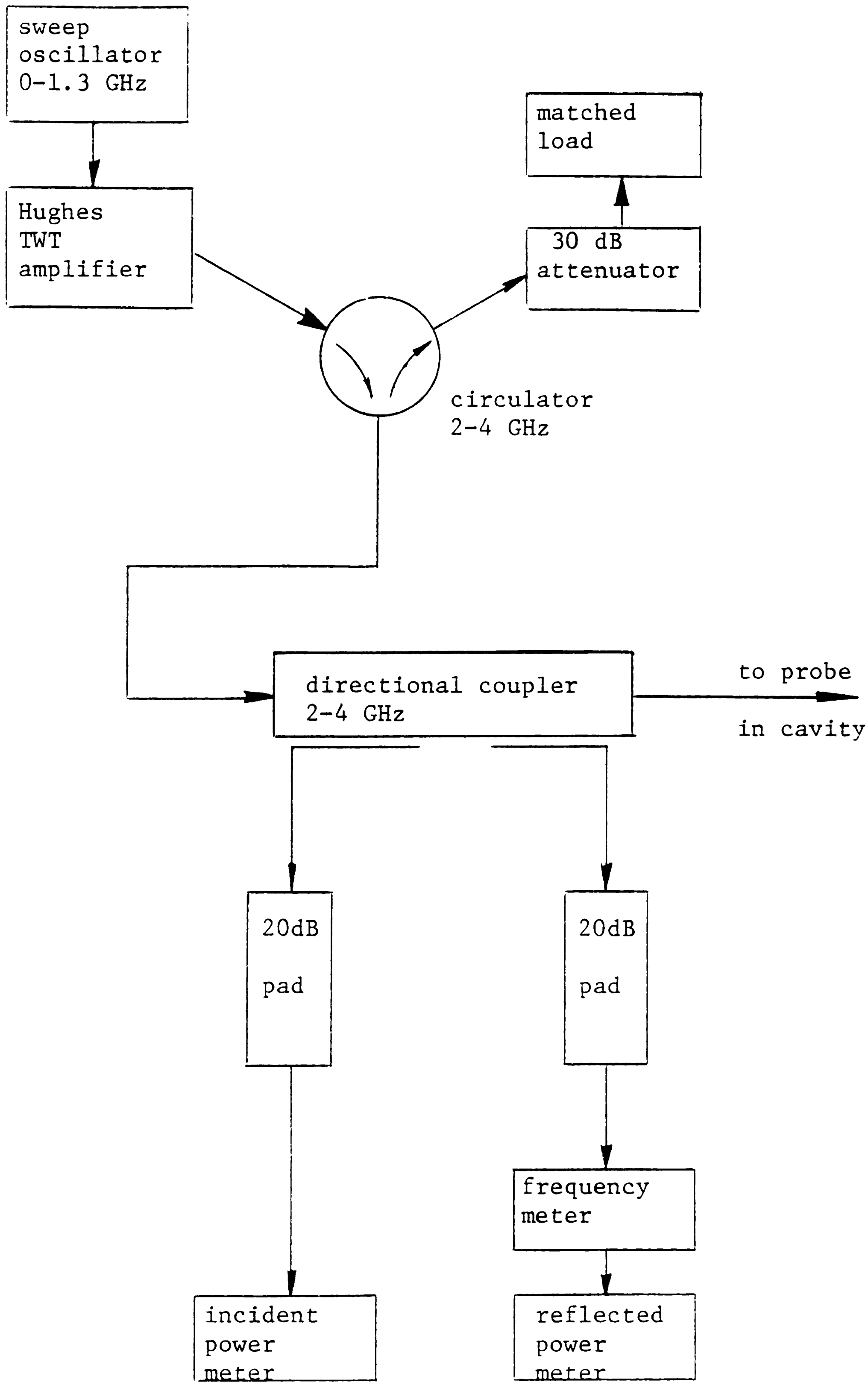

Figure 3.6 Low Frequency, Low Power Circuit for the Coaxial Cavity (850 MHz)

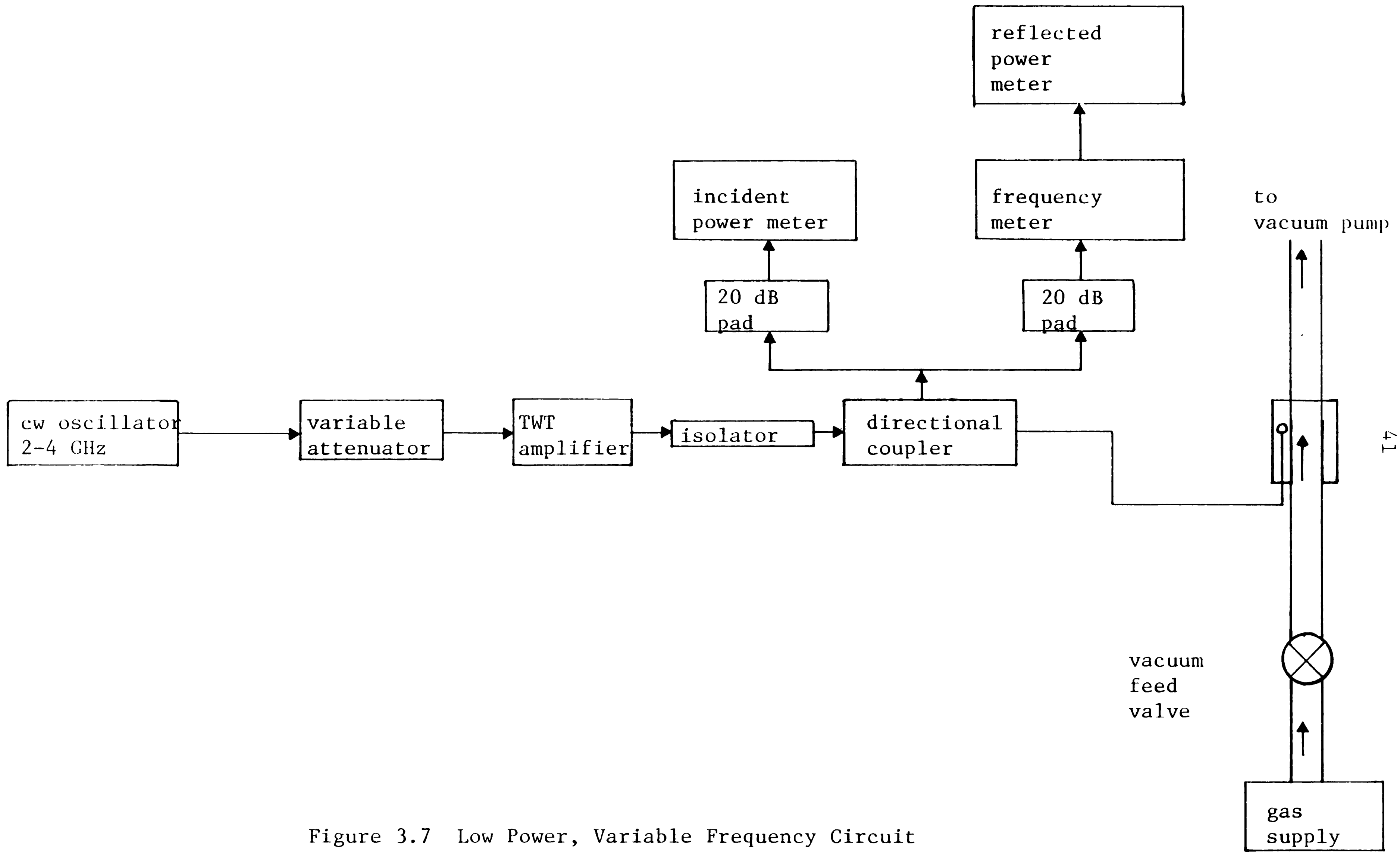

Figure 3.7 Low Power, Variable Frequency Circuit

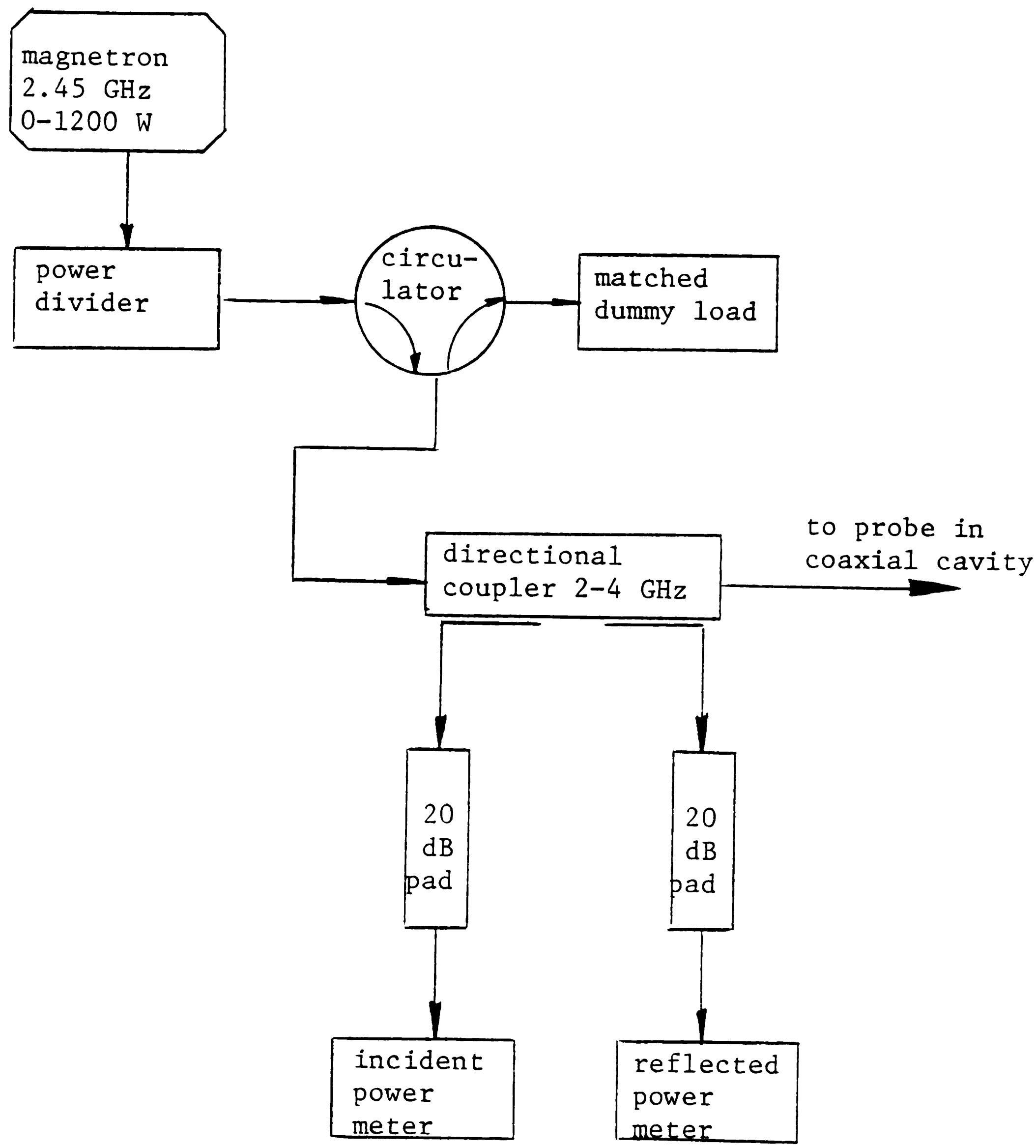

Figure 3.8 High Power Circuit for the Coaxial Cavity

divider. Power to the cavity was regulated by this power divider, equipped with two dummy loads, one of which was water cooled. A water cooled circulator isolates reflected power from the magnetron. The reflected power goes into a matched dummy load connected to the circulator. As in the previous circuits, this incident power passes through a directional coupler used to measure incident and reflected power, and into the cavity. This circuit allowed for variable input power of 0-1200 watts. In practice a maximum of only 50 watts was used, to minimize arcing inside the coaxial cavity to the microcoaxial coupling cable.

The schematic of Figure 3.9 is that used for the cylindrical cavity at high power, 0-1200 watts. Again, the 2.45 GHz magnetron is used with the power divider and 2-4 GHz circulator. The directional coupler is the waveguide type, with the same Hewlett-Packard power meters previously mentioned. From the directional coupler, power passes through a waveguide to coaxial transition to the coupling stub in the cylindrical cavity.

The next diagram, Figure 3.10, shows the circuit employed to excite the plasma with two coaxial cavities. The 2.45 GHz magnetron was used as the power source, but was limited to power inputs of 50 watts to each cavity. After the circulator, the circuit was symmetric for each cavity. Rf power was split by a coaxial "T" located at the output port of the circulator. Operating the cavities in this manner allowed them to be freely coupled to each other. The two coaxial cavities are nearly identical to the one shown in Figures 3.1 and 3.2, with only minor differences in the coupling loops.

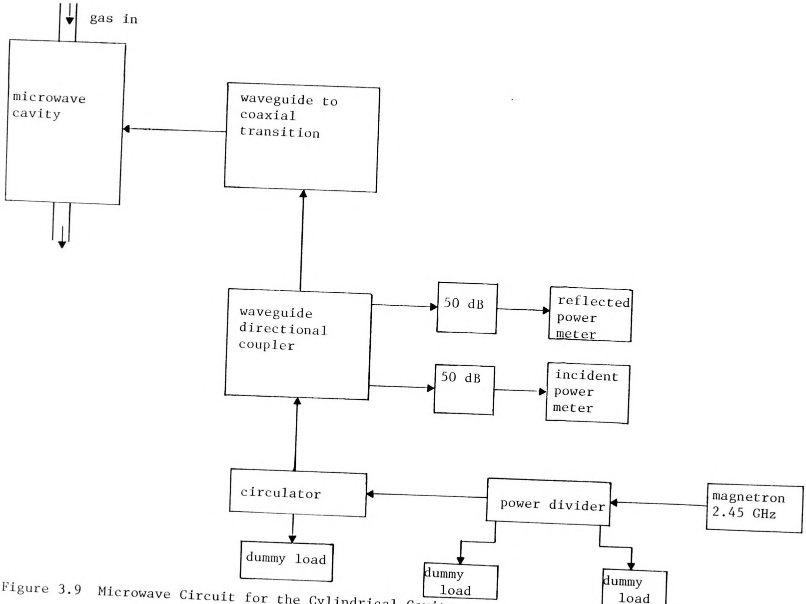

Figure 3.9 Microwave Circuit for the Cylindrical Cavity

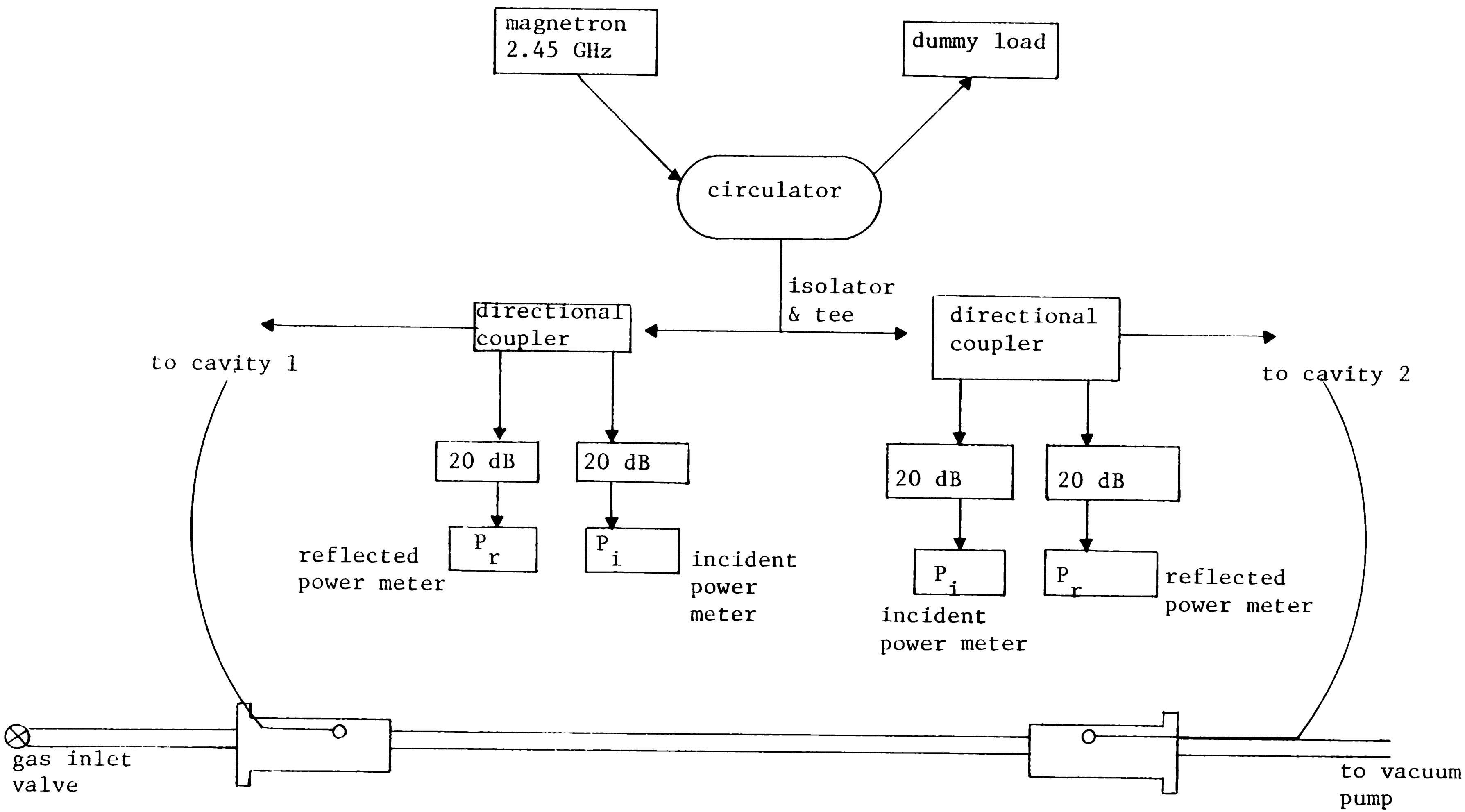

Figure 3.10 Two Cavity Circuit for Doubly-Excited Surface Wave Plasma

3.4 Vacuum Systems

In order to initiate breakdown in the experimental gases the pressure in the tubes containing the gases must be between approximately 50 to 200 microns. Discharges at pressures lower than 50 microns and higher than 200 microns can be maintained by retuning the cavities after breakdown.

Each experimental system was evacuated to 1-10 microns and leak checked before introducing the experimental gases. Leak rates were less than 15 microns per minute.

The vacuum system of the coaxial cavity was evacuated by a Speedivac High Vacuum pump. The source gas was from a tank of Ar, He, or O_2 or from a one or two liter bulb of research grade Ar, Xe, Kr or He-Ne.

A high quality needle valve controlled the pressure of the gas in the small quartz tubes, and Swagelock fittings were used at the joints whenever possible. Nylon tubing connected the quartz tube with other parts of the vacuum system. A Hastings thermocouple gauge was located approximately 2½ feet from the plasma tube. Next to the thermocouple was a mercury manometer followed by a shut-off valve to the pump. This valve was used to control the flow rate of the gas in the tube, on a relative scale only. The Hastings gauge was calibrated in microns of mercury from 0 to 1000. Calibration nomograms were provided by the manufacturer for various gases. Pressures of one torr or greater were read on the manometer. This system is shown in Figure 3.11.

The cylindrical cavity vacuum system, shown in Figure 3.12, was pumped by a high volume Kinney Compound mechanical pump, that could be isolated from the rest of the system by a large butterfly valve, providing a high flow rate or none at all. Pressures were read on a Hastings

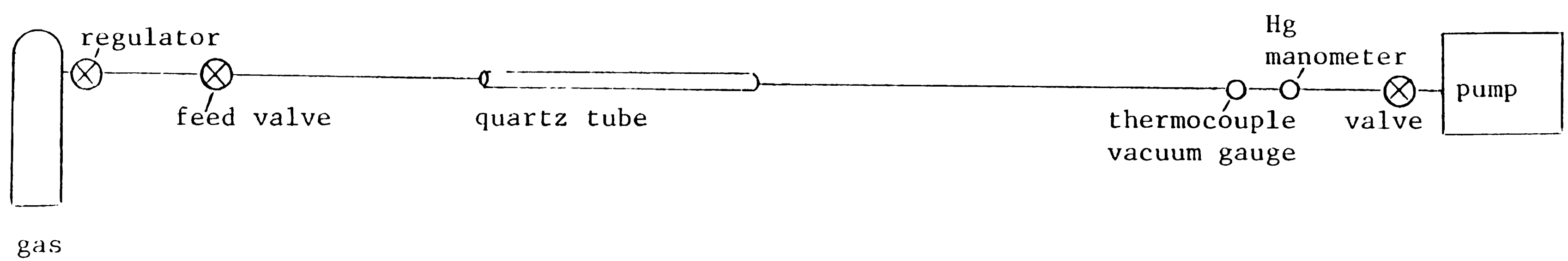

Figure 3.11 Vacuum System for the Coaxial Cavity

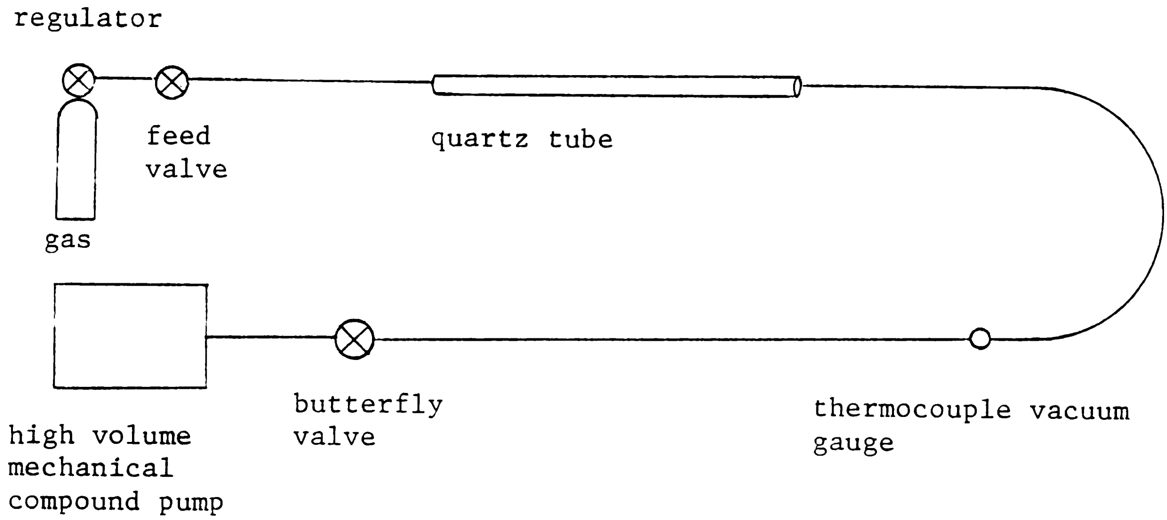

Figure 3.12 Vacuum System for the Cylindrical Cavity

thermocouple gauge located about six feet from the plasma tube (hot gases affected the gauge). This is the same gauge that was used in the coaxial cavity system. Gas pressure was controlled by a Whitey regulator valve. Connective tubing was nylon or copper, with Swagelock fittings. The quartz tubes were fitted with two inch aluminum collars (with O rings), which were attached to the tubes with Torr Seal.

3.5 Safety and Screening of Discharges

Due to the rf radiation hazards, protective screening was used for all experiments. This screening consisted of three basic types: (1) a small screen box or other type of enclosure, used with the coaxial cavities, (2) screening around only the plasma tubes, used with the large cylindrical cavity (another layer of screen was later added to this), and (3) a large screen box, used with a cylindrical cavity.

Figure 3.13 shows the type of enclosures used with the coaxial cavity. The screened box consisted of a 4" x 4" x 16" box with wood sides and square wood endpieces with large openings. Screening was stapled securely all over the box and holes were made in one end just large enough for the quartz tube, and in the other for the cavity. The end plate of the cavity and the coaxial rf input cable extended outside the screen box. The bottom edges of the wood frame were screened, but the bottom of the box was left open. The box was placed on two layers of screen stapled to a piece of plywood on the laboratory table. A flap was formed by the layer of screen on the top, forming a lid that could be stapled down. The staples could be easily removed and the flap lifted, allowing access to the cavity for adjustments. This type of screening is effective if the plasma does not extend outside the box.

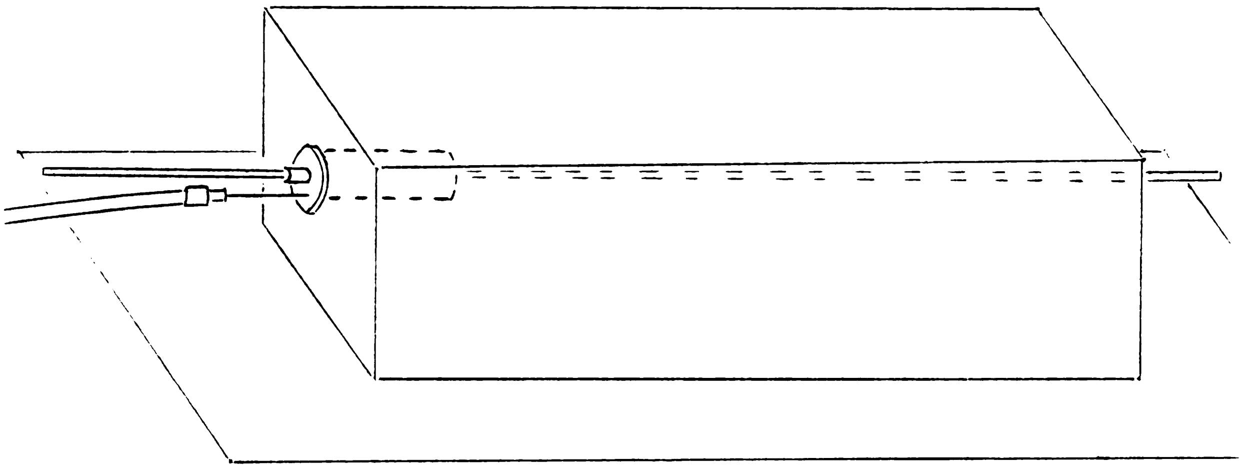

(a) Small Screened Box

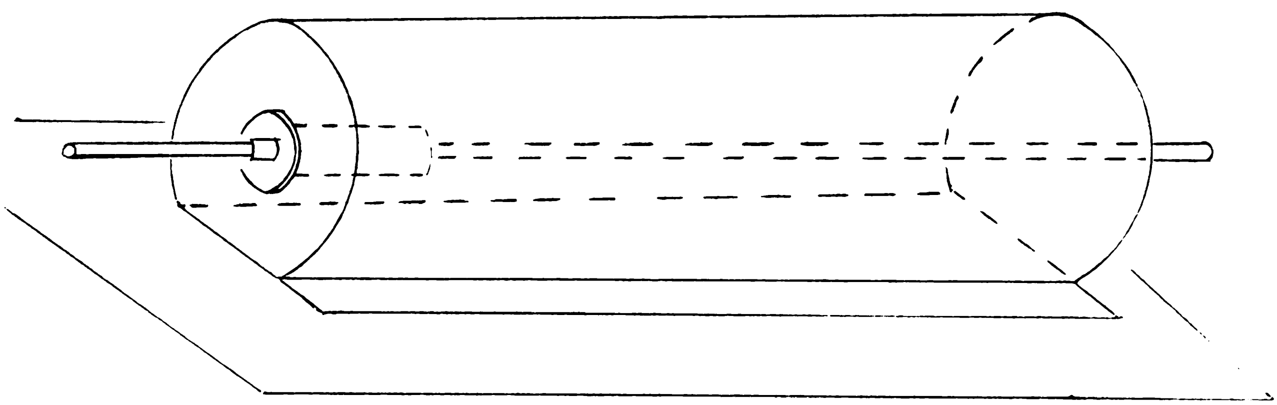

(b) Cylindrical Screen Enclosure

Figure 3.13 Screened Enclosures for the Coaxial Cavity

An alternative to the box (for the coaxial cavity) was a cylindrical enclosure. This is similar to the box but without the wood frame. A large piece of screen is rolled to form a cylinder about six inches in diameter. The longitudinal edges of the screen were stapled several inches apart to the layer of screen on the table. Cardboard was cut to fit the ends and covered with screen, including the edges. These were held in place by the screen cylinder. Again, holes were cut in the ends for the quartz tube and cavity. Another loosely fitting layer of screen was placed over the entire cylindrical enclosure, providing two layers of shielding.

For the larger cylindrical cavity effective shielding was provided by what could be considered local screening. See Figure 3.14. To allow access to the sliding short adjustment screw and the coupling probe, only the quartz tube was screened. On the end where the adjustment screw was located, a two inch cylinder was formed, one end was flared and held to the cavity by a circular plate with screws. The other end was secured to the collars on the end of the quartz tube by means of a large ring clamp, forming a cylindrical waveguide. The other end of the tube used a large cylinder of screen secured to the cavity perimeter by five or six ring clamps that had been opened and then screwed together to form one very large ring clamp. This cylinder tapered to a flat seam which was stapled for close fit around the aluminum collar on the end of the tube. This shielding was made more effective by surrounding the entire tube and cavity with another layer of screen that was open on the ends.

The other (and less effective) type of shielding for the cylindrical cavity was a large box, approximately $2\frac{1}{2}' \times 2\frac{1}{2}' \times 6'$. The frame was made

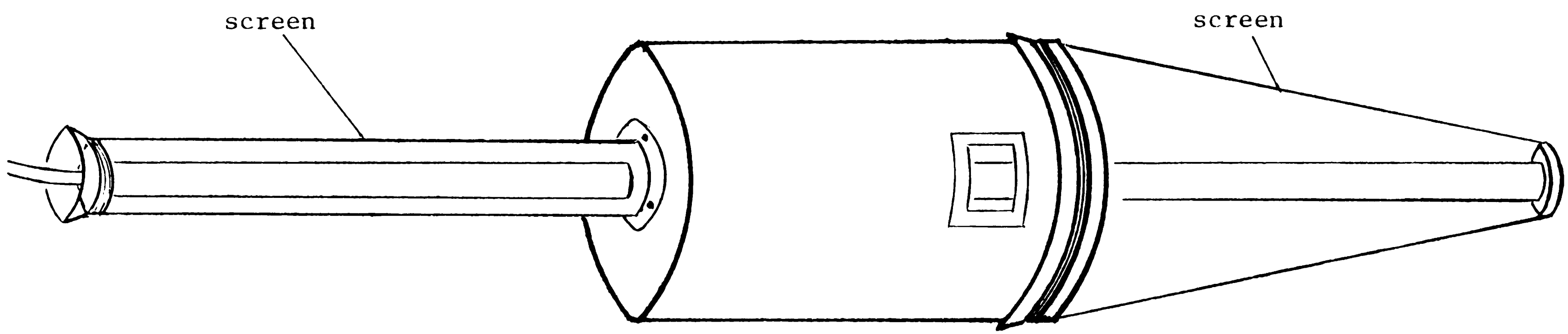

Figure 3.14 Locally Screened Tube in the Cylindrical Cavity

of wood and covered with screen. See Figure 3.15. The lid was hinged to allow access to the cavity and the sliding short was moved by a long rod to the cavity, with a handle outside the screen box. Holes were made in the sides of the box for coupling structures and vacuum tubing. Since energy is allowed to radiate from the microwave cavity and plasma tube, it was found that this type of box becomes a large microwave cavity, which can radiate from the openings in the ends and sides of the screened enclosure.

To prevent damage to the eyes from ultraviolet radiation from an Ar discharge, large sheets of plexiglas were placed on the top and sides of the screen box and plexiglas cylinders were used on the "locally" screened cavity. See Figure 3.16. Goggles were also available.

3.6 Measurement of Relative Electron Density and the RF Argon Spectrum

Although power absorption in the rf surface wave generated discharge was of primary concern, measurements were taken to determine the relative density of the plasma electrons in the coaxial system, using a photodiode, and to approximate the numerical density of the plasma electrons when standing waves could be observed in the tubes of the coaxial and cylindrical cavities.

Since the intensity of emitted light is related to the plasma electron density, relative measurements of the density could be obtained with a photodiode. (Absolute density measurements with a photodiode are possible only if the diode is calibrated for each gas and each pressure.)

The circuit that was used is shown in Figure 3.17. A nine volt radio battery was used to bias the diode, the microammeter measured the photocurrent and the switch was closed only long enough to take readings, so

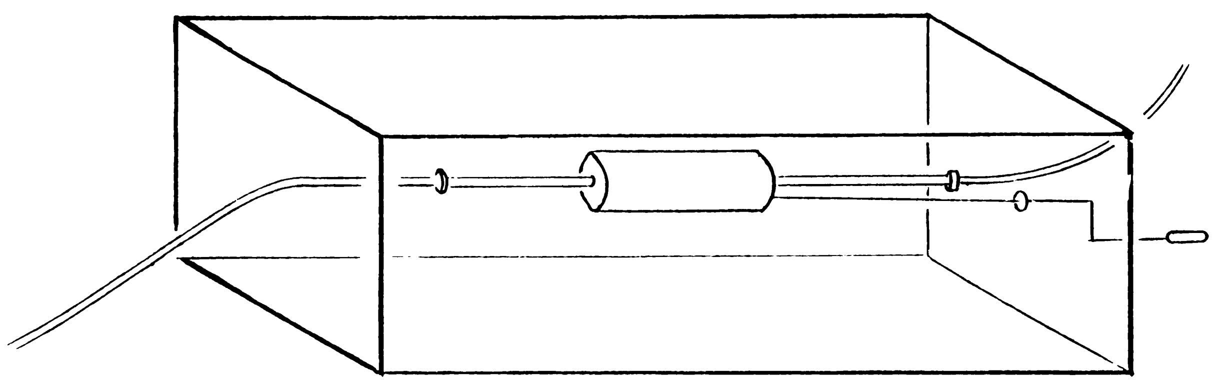

Figure 3.15 Screened Box for the Cylindrical Cavity

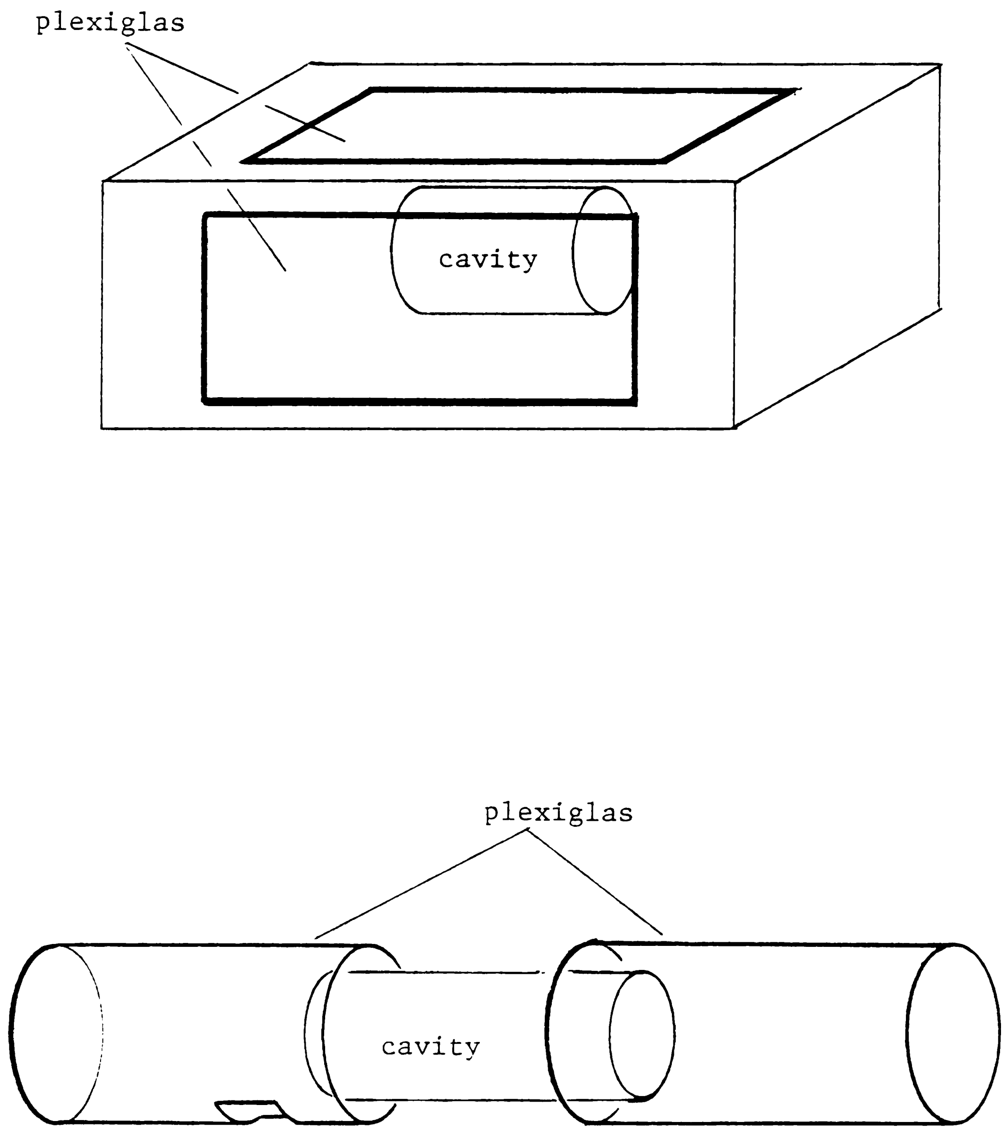

Figure 3.16 Plexiglas Shielding for the Cylindrical Cavity

as to have a minimal effect on the battery.

Figure 3.18 illustrates the location of the photodiode. When used with the coaxial cavity, it was placed adjacent to the end of the cavity and pointed at the center of the plasma tube. Current changes could be read as cavity parameters were changed. Optimum values of cavity parameters could then be determined by considering the power match, absorbed power per unit length of discharge, plasma length, or photocurrent. Alternatively, the photodiode could be moved along the plasma tube to determine the variation of plasma density as a function of position along the tube.

When used with the high power cylindrical cavity, the photodiode could be placed in a hole in the cavity wall near the center of the resonant cavity or located in a wooden block below the plasma tube. The first location provides a determination of relative density as cavity parameters are changed, and the second allows one to determine the variation of plasma density along the plasma column.

An important feature of this method of measurement is that it allows an accurate determination of the length of the standing waves in the plasma columns, by measuring the photocurrent as a function of position. Such standing waves were observed when the two coaxial cavities were used simultaneously, producing travelling waves in both directions along the tube, and in the cylindrical cavity, because the waves were reflected from the metal flanges on each end of the quartz tubes. This standing wave length, along with a plot of the Gould-Trivelpiece dispersion relation (normalized), determines an approximate numerical value for the plasma density at an position along the plasma column. This method was described in Section 2.5.

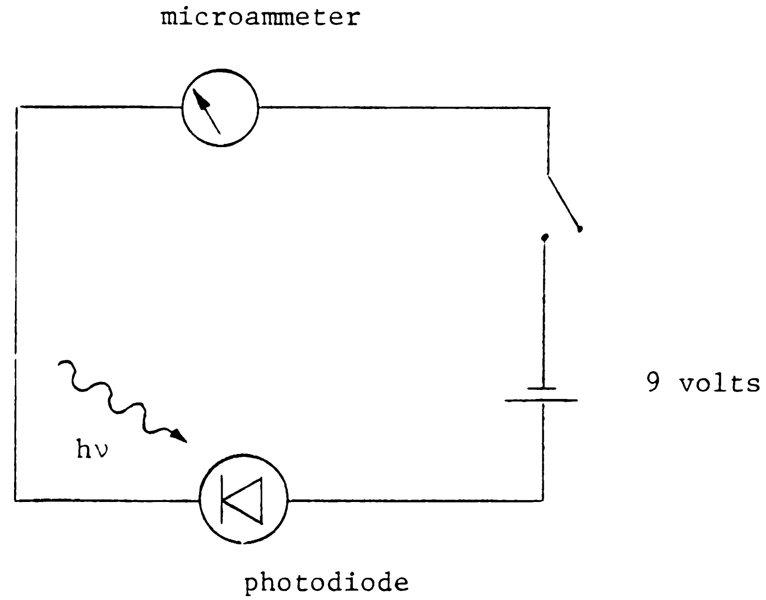

Figure 3.17 Photodiode Circuit

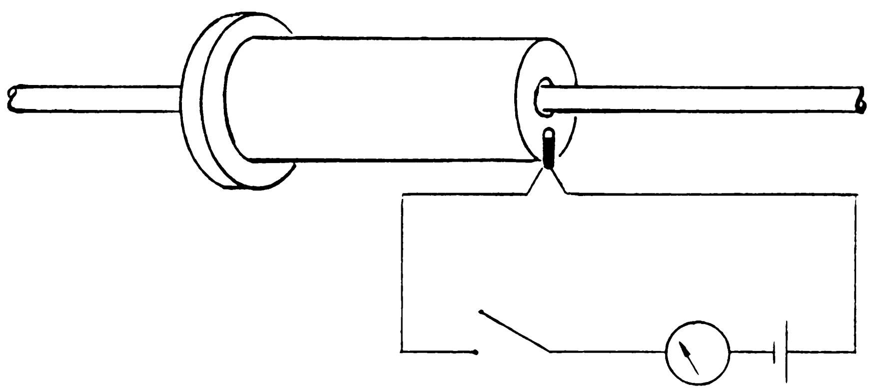

Figure 3.18 Location of Photodiode

A basic spectroscope (such as would be used in introductory physics courses) was used to determine the wave length of the optical radiation from the plasma. The experimental set-up is shown in Figure 3.19. A quartz tube was fitted with plexiglas windows on the ends. The collimator of the spectroscope was pointed along the axis of the plasma tube so that the discharge was viewed end on. The diffraction grating was calibrated with a He-Ne laser of wave length 6328 A. The grating had 600 lines/mm.

As the absorbed power in the plasma was increased, some of the lines of the spectrum increased in intensity. At low powers (up to approximately 500 watts), the discharge was typically pink, becoming blue as the absorbed power increased (to about 1000 watts). This information is useful in determining if certain transitions are present in the discharge. Results from this experiment are discussed and tabulated in Chapter 4.

3.7 General Techniques and Experimental Methods and Comments

Most investigators will agree that a given system will behave differently at different times and/or with different operators. Attempts were constantly made during this investigation to eliminate or minimize inconsistencies, so that all observed behaviors would be reproducible. Various simple techniques and methods that were developed for this purpose will be described in this section.

As stated previously, the coaxial cavity used was a modification of one used earlier by Fredericks and Asmussen. The modifications consisted primarily of tuning screws and finger stock in the cavity. The tuning screws allowed cavity geometries to be easily reproduced during a given experiment or even some time later. Previous to the addition of the screws (which were not on the first design of this cavity), measurements were

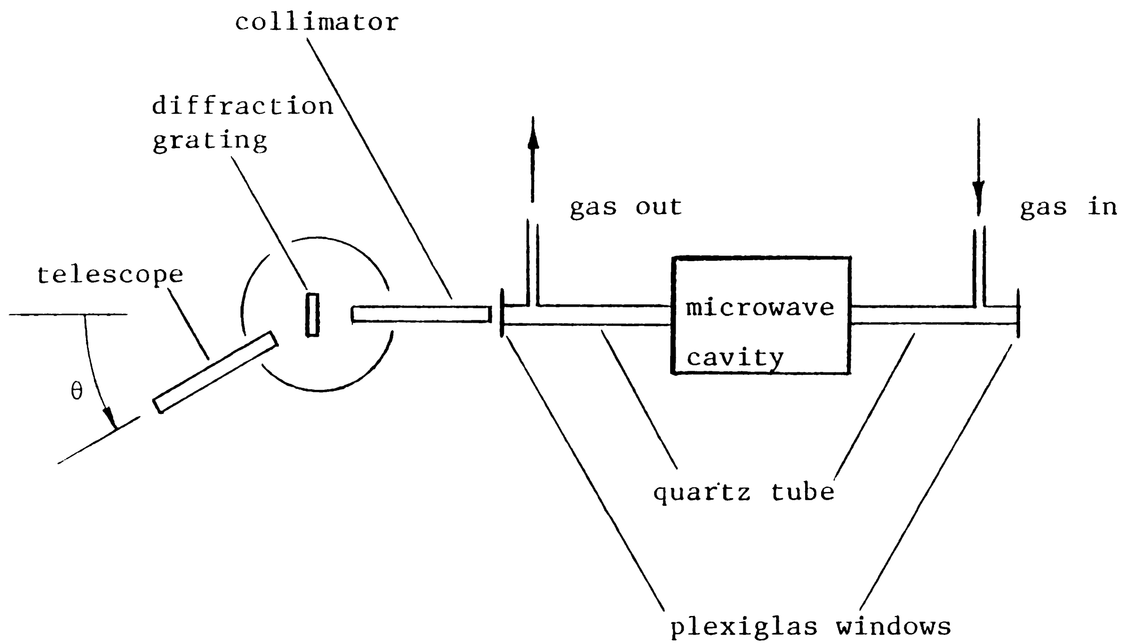

Figure 3.19 Experimental Arrangement for Determining the Wave Length of an RF Ar Discharge

difficult to duplicate due to the sharpness of some of the observed resonances. The tuning screws allowed controlled fine tuning of the cavity.

For a given geometry of the coaxial cavity the discharge and coupling were most sensitive to the position and orientation of the probe. Small axial adjustments of the probe could produce very significant changes in the discharge.

At incident powers of 25 watts or greater, arcing was sometimes observed between the side of the loop and the center conductor, when the magnetic moment of the loop was circumferential, i.e., the plane of the coupling loop was radial. This problem was eliminated by rotating the loop so that its magnetic moment was radial. Arcing to a lesser degree was observed from the loop to the inside of the end plate of the cavity. This was not affected by placing a thin sheet of mica on the end plate. Either the incident power was decreased or the loop was moved away from the end plate. Generally, for incident power less than 30 watts, there was no arcing to the end plate.

Gap length (from the center conductor to the end plate) had significant effects on the discharge and coupling. A 1½ to 2 mm gap appeared to be optimum for most frequencies, though some adjustment was necessary. The center conductor had viewing holes that could be aligned with similar holes in the side of the cavity. For this reason, the center conductor was usually placed at fixed positions, basically rotations of 180°, unless the plasma extended outside the cavity. Discharges could be sustained for longer gaps, if the probe was moved further from the end plate, though coupling was not as good as for short gaps. Two or three mm gaps resulted in power matches of 50 to 70% as compared to generally 80 to 90% for shorter gaps. In addition, the discharges were usually about 20% shorter when experiments were done with longer gaps.

The resonance curve for the cavity length (determined by the position of the sliding short) was not as sharp as resonance curves for the probe and gap, though optimum values were clearly distinguishable. The cavity lengths were generally 1/8 to 1/4 of the free space wave length of the source. For example, a cavity length of approximately 2.1 cm was used for 2.45 GHz. One fourth of the free space wave length is 3.06 cm.

To maintain optimum surface wave coupling, a change in one cavity parameter necessitated a change in the other two. Lengthening the cavity meant that the gap had to be increased and the probe moved away from the end plate. Changing the probe (or gap) implied similar changes in the length (or probe).

For most of the investigations done with the coaxial cavity, at incident powers of about 20 watts, a Tesla coil was needed to initiate breakdown of the gas. A spark anywhere along the two foot quartz tube was sufficient, when the cavity geometry was adjusted properly. If the cavity geometry was not adjusted properly, stable discharges could not be sustained. The Tesla coil was not needed with the cylindrical cavity, since a number of cavity modes overlapped for a given cavity length.

Breakdown occurred for a narrow range of pressures (depending on the gas)--50 to 200 microns. After breakdown, gas pressure could be varied and the cavity tuned to sustain discharges over pressures ranging from about 20 microns to 20 or 30 torr, or greater.

When the coaxial cavity was operated with incident power levels of 50 watts or greater, arcing occurred between the coupling probe and cavity walls or inner conductor. Generally the cavity would get warm to the touch, and the quartz tubes were hot after 15 to 20 minutes with Ar and similar gases, and after only 5 to 10 minutes of operation with He or O_2. When the power levels approached 100 watts, as it did on two or three occasions, the solder holding the coupling probe melted slowly, allowing the probe to disorient itself. The effect was not immediately obvious but became evident after several attempts to reproduce previous results of the same day. During one experiment, 200 watts was incident on the cavity, which caused the solder of the probe to melt, and also resulted in a split in the outer conductor of the microcoaxial cable used for the coupling loop.

One interesting feature of the coaxial cavity was the difference in the nature of the discharge when the type of power source was changed. With a continuous wave oscillator at a frequency of 2.45 GHz, discharges could be sustained over large pressure ranges, but always needed to be initiated with a Tesla coil. With the magnetron as source (square wave output at 2.45 GHz), the sustaining pressure range was narrower, but the plasmas were longer for a given absorbed power and usually were self-starting.

Rectangular loops were also tried as coupling probes. These had a tendency to arc from the corners and the surface wave coupling was not as good as when circular loops were used.

There is a reasonable probability that the length of the microcoaxial cable between the N-type connector and the loop affected the nature of the coupling, however, this was not investigated.

The cylindrical cavity could be operated with an incident power of 0-1200 watts. This was limited by the magnetron that was used. The S-band waveguide directional couplers were calibrated in previous experiments such that the actual power levels were 1.3 times those read from the power meters. Maximum incident power obtained was 900 watts as read from the power meter, indicating 1170 watts available from the magnetron.

The following simple procedure was adopted when tuning the cylindrical cavity: probe position was determined--this was relatively arbitrary since many different positions resulted in long discharges for the cylindrical cavity, gauge gas pressure was fixed to approximately 150 microns, cavity length adjusted for minimum power reflection. By this time a discharge was usually present. The tube was adjusted for minimum power reflection and cavity length was readjusted as pressures were changed. The whole starting procedure required less than two minutes. After the discharge was present, retuning of the cavity was obtained in 5 to 10 seconds as pressures were changed.

The Tesla coil was not needed with the cylindrical cavity. When the cavity length was properly adjusted and gas pressure was about 150 microns, the plasma was self-starting. Once the plasma was initiated, the cavity length, plasma pressure and tube position could all be adjusted for optimum coupling, usually resulting in a power match (the ratio of absorbed power to incident power) of 90 to 98%. Changing the cavity length or tube position generally resulted in a significant change in the power match and in the plasma length.

While cavity length, probe position and gas pressure could all be varied in a controlled and reproducible manner, the effect of the position of the quartz tube within the cavity was a poorly understood, though very significant, factor when coupling to the surface wave plasmas. With the tube centered in the cavity by using snugly fitting collars, the power match was generally so poor that the reflected power on the meters was greater than the incident power. Moving one end of the tube up to 10^{o} off the cavity axis could result in a 90 to 95% power match.

Arcing similar to that of the coaxial cavity was observed at high power levels (400 watts or greater on the power meters) when: (1) the fingerstock of the sliding short was not tight against the inside wall of the cavity, (2) when collars to support the quartz tube were not seated tightly in the cavity, (3) when the screening around the quartz tube was not completely sealed, and (4) if the finger stock of the sliding short approached the probe, 5 mm or less, during the tuning of the cavity. In addition to this, the sliding was short was water cooled by ¼ inch copper tubes soldered to its bottom. These tubes passed through holes in the bottom of the cavity and arcing occurred at these points.

Fortunately, all of these problems had remedies: (1) the fingerstock could be bent by hand to fit the cavity wall more tightly, (2) holes were tapped in the end plates of the cavity so that the collars could be held in place with screws, (3) screening around the tube was clamped to the end flanges of the tube or stapled shut (the staples provided a good seal that could be easily removed for repairs and modifications), and (4) the cavity was operated at a length that kept the probe 4 or 5 cm from the fingerstock. Arcing around the water cooling tubes was prevented by sliding a flat washer around the tube to the outside of the end plate of the cavity, and holding it there with a spring around the tube.

Very often, the plasma was not symmetric with respect to the cavity. The screens around the tube were unequal in length, causing one end of the tube to extend further from the cavity than the other end. The "short" end of the tube would fill with plasma before the other end. As input power increased, the intensity of the discharge in the short end of the tube increased, while the discharge in the long end would lengthen to fill the tube and then become brighter.

The dual cavity system presented a cavity coupling problem. Initially, this system was operated with the two cavities isolated from each other and from the rest of the circuit by an isolator and a circulator. The cavities coupled to each other by means of the surface waves propagating along the quartz tube. An increase in the coupling efficiency of one led to a decrease in the coupling efficiency of the other. As the plasma in one lengthened, the other shortened. In fact, when the cavities were 15 to 20 cm apart, a gap of approximately 2 mm consistently separated the discharges of the cavities (so that there were two) and moved back and forth as the cavities were adjusted. Thus the cavities could not be uncoupled.

Later, the cavities were allowed to couple freely to each other, but isolated from the rest of the circuit. This is the schematic shown in Figure 3.10. The cavities were operated at an incident power of up to 40 watts each, from the magnetron. They could be adjusted to give symmetric discharges in terms of coupling and plasma length. A small gap existed between the discharges at an incident power of about 20 watts or less. This was overcome when the incident power was increased, though the point where the discharges joined was slightly dimmer than the rest of the plasma. In general, this discharge had to be started with a Tesla coil. A standing wave pattern in the intensity of the discharge was observed.

The microwave circuits presented no problems, provided the cable connections were tight. Loose connections resulted in losses that could not be corrected by cavity coupling. Thus the connections were checked occasionally, particularly when incident power could not be coupled into the plasma more efficiently than 60%. Cable connections apply only to the coaxial cavity, as the cylindrical cavity circuit consisted of waveguides. The waveguide joints were checked for microwave radiation leaks, with a waveguide to coaxial transition connected to a power meter. Though uncalibrated, this technique of radiation monitoring proved effective since the coupler functioned as a receiving aperture and the power meter could be set to very sensitive scales. This "detector" was used as a leak detector to determine if various parts of the system were radiating. It was also placed between the cavity and operator during experiments and used as a continuous monitor. Though the actual calibration of this type of detector may be open to question, it was found by direct comparison with a commercial rf leak detector to be more sensitive to low levels of radiation. It cannot, however, pinpoint an rf leak as well as the commercial detector.

Whenever possible, Swagelock fittings were used on all vacuum tubes and pipes. New fittings are preferable to used ones which may become bent or stretched with much use. The small quartz tubes used in the coaxial cavity were fitted with rubber O rings and Swagelock fittings, without the ferrule. The quartz tubes that were used with the cylindrical cavity were fitted with two inch aluminum flanges and sealed with Torr Seal. These flanges were grooved for an O ring and butt jointed with another flange leading to tubes with Swagelock fittings.

The most straightforward method of dealing with vacuum systems is to assemble the system one section at a time, with the gauges included, and check leak rates. When the first section is determined to be as leak tight as desired, another section is added to the existing one and checked. The total system is then built a piece at a time and leaks have been found and sealed before the system is completely assembled. In the leak checking, time must be allowed for outgasing of the system before isolating the system from the pump.

Hysteresis in the measurement of absorbed power per unit length of discharge was observed in nearly all of the experiments in which gas pressure was varied. Starting at low pressures and working up gave different results than starting at high pressures and working down. Such effects were reported by Fredericks and Asmussen (10). In one experiment, the pressure cycle from several torr to a few tens of microns was completed several times, without once getting the same P/L for the same pressure but at different times.

In conclusion, experience shows that tuning capability of cavity length, probe position, gas pressure and tube position within the cavity are necessary to couple energy efficiently into the surface wave discharge. All joints and screens for rf shielding must be tightly secured to prevent arcing and radiation leaks. Each system has power limitations which are not obvious without some testing and subsequent repair, if the limits are to be found. Problems with vacuum systems can be minimized by assembling and the checking the system one piece at a time.

CHAPTER IV

EXPERIMENTAL RESULTS

4.1 Introduction

This chapter will present a summary of the results of over 150 experiments, performed with the coaxial and cylindrical cavities, over a period of about 1¼ year. Each of the experiments performed with the coaxial cavity typically included 10 to 15 data readings, while those with the cylindrical cavity included 6 to 10 readings.

The primary measurement with both rf surface wave excited plasma sources was the absorbed rf power per unit length of discharge. This ratio is labeled as P_a/L_p, or simply P/L, where P_a refers to the absorbed power, which is determined as the difference between incident and reflected rf powers, measured by power meters, and L_p is the length of the plasma, measured with a 30 cm rule or a meter stick.

During early experiments with the coaxial cavity, important plasma-cavity system parameters were identified; they were (1) gas pressure, (2) absorbed power, (3) tube or plasma diameter, (4) excitation frequency and source type, (5) gas type, and (6) coupling and cavity geometry. In most cases, these parameters are interrelated. Thus, experiments were devised to isolate each variable from the others to a significant degree.

Though the procedures followed to obtain these experimental results will be discussed in the appropriate sections, some general comments are in order at this point. For the coaxial cavity, the neutral gas pressure was initially set at approximately 100 to 150 microns before applying power to the cavity-plasma system. Coupling geometry was adjusted and the discharge started with the spark from a Tesla coil. In some cases, the discharge started without the Tesla coil. The gap length, cavity length and coupling probe were then adjusted to yield a minimum reflected power for an rf input power of 15 watts or greater. Small changes in coupling probe position were made to lengthen the discharge if the reflected power showed only a small increase. The experimental variable being studied would then be changed as readings were taken, without further adjustment of any other parameters, except in some cases, immeasurably fine tuning of the coupling probe. Light intensity measurements were taken with the photodiode as close to the end of the cavity as possible. See Section 3.6 and Section 4.7.

For the cylindrical cavity, results to be presented are P/L as a function of (1) gas pressure, (2) absorbed power, (3) tube or plasma diameter, and (4) gas type. Standing wave patterns could be observed in the discharge so that the method discussed in Chapter 2 was used to estimate the plasma electron density. Finally, optical wavelengths of the "bright" lines in the spectrum of an Ar discharge were experimentally determined and will be discussed.

In general, the experimental procedures used with the cylindrical cavity were similar to those used with the coaxial cavity. The simpler nature of the cylindrical cavity allowed quick retuning of the cavity-plasma system before each reading was taken. The objective of the tuning was to minimize reflected power from the system. If a change in the variable to be investigated produced a significant change in the reflected power--such as from 10 to 20 watts, the length of the cavity was retuned.

This adjustment was generally less than ½ mm. Breakdown of the discharge in the cylindrical cavity was spontaneous when the cavity was tuned to an eigenlength. Maximum length of the discharge with minimal reflected power was then achieved by retuning the cavity. Initial pressures for breakdown were 100 to 200 microns for 200 watts of rf input power. After breakdown the system was adjusted to the desired experimental conditions.

The chapter will be concluded with the results obtained from a system using two coaxial cavities, i.e., a doubly excited surface wave plasma. In some cases, two separate discharges were observed, while in others one discharge coupled the two cavities and standing wave patterns were observed. A calculation of the approximate plasma electron density will be presented, based on the observed standing wave patterns.

Each of the following sections will be organized in the following manner: (1) discussion of the motivation for the experiments or type of experiments, (2) a statement of the experimental problem, (3) the important physical parameters in the experiments and the procedure that was followed to obtain the data, (4) presentation of the results in the form of graphs and tables, and (5) conclusions that can be drawn from the analysis of the results.

4.2 P/L vs. Pressure: Coaxial Cavity

When these experiments were begun it was immediately obvious that gas pressure affected the length of the surface wave generated plasmas. In particular, the plasma length is strongly dependent on pressure, when other parameters are held constant. Incident and reflected powers are also affected by changes in pressure and these, in turn, affect the absorbed power. The pressure dependence of the surface wave generated plasma was studied by measuring the absorbed rf power per unit length of plasma, which is designated as P/L.

Many experiments were performed with a number of tubes of different diameters to determine the dependence of P/L on gas pressure. For the purposes of reference only those performed in a 4 mm quartz tube, excited at a frequency of 2.45 GHz (from the magnetron), will be discussed. An exception to this is the experiment with O_2, which was performed in a 2 mm tube. Besides pressure, the absorbed power, cavity length, gap length and probe position all affect the length of the discharge and hence the ratio P/L. Thus these quantities will be marked on the graphs, since they were not all the same for each experiment.

The procedure for breakdown of the discharge was to adjust the cavity length to between 2 and 3 cm (roughly ¼ of the free space wave length of the excitation source). The gap was set to 1 or 2 mm. After pumping the tube to several microns to outgas, gas was bled into the discharge tube to a pressure of several hundred microns, and power was applied to the plasma-cavity system. A Tesla coil was placed near the discharge tube close to the cavity and allowed to arc to the tube while the cavity length, gap and probe were adjusted by trial and error until a discharge was obtained. The Tesla coil was removed and cavity parameters were adjusted until a discharge 5 cm or longer was obtained. When this occurred, reflected power was usually of the order of several watts, while the incident power was 15 to 20 watts. Initial experiments were performed simply to obtain a reproducible discharge and eventually to optimize it in terms of length and reflected power. Experience with the system allowed this start-up procedure to be reduced to several minutes.

The experimental procedure to determine the variation of P/L with gas pressure was to simply vary the pressure of the gas discharge in the tube, without changing the other parameters of the cavity. In all of the experiments, the absorbed power remained nearly constant. In a few instances, very high or very low pressures caused a mismatch of the system to the power source. If the discharge was retuned this match could be recovered and the surface wave could be sustained over a wider pressure range. Retuning consisted primarily of a slight adjustment of the coupling probe. The results obtained from this procedure are shown in Figures 4.1 through 4.5.

Figure 4.1 is the P/L vs. pressure curve for Ar. The points shown constitute two separate experiments. The same cavity length was used in both, thus the variations between the two are small. An interesting feature of the curve is that the power match (P_a/P_i) is nearly constant over the wide pressure range of 200 microns to 3 or 4 torr. Even beyond this range, P/L is relatively constant between .3 and .4 W/cm. In general, the observed values of P/L range from .25 to .5 W/cm for an absorbed power of 15 to 20 watts.

Figure 4.2 is the same curve for Kr. Power match is 10 to 15% lower than for Ar, but relatively constant at about 60%. The P/L is also lower than for Ar, between .2 and .3 W/cm and roughly constant over the entire pressure range. Kr and Xe (to be discussed next) presented some problem in the determination of the actual pressure of the gas. In both cases, the corrected values as indicated on the nomograms provided by the manufacturer of the thermocouple vacuum gauge were very much lower than readings taken at the same time from a Hg manometer in the vacuum system. This explains the lack of data points in the region from 350 microns to 4 torr. Gauge readings for these pressures were higher than the values

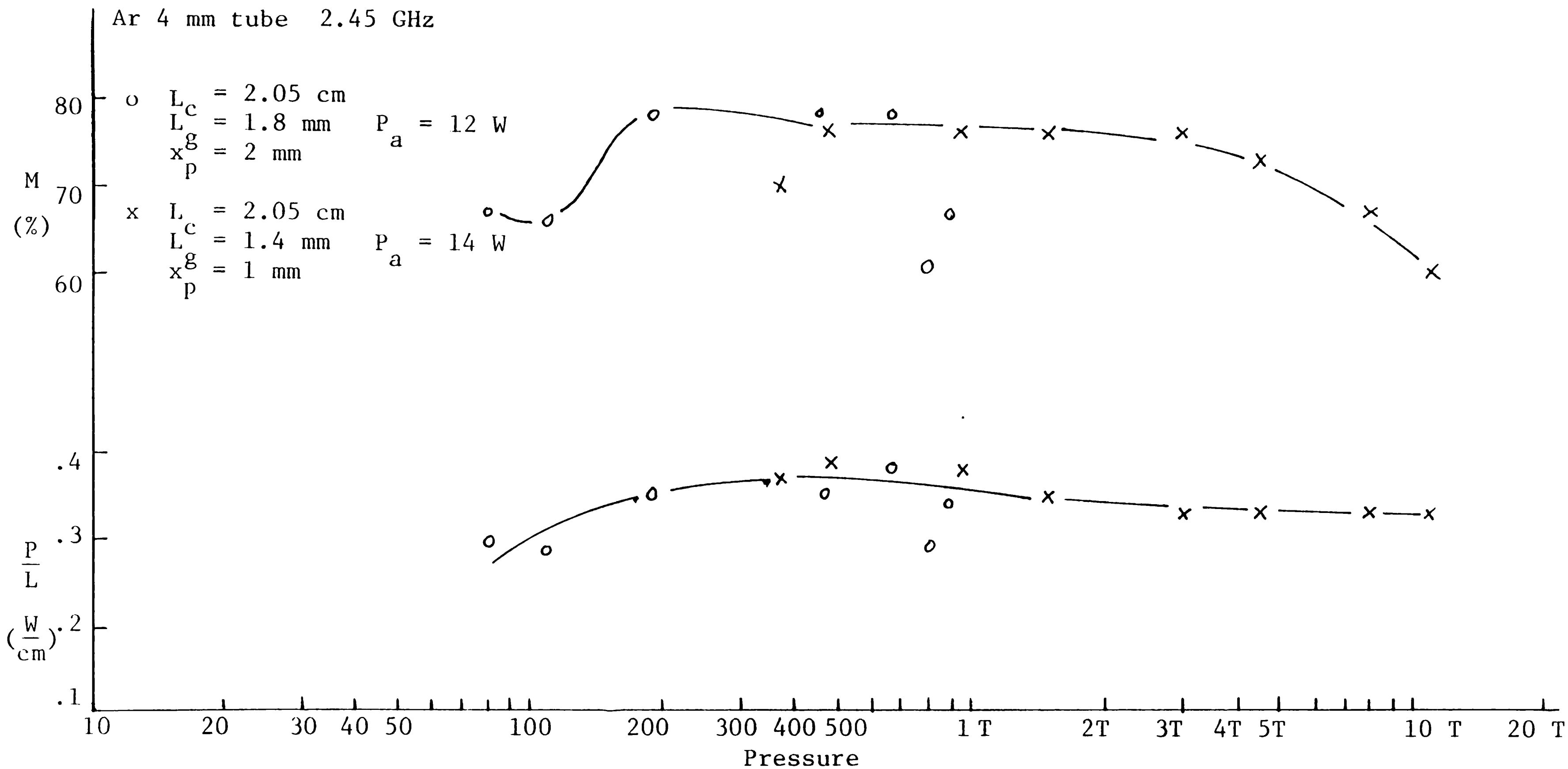

Figure 4.1 P/L vs. Pressure for Ar in the Coaxial Cavity

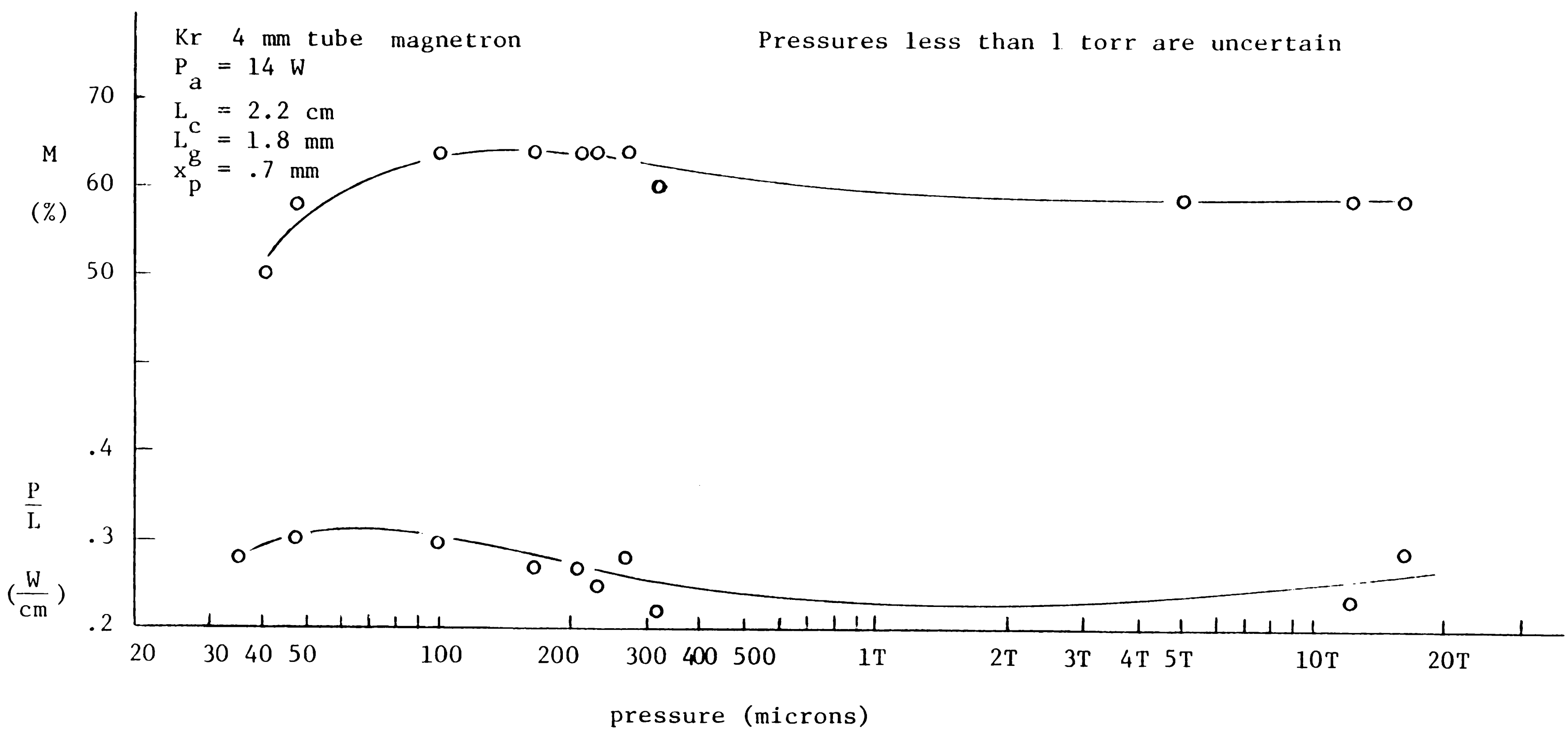

Figure 4.2 P/L vs. Pressure for Kr in the Coaxial Cavity

shown on the graphs, which are values determined from the pressure nomograms. Pressures at 5 torr and above were read directly from the manometer. The lower nomogram readings, 100 microns or less, are probably close to the actual value of the pressure (which is unknown). It should be noted that the points from 200 to 400 microns (actual pressure) should lie somewhere between 200 microns and probably 4 torr. Despite this problem, it is obvious that the power match and P/L remain roughly constant over the wide pressure range shown.

P/L vs. pressure for Xe is shown in Figure 4.3. Pressure determination was again a problem, but not as significant, since pressures from .5 torr or greater were read from the manometer. Though the power match shows only a slight decrease as the pressure rises over 2 torr, note that it is much lower than for the other gases--40% as compared to 60 and 75%. The value of P/L is also lower, around .2 W/cm, but this may be somewhat misleading. A low value of P/L is due to production of a long plasma with a small amount of absorbed power. However, the small value of absorbed power may be, as in this case, due to a mismatch of the plasma-cavity system. Incident power may be high, but so is the reflected power as shown on the power meters, resulting in a low value of P/L. One might also argue that with very little power absorbed by the gas, the plasma produced would not be as long as the case when a great deal of power is absorbed. This is not always the case, because a small adjustment of the coupling probe or cavity gap could be made to produce a mismatch of the system, but the plasma length did not always decrease in proportion to the rise in reflected power. This is the reason the plasma-cavity system was usually tuned to produce the best possible power match, while maximizing the plasma length was the second priority.

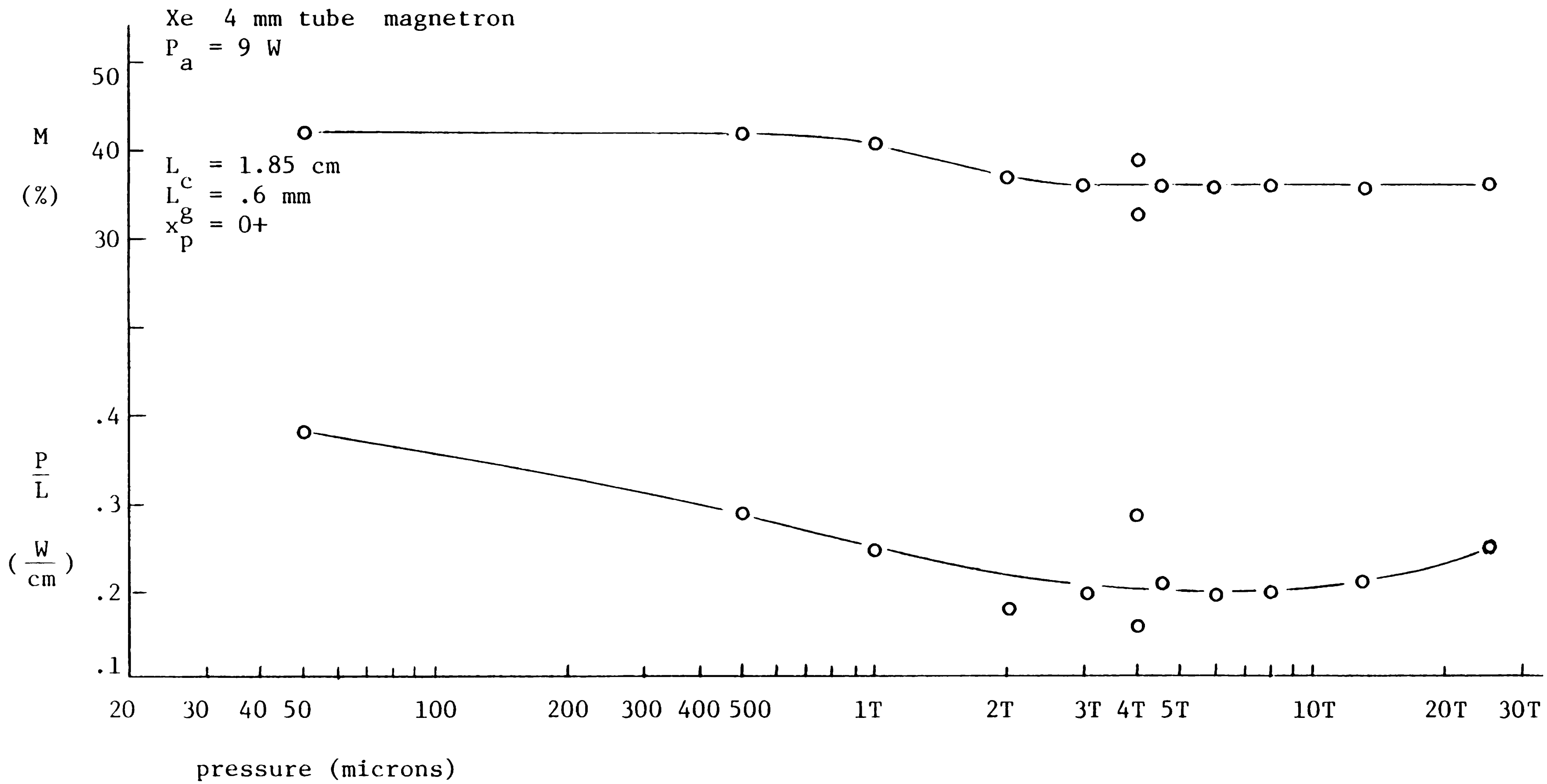

Figure 4.3 P/L vs. Pressure for Xe in the Coaxial Cavity

Variation of He power match with pressure, Figure 4.4, shows that a larger fraction of the incident power was coupled into the plasma-cavity system, and remained relatively constant over the pressure range shown. The lowest pressures shown are not as low as some of those for the other gases, because a He discharge could not be sustained at lower pressures, for the indicated absorbed power. (Discharges could be sustained over a greater pressure range at higher absorbed powers.) P/L remains between 2 and 3 W/cm for pressures up to 1 torr, and rises steadily to 6.7 W/cm at 11 torr.

The behavior of O_2 power match and P/L with pressure is shown in Figure 4.5. As with He a high power match was achieved, about 85%. It remains relatively constant over the pressure range shown--from 35 microns to 900 microns. At this point the discharge was extinguished. P/L for O_2 rises more rapidly with pressure than for He, and is not constant over any pressure regime.

For all of the gases studied, one can see that the power match is nearly constant over pressures ranging from roughly 50 microns up to 10 torr, depending on the gas. For the heavier inert gases--Ar, Kr, and Xe, P/L is nearly constant over most of the pressure range for which a discharge can be sustained without retuning; He and O_2 show an exponential rise with pressure.

4.3 P/L vs. P_a: Coaxial Cavity

One of the most desirable features of any experimental system is that results should be reproducible. The experiments just described presented problems in this aspect until it was realized that very often, incident or absorbed rf power levels were varied slightly, and unintentionally,

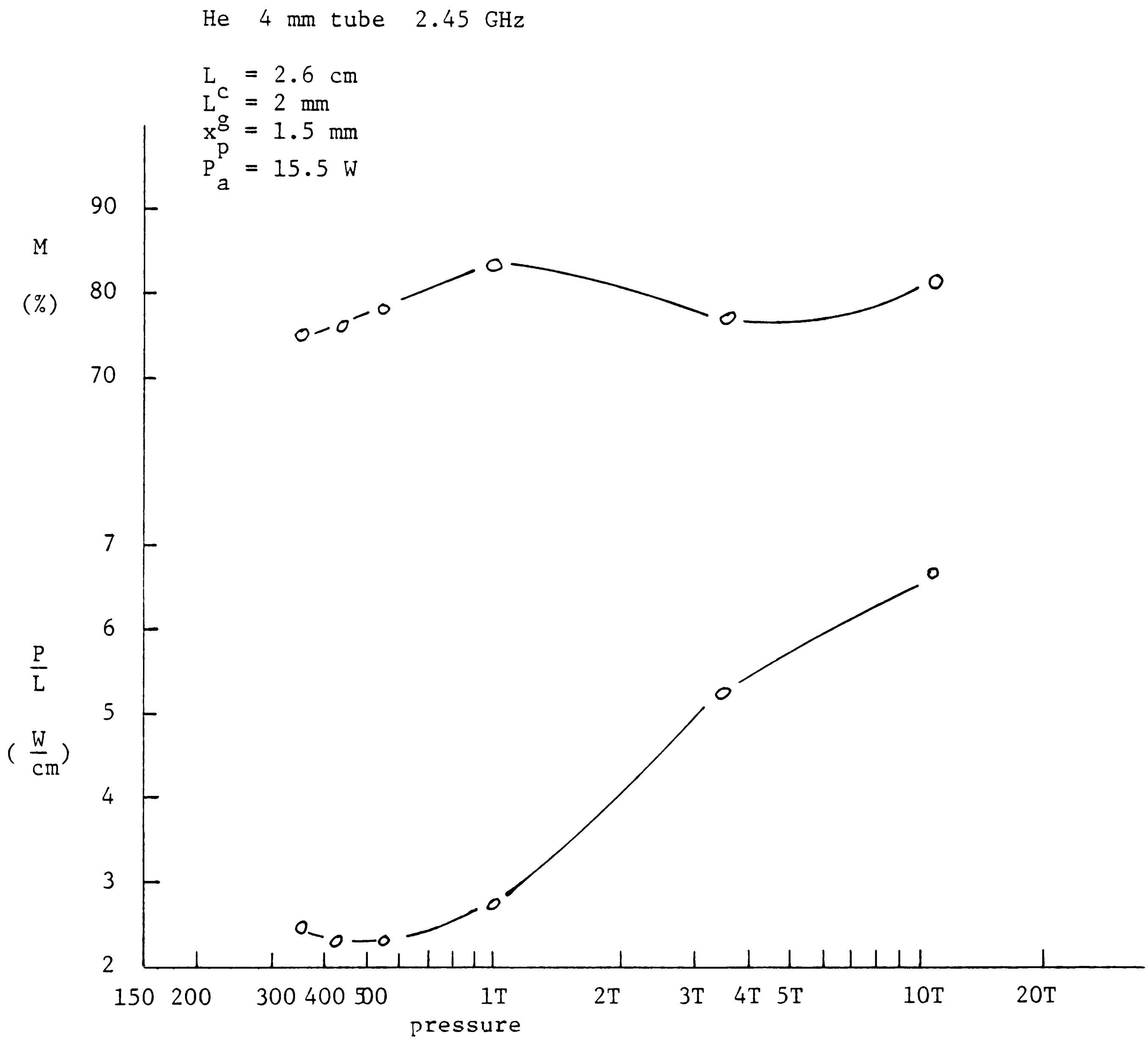

Figure 4.4 P/L vs. Pressure for He in the Coaxial Cavity

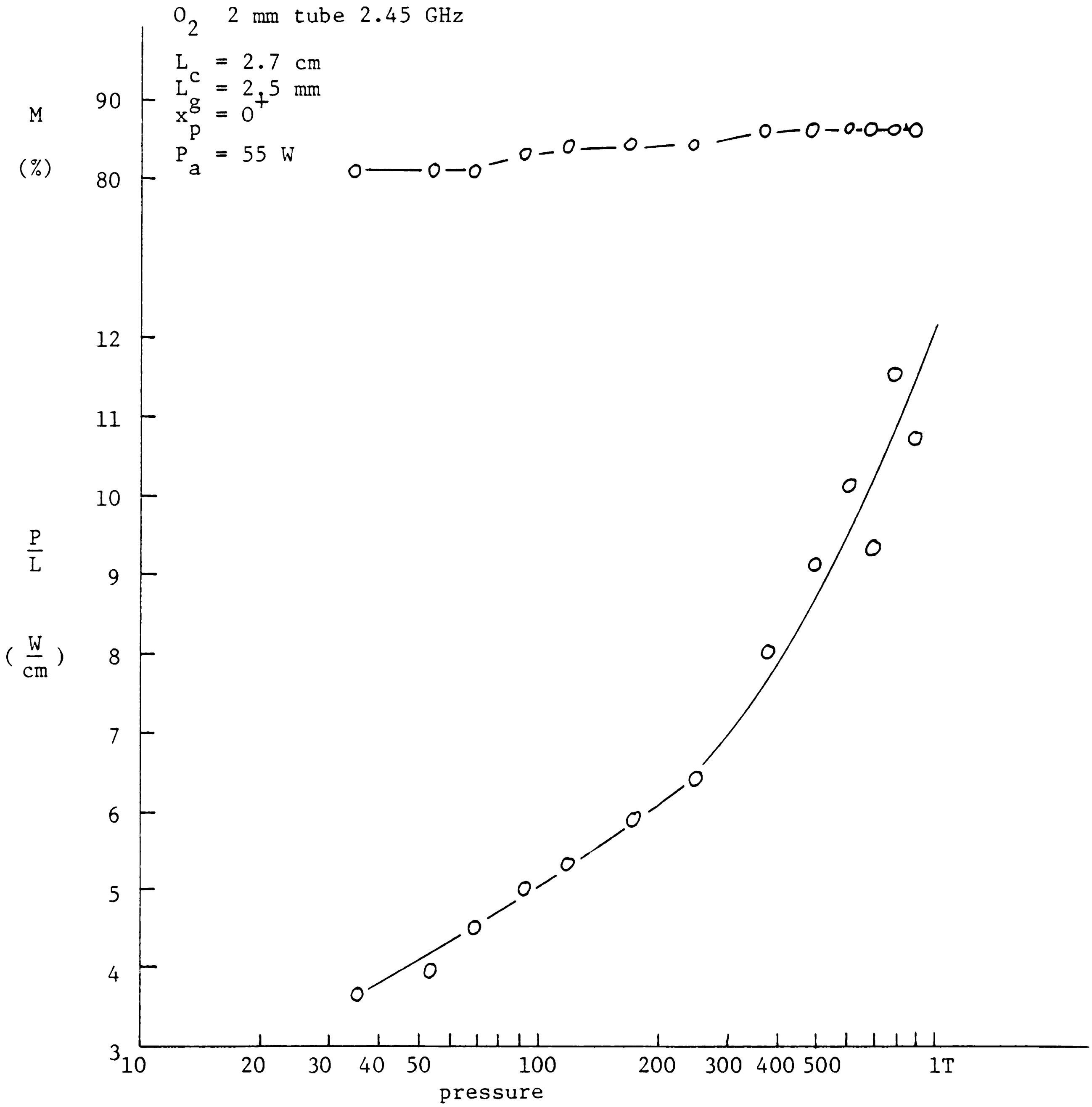

Figure 4.5 P/L vs. Pressure for O_2 in the Coaxial Cavity

from one experiment to another, by 2, 3 or even 5 watts. Comparison of curves showed that P/L was generally higher for higher absorbed powers. Additionally, papers in the literature discussed results at different power levels, being constant for a given report but differing from one group to another. Correlating results from experiments performed at different power levels is facilitated by an understanding of how the power absorption per unit length depends on the absorbed power in the plasma. The experiments described in this section were designed to determine how the power match (P_a/P_i, i.e., ratio of absorbed to incident power) and P/L depended on the power absorbed by the plasma-cavity system.

As in the previous experiments, the tube bore is 4 mm and excitation frequency is 2.45 GHz from a magnetron. The same gases were used. Cavity dimensions and pressures will be shown on the individual graphs.

In this set of experiments the variable is the absorbed power. In performing the experiment, breakdown was achieved as described in Section 4.2, and the cavity was adjusted for long plasma with minimum reflected power. The pressure was constant and chosen so that the discharge length was close to a maximum, or P/L was a minimum, based on the experiments described in Section 4.2. The only change made after this point was to increase the incident power to the cavity, starting from the lowest value for which a discharge could be sustained.

The results of one of the first experiments performed to determine absorbed power dependence is shown in Figure 4.6. Cavity dimensions are as shown on the figure. No changes were made in the experimental system when using different gases, except to change the bottle at the gas inlet tube. The diagram indicates that a low flow rate was used, though the flow rate was not measured. The inlet and exhaust valves were simply

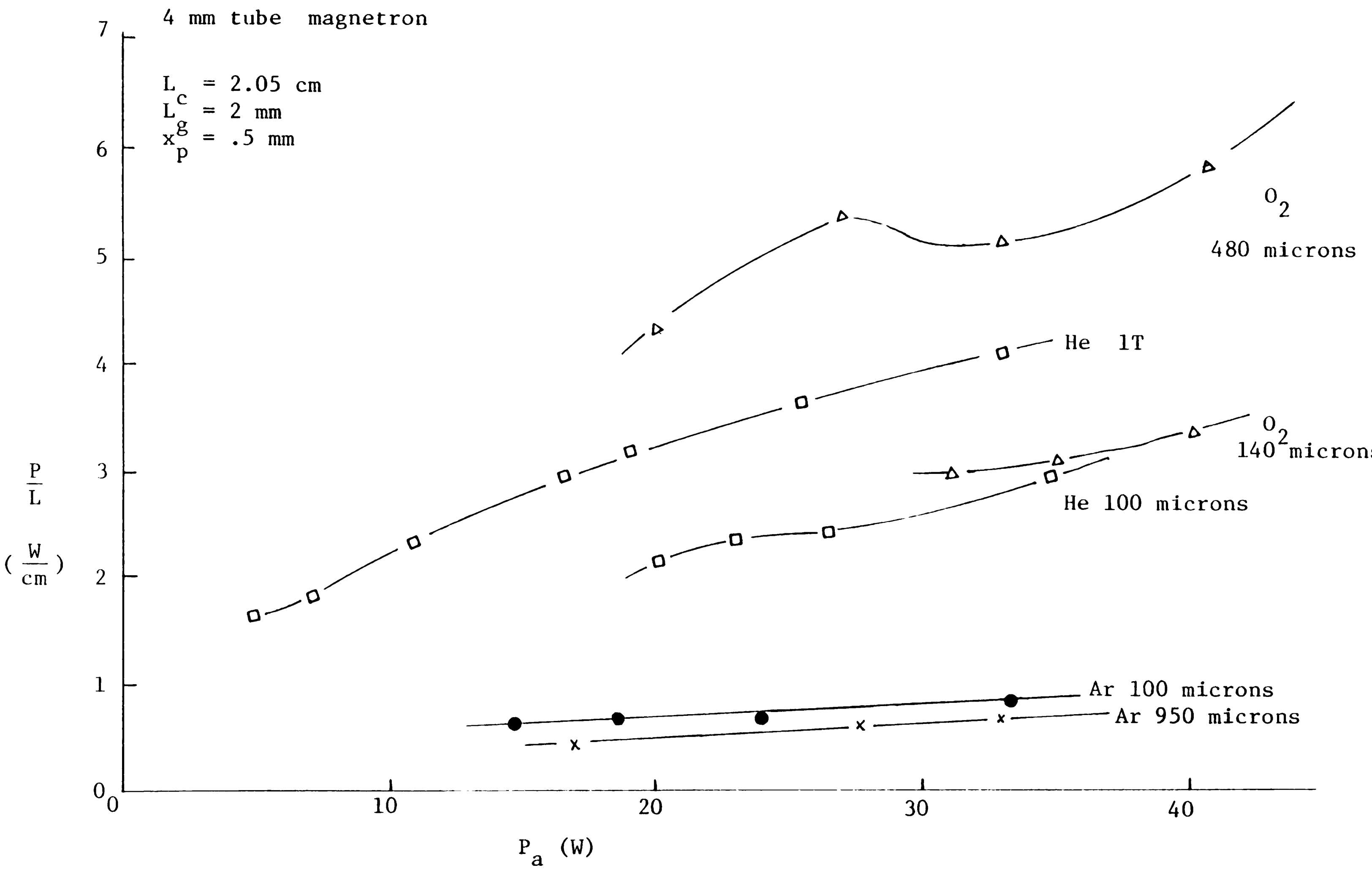

Figure 4.6 P/L vs. P_a as a Function of Gas in the Coaxial Cavity

nearly closed, open just enough to keep the gas fresh. The results shown for Ar, He, and O_2 correlate with the values of P/L from the previous experiments, i.e., P/L was higher for O_2 than for He, and higher for He than for Ar. Obviously the pressure has an effect on the curves, particularly for He and O_2. Ar shows a slight linear increase with absorbed power, and exhibits little variation with pressure, as shown by the 100 micron and 950 micron curves. He was shown to be more sensitive to pressure (100 microns and 1 torr curves), and is more sensitive than Ar to change in absorbed power. Over small power ranges, the curve could be approximated as linear, the slope is greater than that of the Ar line. O_2 (very sensitive to pressure variations) also shows a general increase in P/L with absorbed power, though it is not linear.

The following four figures, Figures 4.7, 4.8, 4.9 and 4.10, show the results of the same experiments performed with research grade Ar, Kr, Xe and He over an absorbed power range of approximately 8 to 28 watts, depending on the gas. Power matches for these experiments were all of the order of 75 to 80%, increasing with absorbed power, as shown for Ar, Kr, and Xe.

As can be seen, the P/L dependence for Ar is nearly linear with absorbed power, while the power match increases and levels off at about 20 watts, at approximately 77%. The Kr P/L curve shows a nearly linear variation with absorbed power, the slope of which is close to that of Ar, though the values are .03 to .05 W/cm higher for most of the curve. As with Ar, the power match for Kr rises and saturates at an absorbed power of about 20 watts, the match being 73%. The P/L curve for Xe is also approximately linear with P_a; the values are about .07 W/cm lower than for the other gases and the slope of the line is roughly the same. For

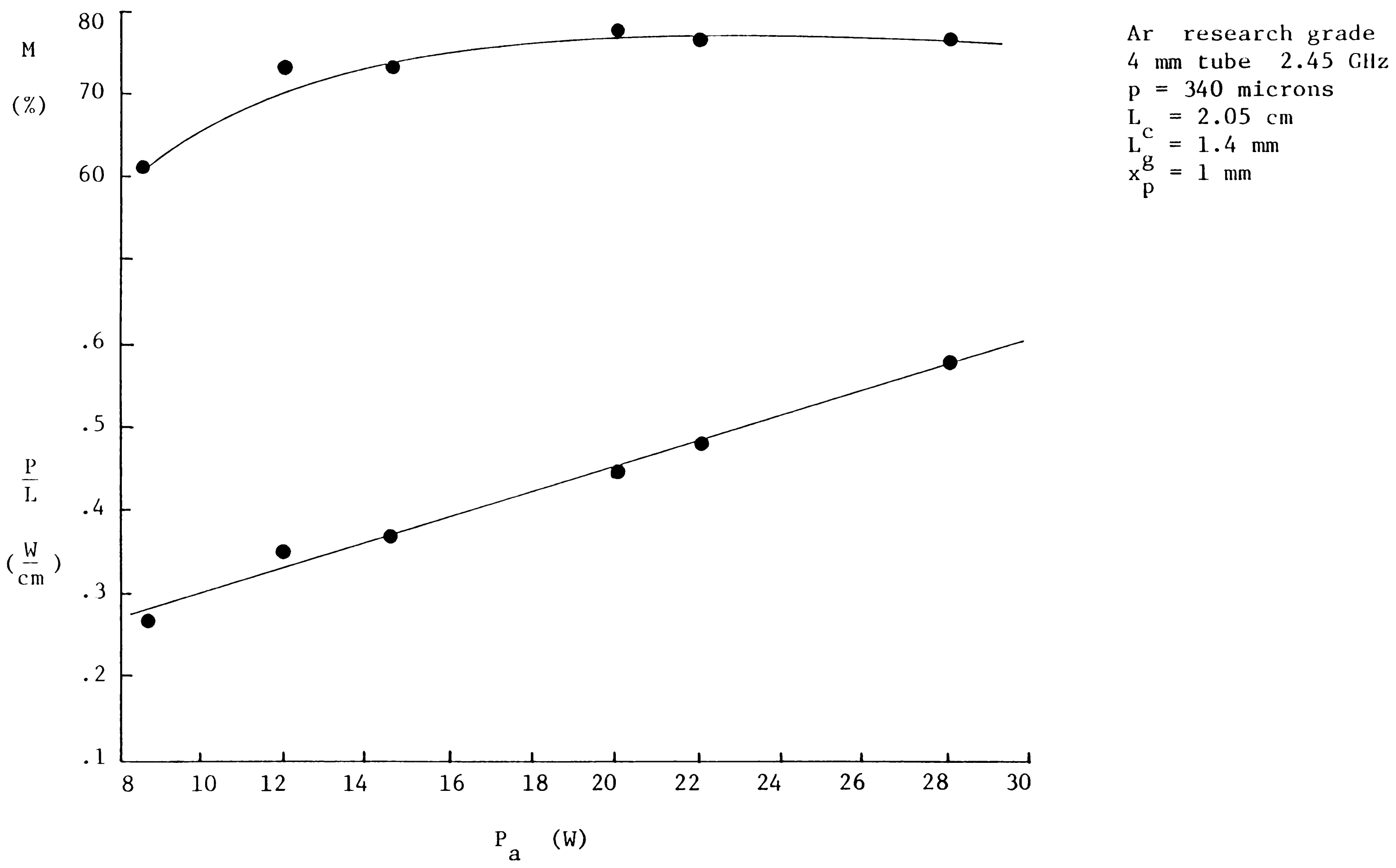

Figure 4.7 P/L vs. P_a for Research Grade Ar in the Coaxial Cavity

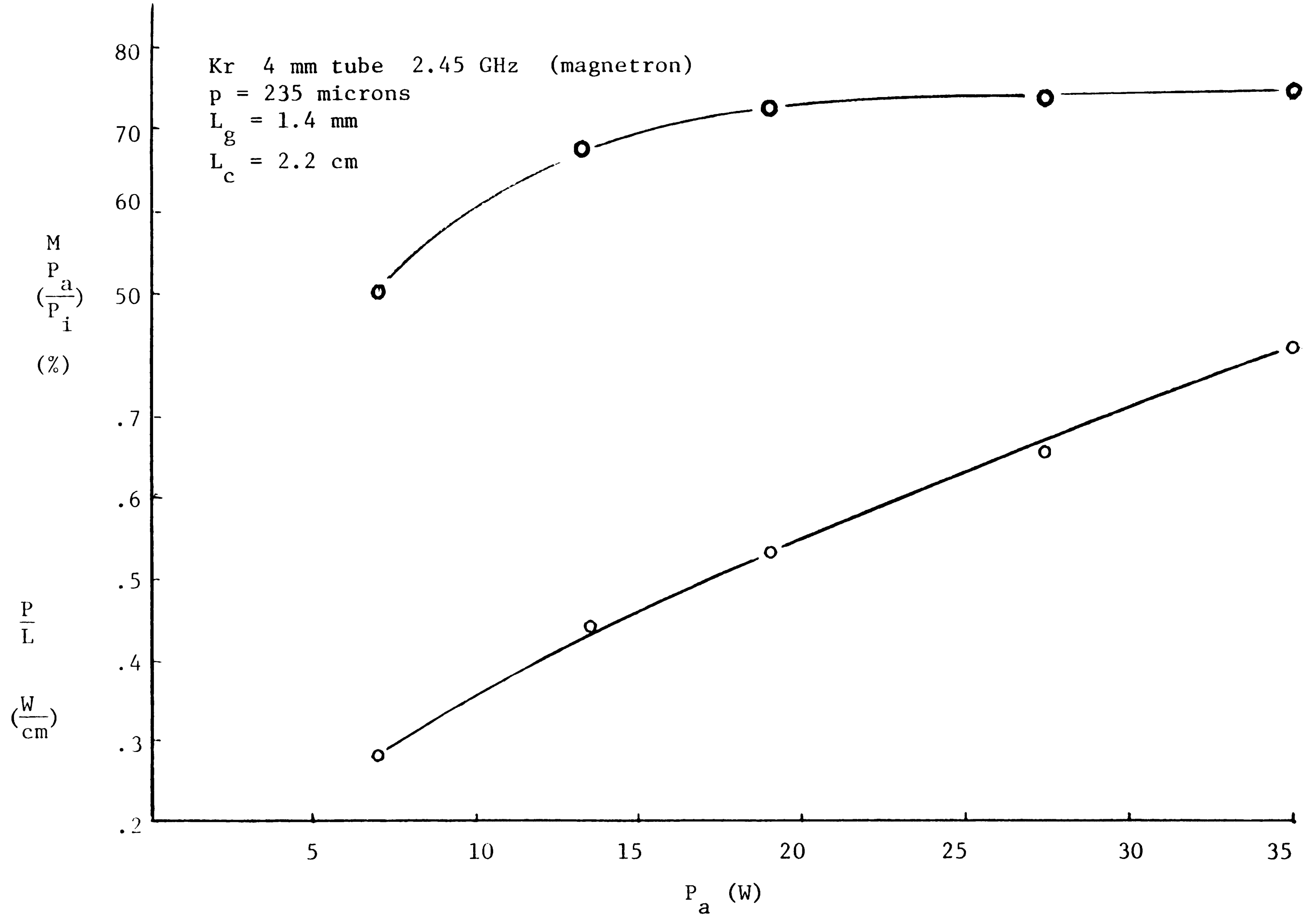

Figure 4.8 P/L vs. P_a for Kr in the Coaxial Cavity

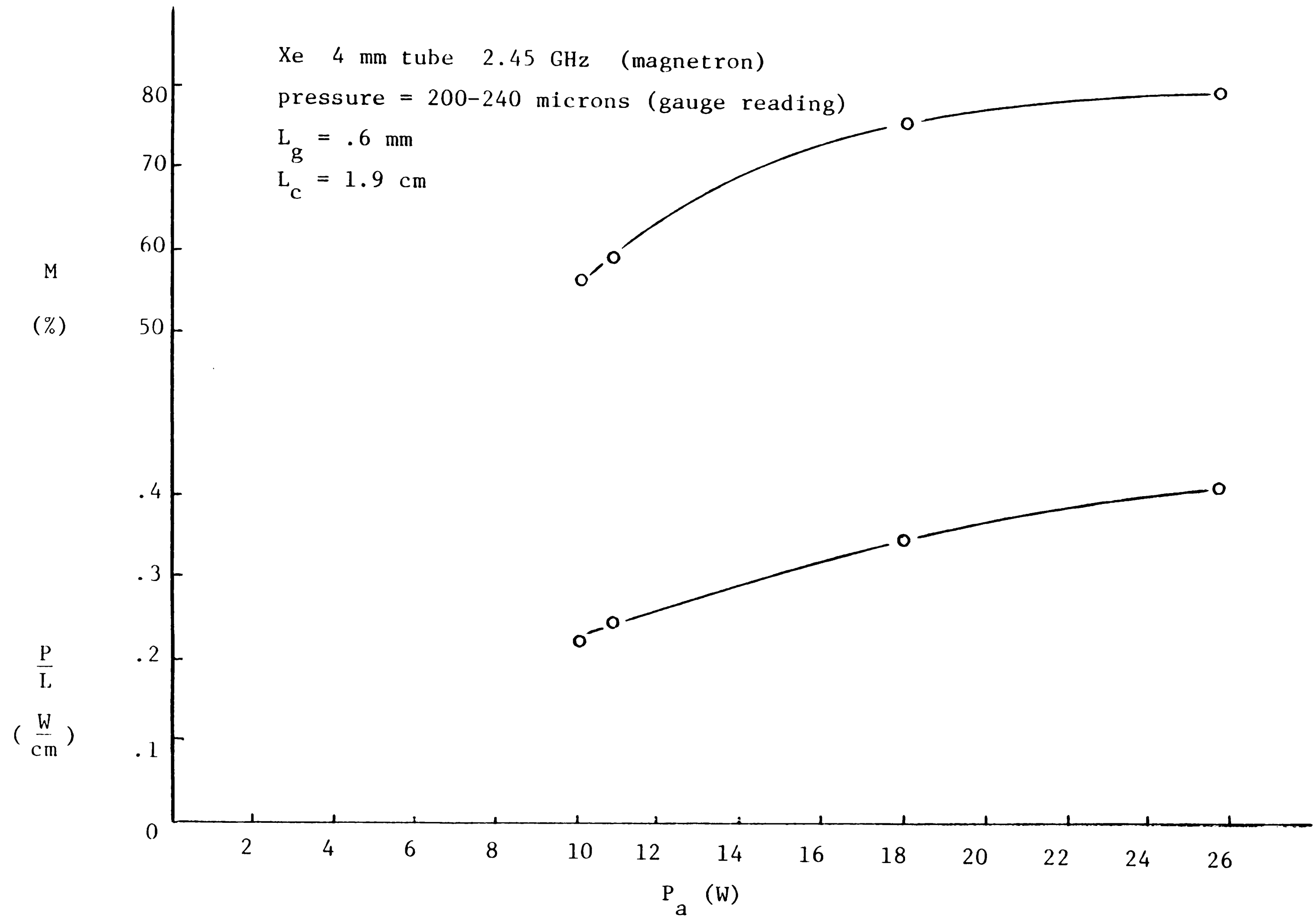

Figure 4.9 P/L vs. P_a for Xe in the Coaxial Cavity

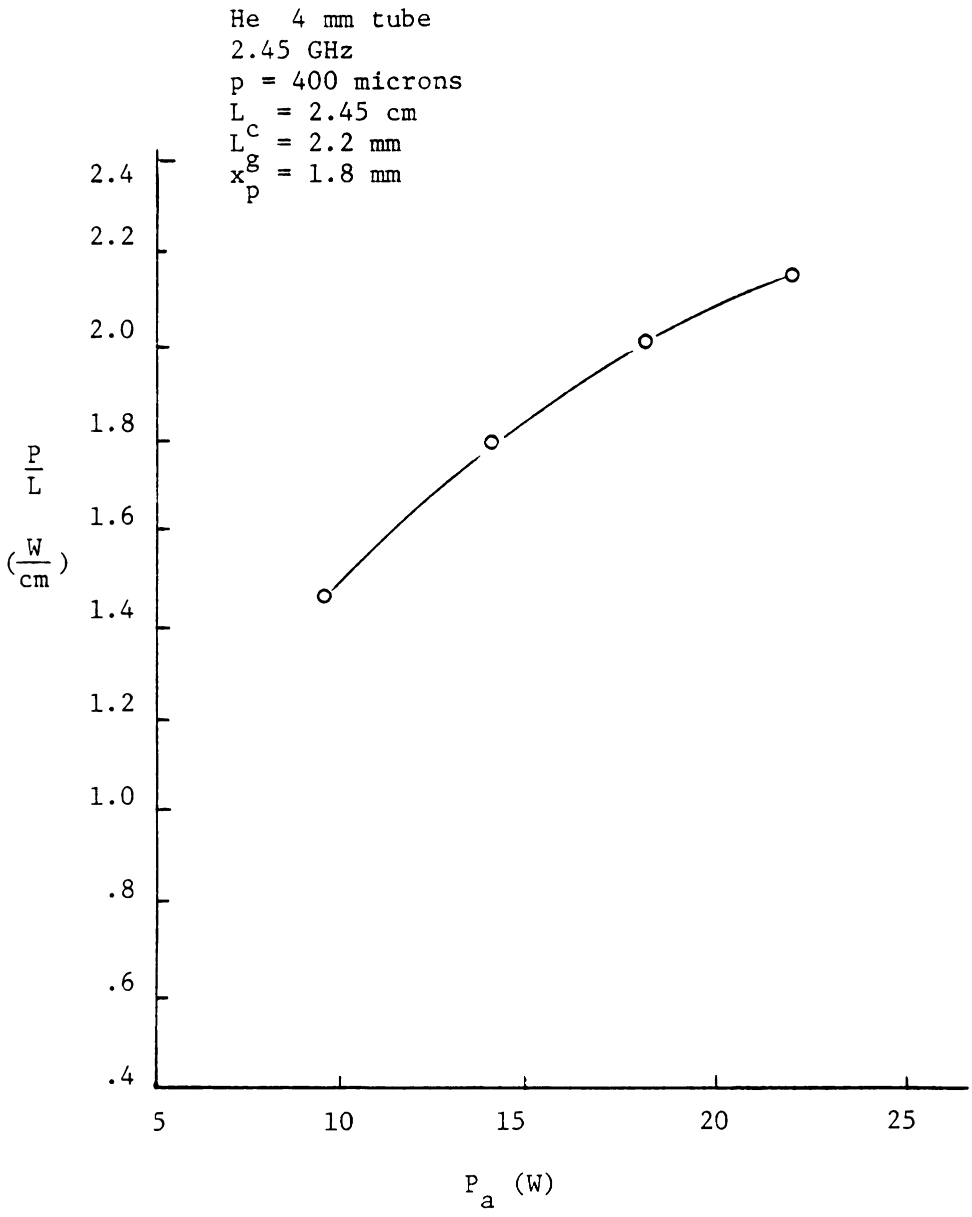

Figure 4.10 P/L vs. P_a for He in the Coaxial Cavity

the data shown, the power match does not quite saturate (maximum absorbed power was 26 watts). Extrapolation would suggest that saturation would occur around 30 watts. The curve shown for He is similar to that shown in Figure 4.6, except that the values of P/L are about .5 to 1 W/cm lower than in the earlier figure. This curve was taken from a set of experiments in which the gap length was being varied, to determine optimum cavity geometry. This is one of the optimum curves.

Overall, one can see that the value of P/L for all of the gases increases linearly or nearly so as absorbed power increases; the values for Ar, Kr, and Xe are all similar as are their slopes. Numerical values of P/L for each of these gases is less than 1 W/cm over the power ranges shown. P/L for He and O_2 are larger by a factor of 4 or 5 compared to the other gases. The power match curves indicate that the relative amount of energy that can be coupled into the plasma-cavity system increases as the power absorbed by the system increases, within the incident power ranges stated (0 - 28 watts).

4.4 P/L and Power Density vs. Tube Inner Diameter: Coaxial Cavity

As with previous experiments, one of the motivational factors for varying the tube diameter was to understand the effect of the tube diameter on the properties of the surface wave discharge. The available cavity system plays an important role in determining what tube sizes will be used, as does the objective of the experiment. For example, some types of lasers may require a high power density (W/cm^3) as compared to applications of microwave discharges to plasma chemistry. To determine the influence of tube size on the P/L of the discharge and also on the power density, different sized tubes were inserted into the coaxial cavity, while attempting to hold other parameters constant.

As usual, the relevant parameters are shown on the figures. In general, pressures around 200 microns were used, these pressures give low values of P/L for Ar and He (other gases also, although these are not included here). Cavity length was about 2 cm, gap varied between 1.5 and 2 mm, and probe position was adjusted for optimum coupling. The method used was to obtain a complete set of readings (P/L vs. pressure or P/L vs. P_a), change the tube and repeat the experiment, with adjustment of the plasma-cavity system for best power match.

Figure 4.11 illustrates the variation of power density as a function of tube cross section for Ar. Taking a pressure of 225 microns for reference, one can see that the power density is approximately inversely proportional to the tube cross section. There is a large variation in power density--2 to 25 W/cm^3--and a less dramatic variation in P/L, which ranges between .65 to .8 W/cm. It would appear that P/L increases nearly linearly as the cross section increases, for 4, 5, and 7 mm tubes, as is shown in Figure 4.12. However, P/L increases significantly for the 2 mm tube, suggesting that there may be an optimum tube size for this cavity.

In keeping with other types of experiments, it was considered desirable to determine P/L vs. tube diameter as the absorbed power increased. This was done for Ar and He. There is the indication that an optimum tube size may exist. The 4 mm tube exhibits a better power match (Ar) and lower P/L (Ar, He) than other tubes shown in Figure 4.13 and 4.14.

Overall, the curves suggest that P/L may reach a minimum for a tube diameter of 4 mm, and increases as the tube gets larger or smaller.

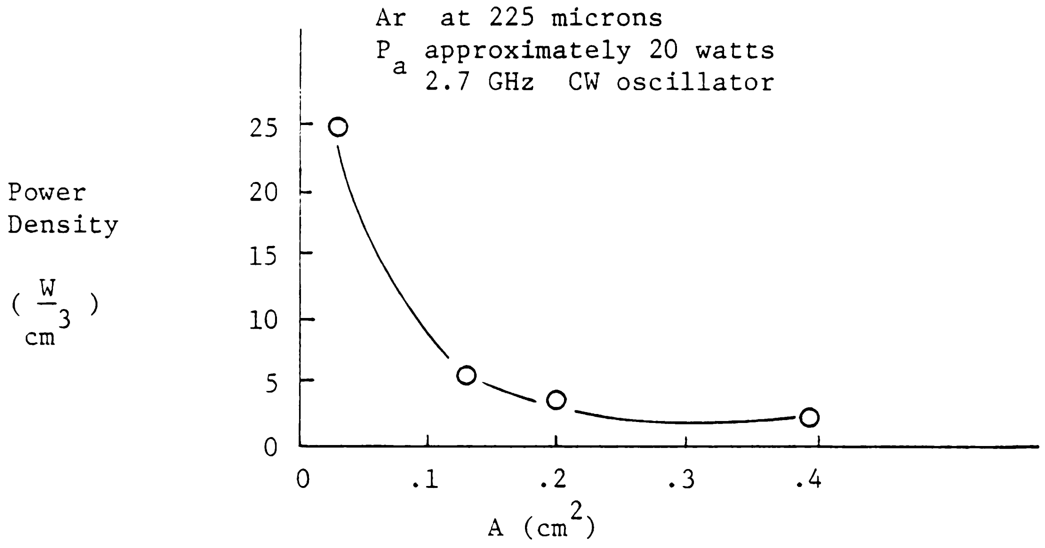

Figure 4.11 Power Density vs. Tube Cross Section in the Coaxial Cavity

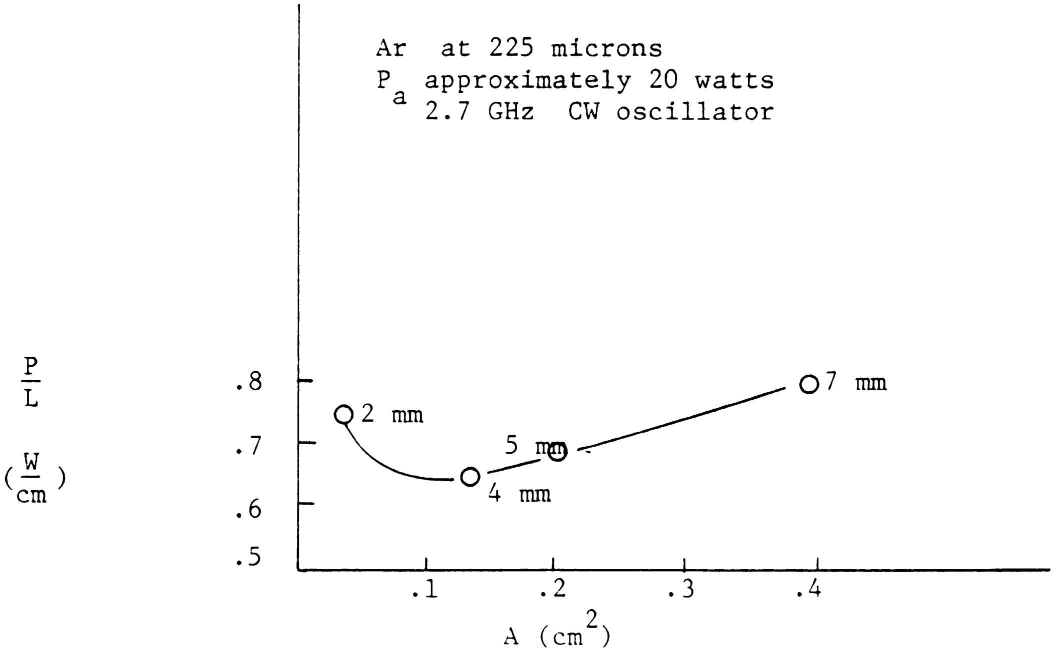

Figure 4.12 P/L vs. Tube Cross Section in the Coaxial Cavity

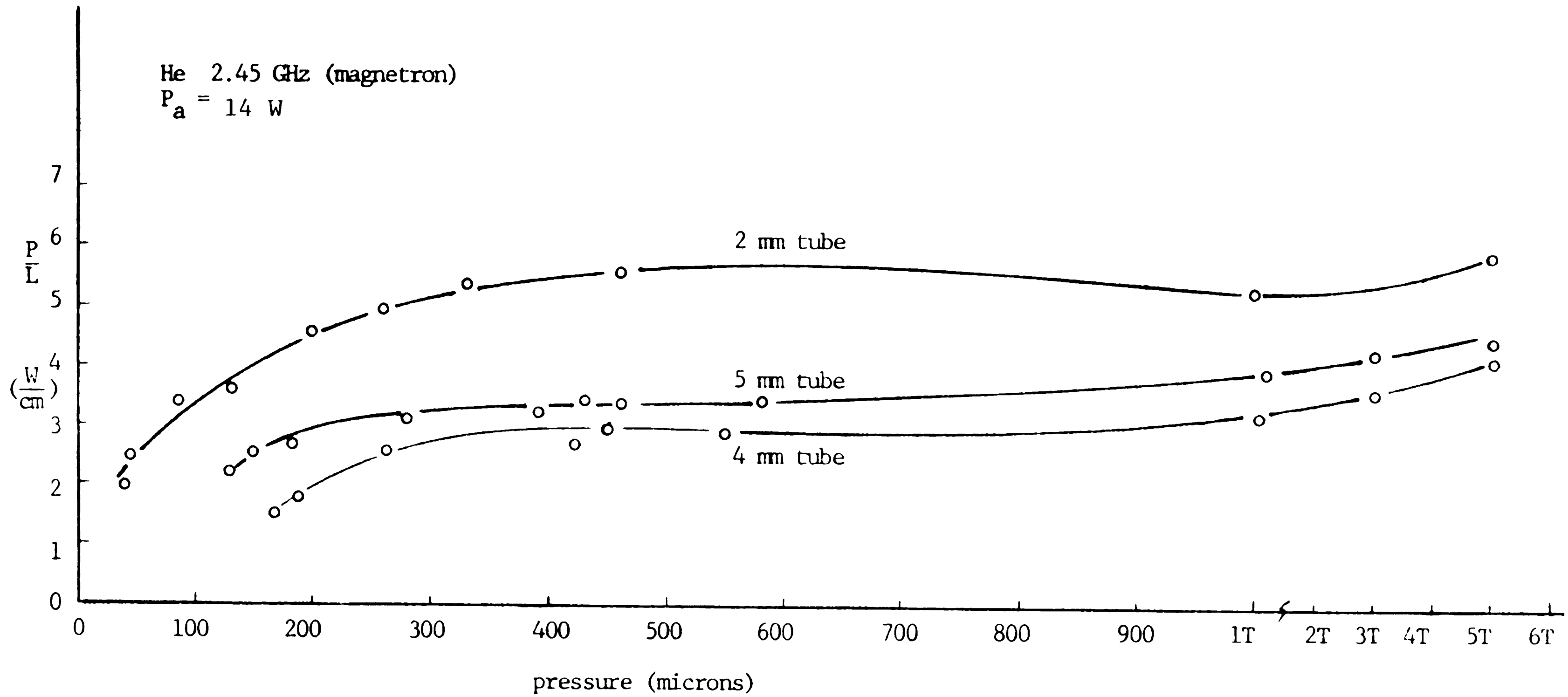

Figure 4.13 P/L vs. Pressure for He as a Function of Tube Size in the Coaxial Cavity

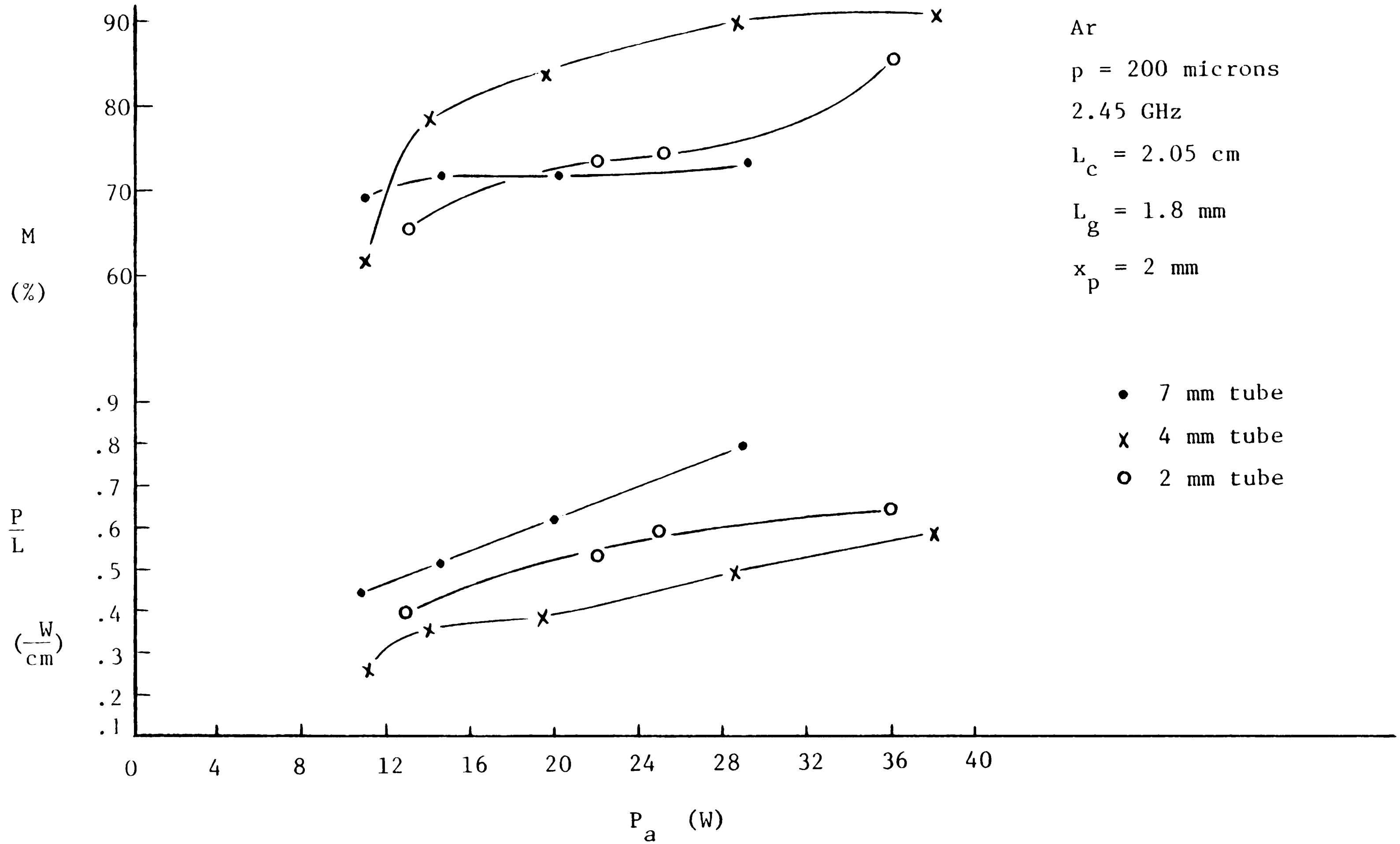

Figure 4.14 P/L vs. P_a as a Function of Tube Diameter for Ar in the Coaxial Cavity

4.5 P/L vs. Excitation Frequency and Source Type: Coaxial Cavity

Examination of the literature dealing with microwave sustained discharges reveals wide differences in the excitation frequencies used and also in the type of power source. To compare results of different groups is difficult unless one understands how the surface wave behavior of the discharge at one frequency is related to the surface wave behavior at another frequency. In addition, it was found that surface waves sustained longer plasmas with a magnetron as the power source than when a CW oscillator was used, with other parameters the same for both sources. The following experiments were designed to determine the variation of P/L vs. pressure at different frequencies from a CW oscillator, then a particular pressure was chosen for comparison. In addition, a direct comparison of P/L vs. pressure and P/L vs. absorbed power for Ar using a CW oscillator and a magnetron was made.

To determine the dependence of P/L on frequency, a CW oscillator was used as a power source. Experimental gases were Ar and He in a 4 mm tube, absorbed power was approximately 15 to 20 watts for each frequency, and common pressures were chosen from P/L vs. pressure curves. In order to maintain optimum coupling, the cavity length, gap and probe position were adjusted with each change in frequency.

To compare the dependence of surface wave behavior on source type, the magnetron was used to generate P/L vs. P_a and P/L vs. pressure curves for Ar, then the power input cable was changed to the CW oscillator, operating at a frequency of 2.45 GHz, as determined by a frequency meter. Minor adjustments were made in the position of the coupling probe to maintain long plasmas with minimum reflected power.

Figure 4.15 shows the variation in P/L as the frequency of the source

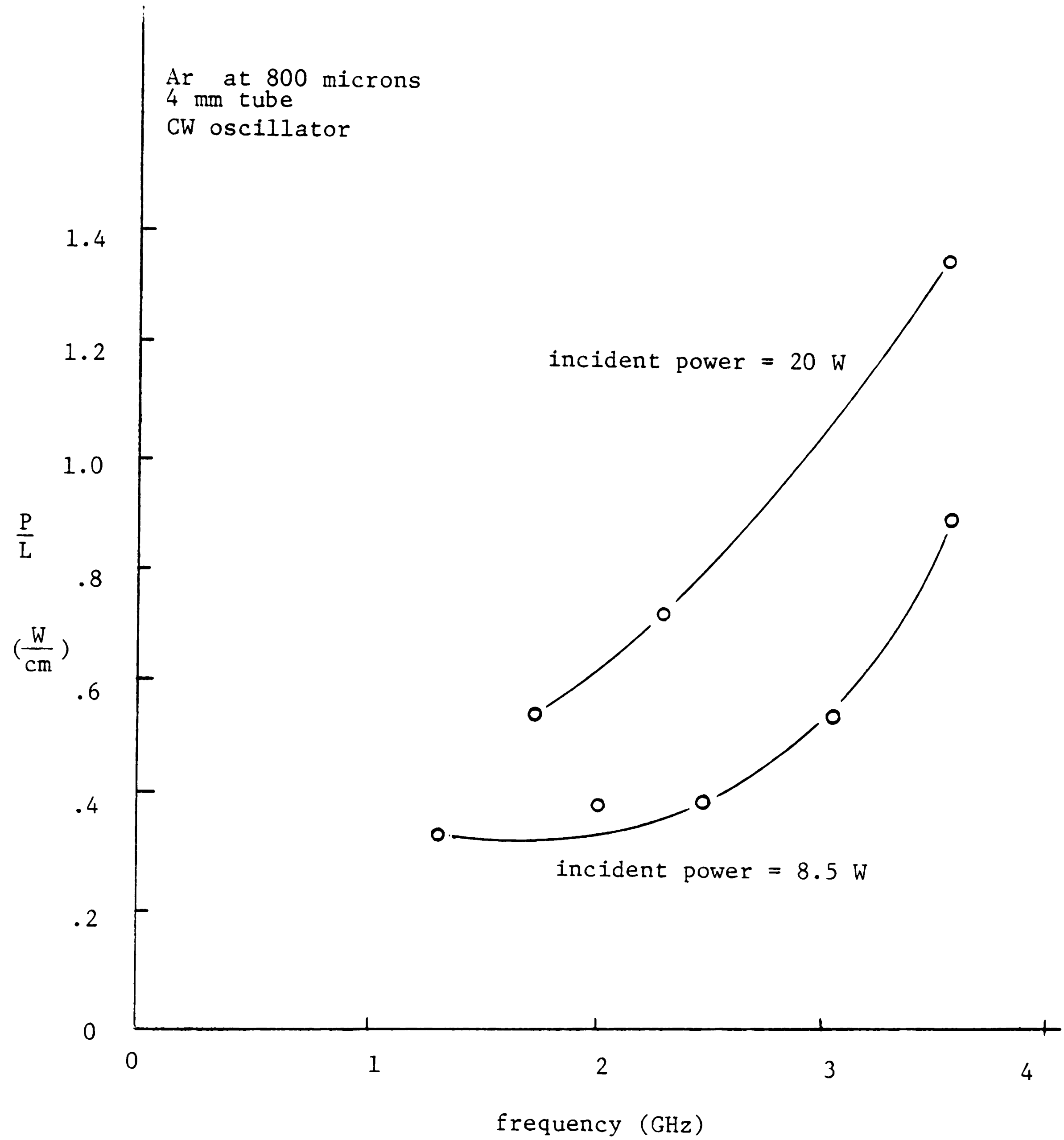

Figure 4.15 P/L vs. Frequency for Ar in the Coaxial Cavity

was changed for Ar. A definite increase is obvious, meaning that more power was supplied to the discharge gas to get a plasma of a given length, at higher frequencies.

Results from He experiments performed using the same procedure are given in Figure 4.16. The same general trend is apparent, i.e., increasing P/L with frequency.

It should be noted here that the values used to determine these curves are minimal values from P/L vs. pressure curves, all occurring near the pressure indicated in the figure.

A difference in P/L was noted for Ar plasmas when changing from the CW oscillator to the magnetron. Experimental curves for the different sources were significantly different as was breakdown of the gas. Figure 4.17 compares the P/L vs. pressure curve for each source. P/L increases with pressure for the oscillator, while it exhibits a minimum at about 150 microns when the magnetron is used as the source. Note also that the values of P/L are two to three times lower for the magnetron. The P/L vs. P_a curves, Figure 4.18, have a similar shape for the two sources, however, values for the magnetron are roughly 1/3 those for the oscillator.

The ranges of the pressures at which the discharge can be sustained is different for the two sources. From the same figures, one can see that the magnetron can sustain a discharge over a range of only 20 to 300 microns (at P_a = 9 watts), while the CW oscillator can sustain a discharge from 20 to over 600 microns (same P_a). Breakdown power for the magnetron was about 6 watts, while for the oscillator it was approximately 4 watts. However, the discharges excited by the oscillator had to be initiated with a Tesla coil, while those excited by the magnetron did not.

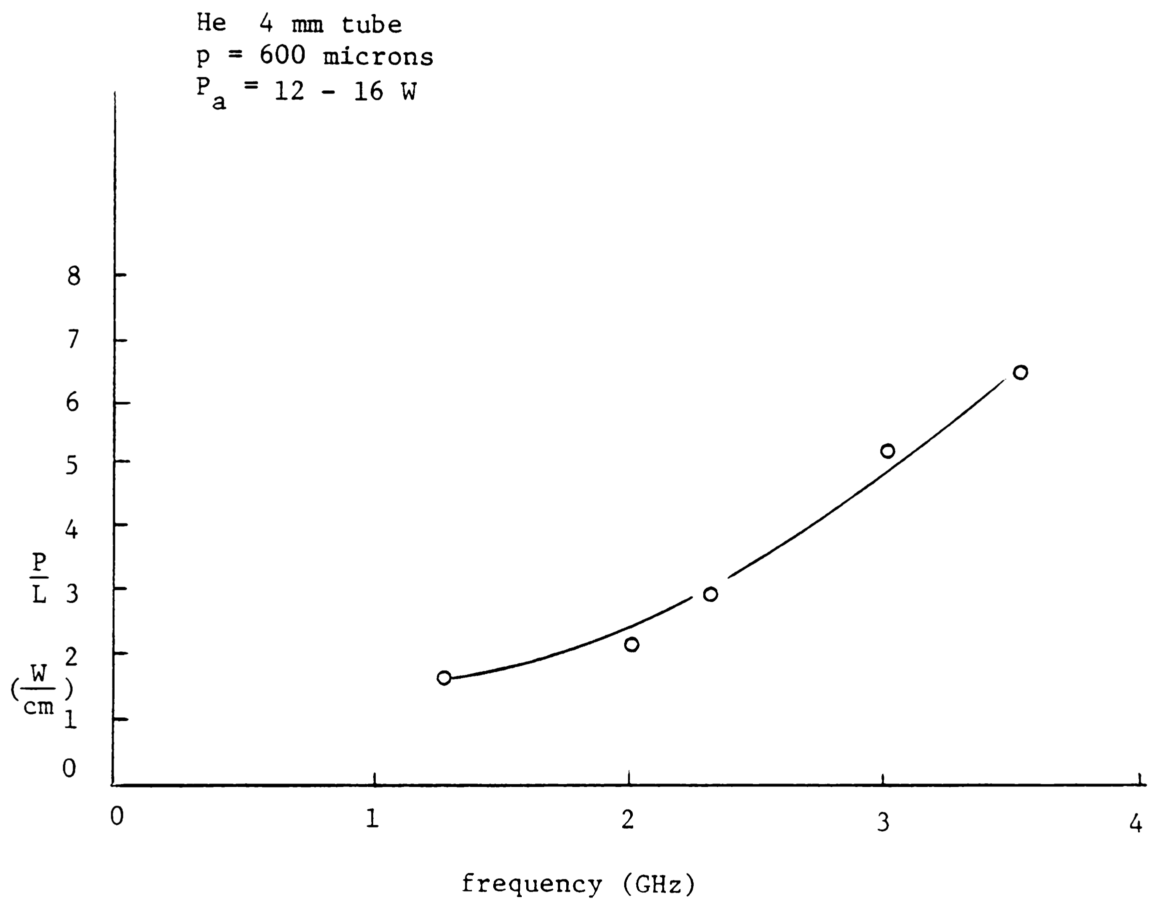

Figure 4.16 P/L vs. Frequency for He in the Coaxial Cavity

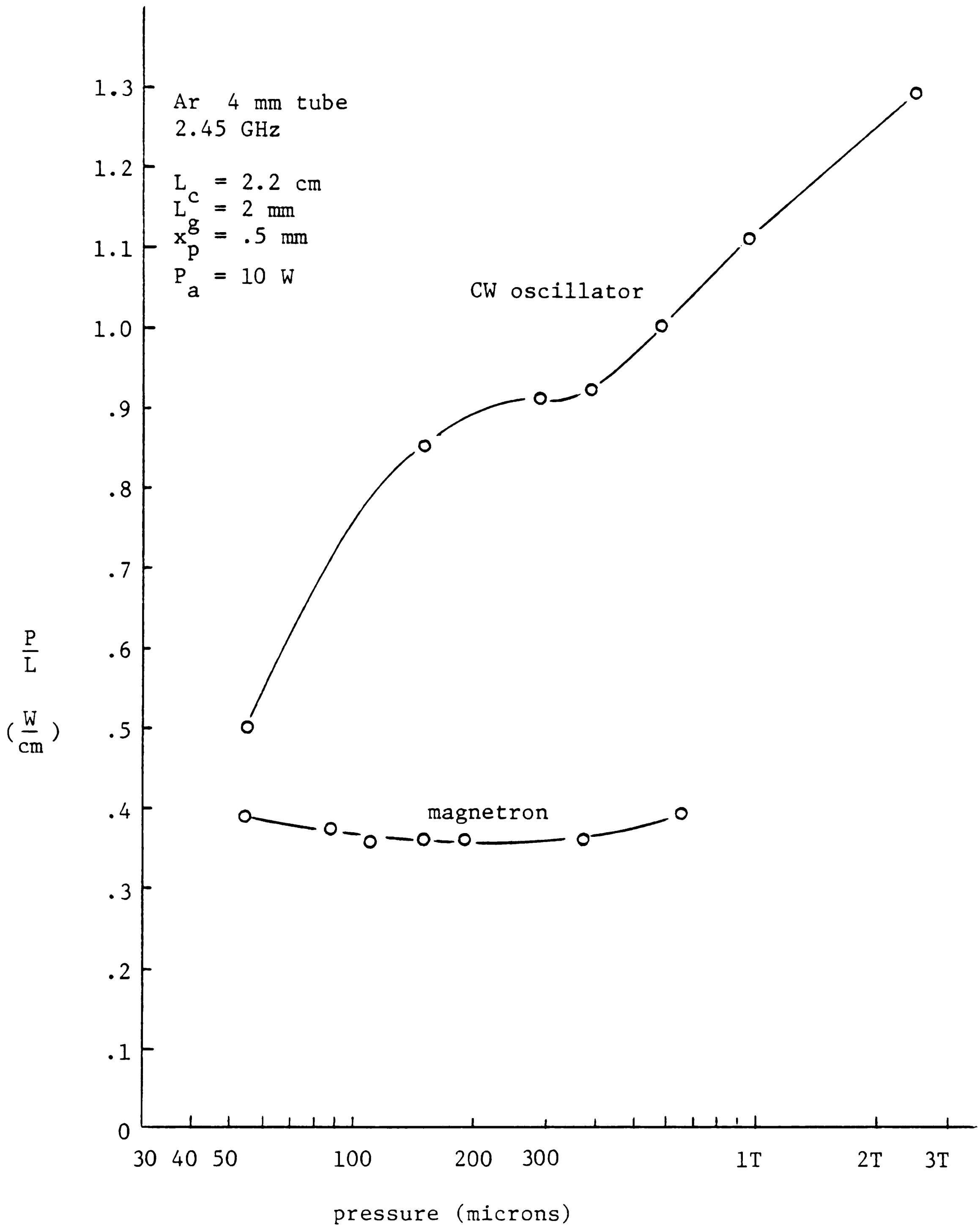

Figure 4.17 P/L vs. Pressure as a Function of Power Source for Ar in the Coaxial Cavity

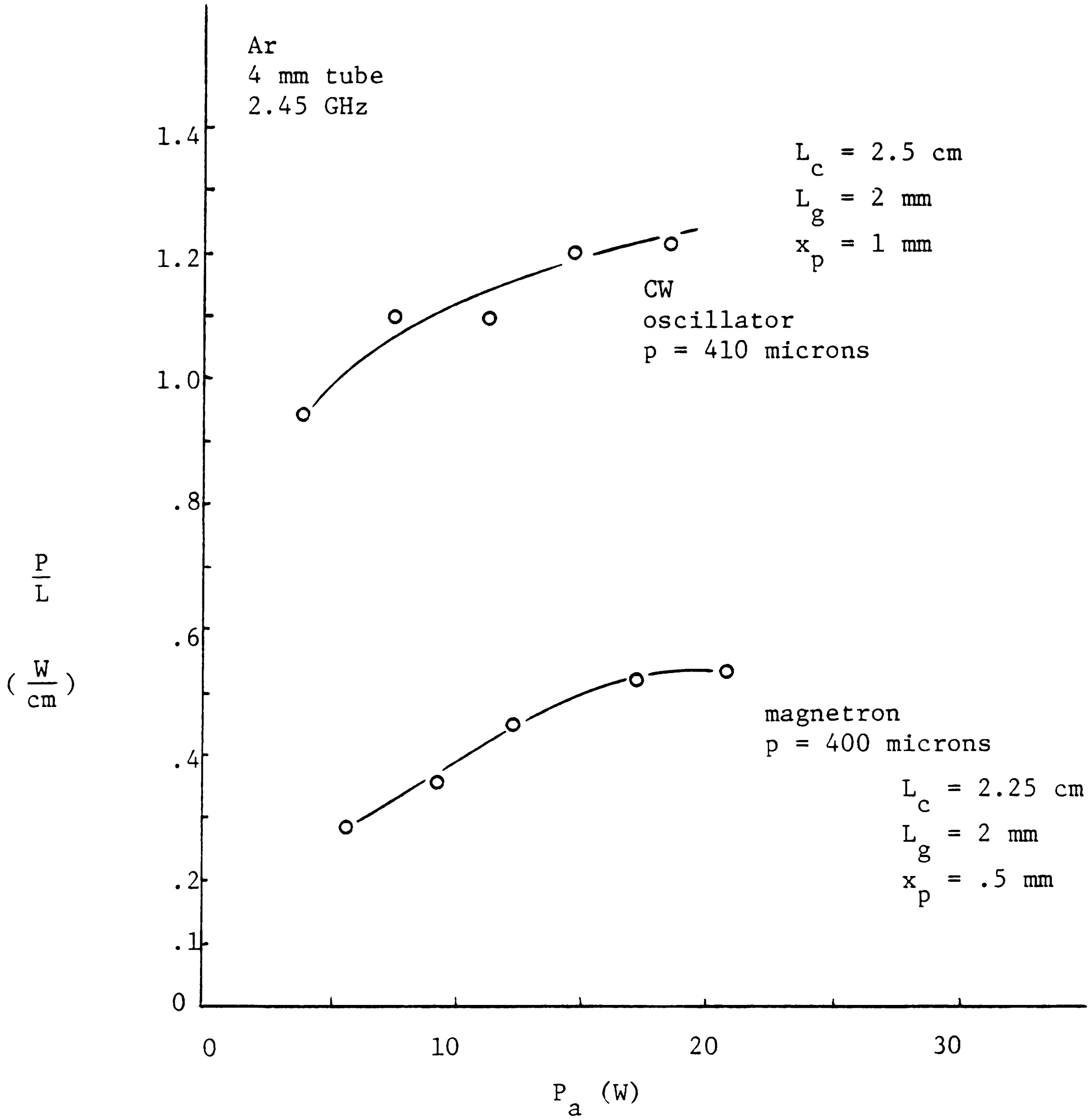

Figure 4.18 P/L vs. P_a for the Coaxial Cavity with Different Power Sources

From the figures, then, one can see that P/L decreases as excitation frequency decreases (this may be an indication of a lower plasma density), and P/L is significantly lower for a magnetron than for the CW oscillator.

4.6 P/L vs. Gas Type: Coaxial Cavity

To expect significant differences in P/L for various gases under similar conditions is natural, and one might wonder whether a general trend can be found for a given property of the gases, for example, ionization potential. From the experiments already discussed, data was extracted to make the graph shown in Figure 4.19. Thus, a single experiment was not performed, rather these data are taken from several experiments.

The same reference conditions were used here as in other experiments: excitation by a magnetron at 2.45 GHz, 4 mm tube, and gas pressure of approximately 225 microns. These experiments were performed within two or three days. The "error" bars shown are the ranges of P/L that were obtained with variation of the cavity geometry and absorbed power levels of 14 to 20 watts. Power densities are shown in the insert, ranging from 2 or 3 W/cm^3 for the more easily ionized gases to 20 W/cm^3 for He. Ionization potential for the He-Ne mix was determined by simply taking a weighted average based on the proportion of He to Ne.

Figure 4.19 shows that P/L obviously increases with the ionization potential of the gas.

4.7 Cavity Geometry Effects: Coaxial Cavity

During the course of experimentation, dependence of P/L and plasma length on cavity length, gap, loop position and orientation became obvious.

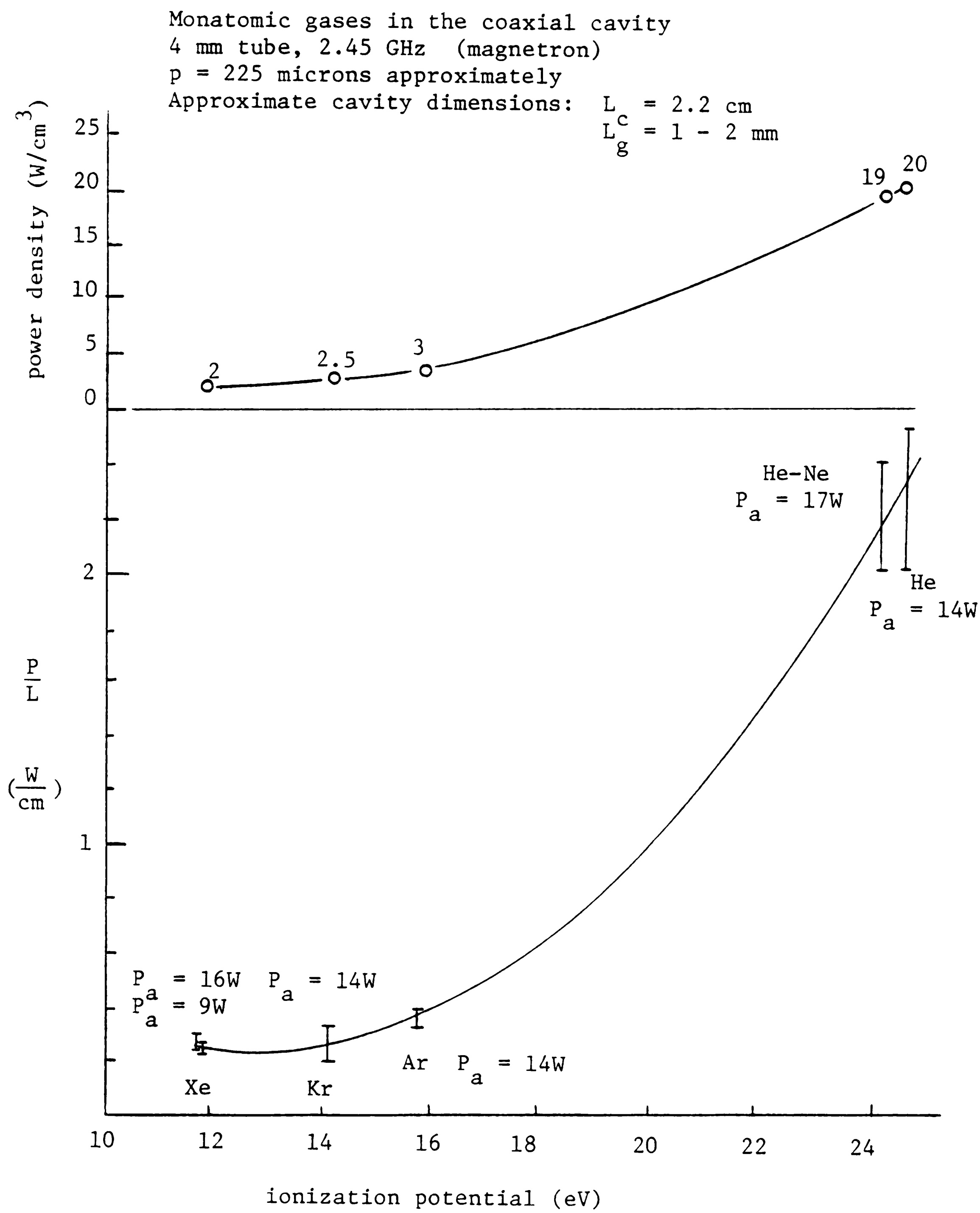

Figure 4.19 P/L vs. Ionization Potential of Gas in the Coaxial Cavity

Such a dependence makes the capability to change geometry a desirable feature in cavity design. This tuning capability can be used to couple energy efficiently into the discharge.

The factors that contribute to the tuning of the cavity-plasma system are (1) probe position, (2) gap length, (3) cavity length, (4) orientation of the probe, and (5) shape and size of the probe. The effects of probe position are discussed briefly. Gap and cavity length were investigated in detail while probe orientation was examined briefly. Probe size and shape warrant further study.

Experimentally, the probe position is probably the most sensitive of all the cavity parameters. Movements of .1 or .2 mm cause dramatic changes in plasma length, power match and light intensity from the discharge. Measurements of probe position in the experiments reported here were made with a scale marked in millimeters. Thus the experimental values of the probe position are only approximate. Small adjustments were usually too small to measure (and record). Some of the figures indicate that the probe position was 0^+, which means that the probe was almost touching the end plate of the cavity.

The discharge is also sensitive to the gap length between the inner conductor and cavity end plate. Experimental curves, Figures 4.20 and 4.21, show the dependence of power match, discharge light intensity, discharge length and P/L on the gap for Ar and Xe, respectively. Power match, plasma length and P/L were determined in the same manner as in previous experiments. The photocurrent was determined with a photodiode placed as close to the end of the cavity as possible, in a small holder and pointed at the center of the plasma tube. Cavity length, gap and probe position were adjusted to produce the best power match. To obtain the experimental points, the gap length was varied without changing the other parameters. It should be noted that the discharge could be sustained over a wide range of gap lengths, i.e., from .4 mm to cavity length. When the gap length is equal to the cavity length, the center conductor is no longer in the cavity, the geometry is that of a simple cylindrical cavity. The power match is not as great for long gaps as for gaps in the 2 mm range (which is 90% or greater).

Referring to Figure 4.20 for Ar, there is no particular gap length that will optimize all four of the experimentally measured parameters. For example, P/L is lowest for a 1.0 mm gap, intensity is highest for a 1.4 mm gap, power match is maximum at 1.8 mm and plasma length is longest for 2 mm. Another experimental parameter of importance is the power density (W/cm^3). This can be determined by dividing P/L by the tube cross-sectional area. Note from Figure 4.20 that the discharge light intensity and P/L follow a similar pattern as the gap is varied. Since the light intensity can be used as a measure of the plasma density, so can P/L. Nearly all of the experimental curves follow this pattern. In tuning the cavity, one must decide which factor is to be maximized, since it is unlikely that all can be maximized simultaneously.

Xenon, Figure 4.21, exhibits a slightly different trend. A .6 mm gap results in maximization or near maximization of power match, plasma length and P/L. A 2.2 mm gap optimizes power match again, and discharge intensity. A generalization for both Ar and Xe is that the longer gaps produce brighter (denser), shorter plasmas, while the converse is true for shorter gaps.

Cavity length also affects the behavior of the discharge but a larger variation is needed to produce dramatic changes. Representative of this

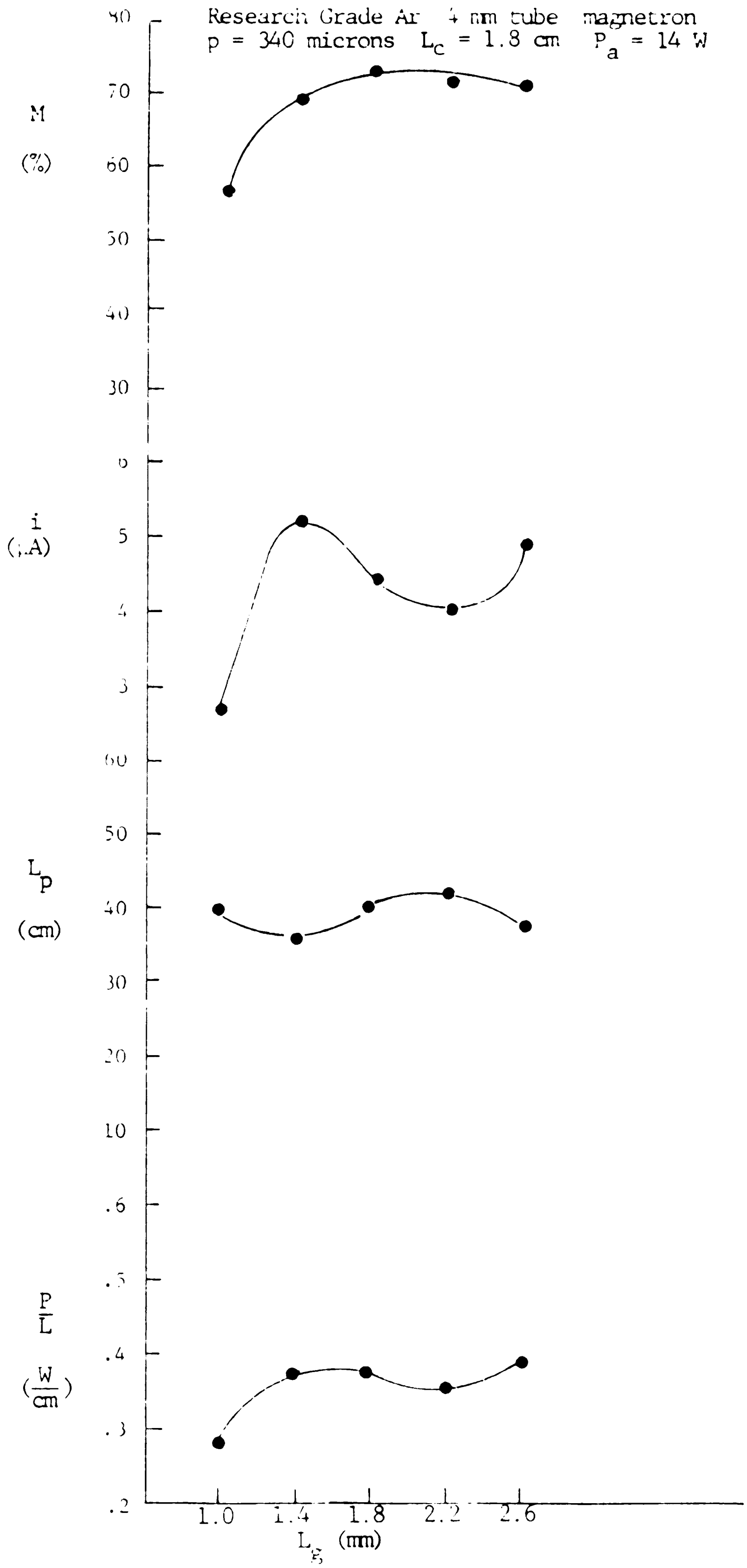

Figure 4.20 P/L vs. Coaxial Cavity Gap Length for Ar

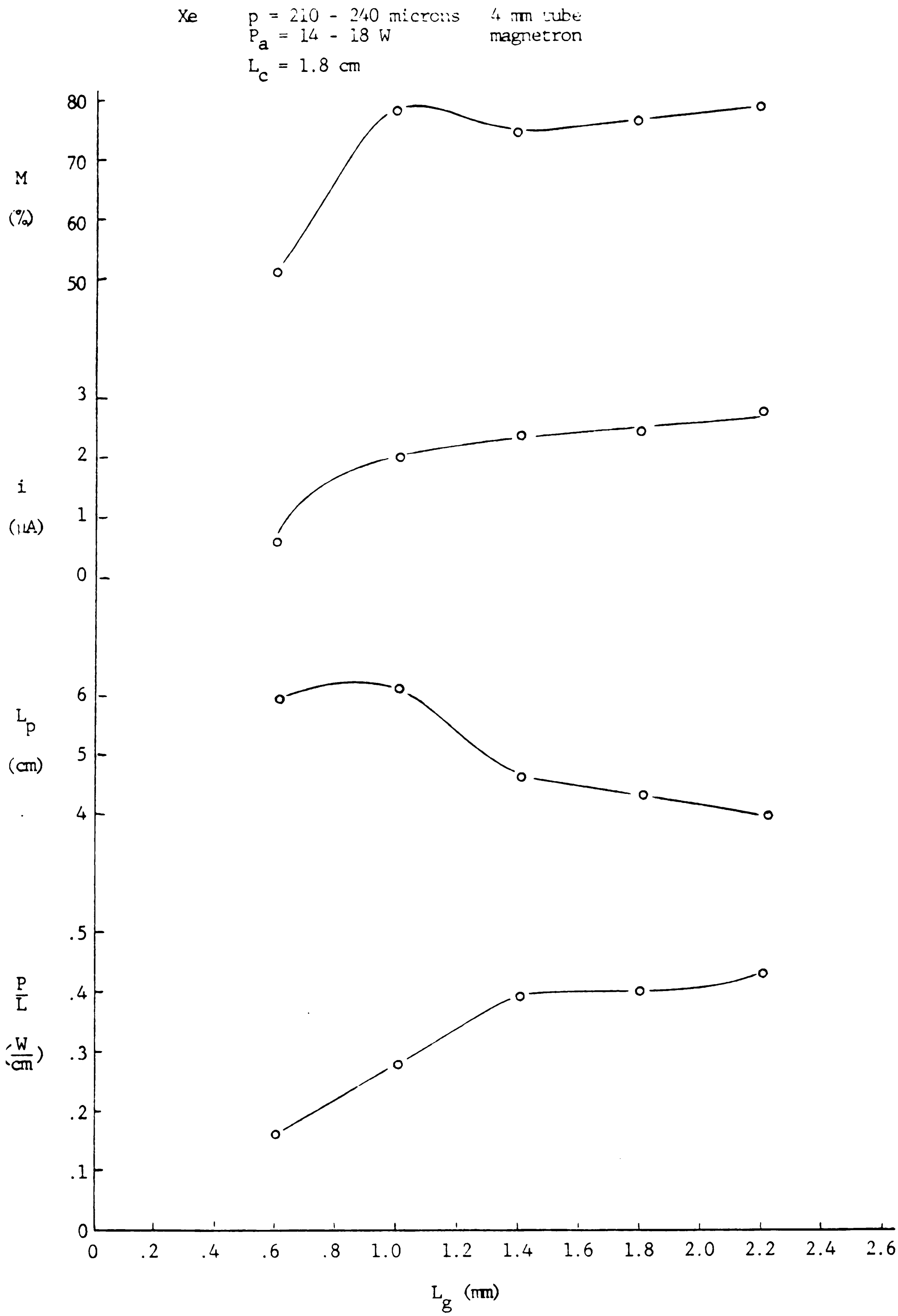

Figure 4.21 P/L vs. Coaxial Cavity Gap Length for Xe

dependence are Figures 4.22, 4.23, and 4.24, showing the variation of power match, discharge light intensity, plasma length and P/L as functions of cavity length for Ar, Xe, and He, respectively. These curves were taken by tuning the cavity for maximum power match at a cavity length of about 2.2 cm, then varying the cavity length from the shortest possible distances over which a discharge could be sustained to longer distances, without changing other parameters. As with the gap, cavity length could be varied over a wide range; about 1 cm to 5 cm was used, when the gap was 1.4 or 1.8 mm and incident power was about 25 watts.

Referring to the experimental curves, one can see that for each of the gases, there is a small range of cavity lengths in which each of the parameters can be nearly optimized simultaneously, thus avoiding significant trade-offs. One should note that the optimum cavity length for all three gases is approximately 2.1 cm, though the gases exhibit different behaviors as the length is changed. The common cavity length is due more to the microwave excitation frequency. As the frequency is lowered, the free space wavelength of the source increases, necessitating an increase in the cavity length. At a frequency of 2.45 GHz, discharges could not be sustained for a cavity length of less than approximately 1.5 cm.

Figure 4.25 shows that as the cavity length is increased, the gap must be increased and the distance between the coupling loop and cavity end plate must be increased to maintain the highest possible power match. This curve was obtained by adjusting the gap and probe position after each variation of the cavity length. The power match over the region shown varied from about 95% to approximately 50% at the longer cavity lengths (not shown).

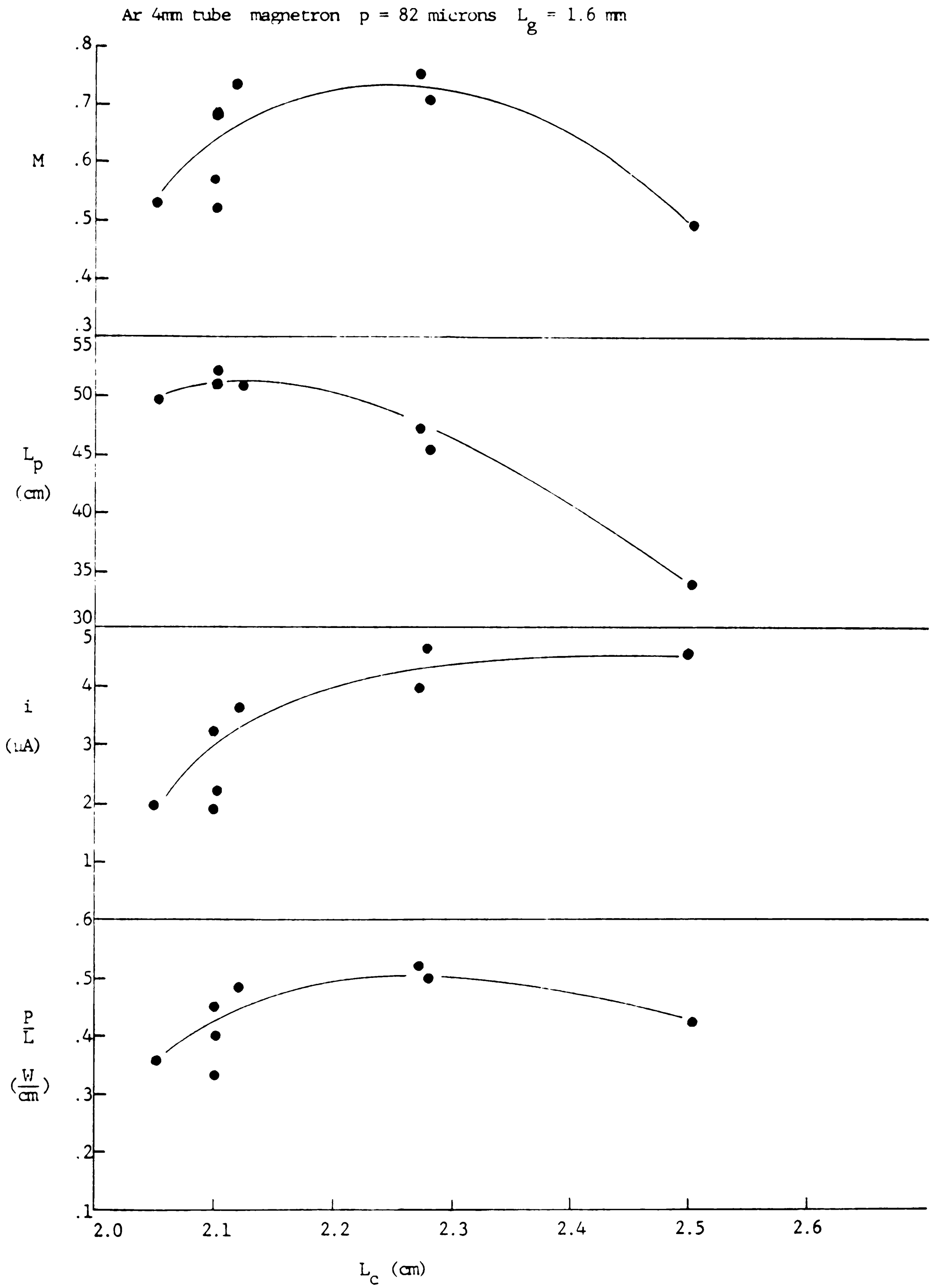

Figure 4.22 P/L vs. Cavity Length for Ar in the Coaxial Cavity

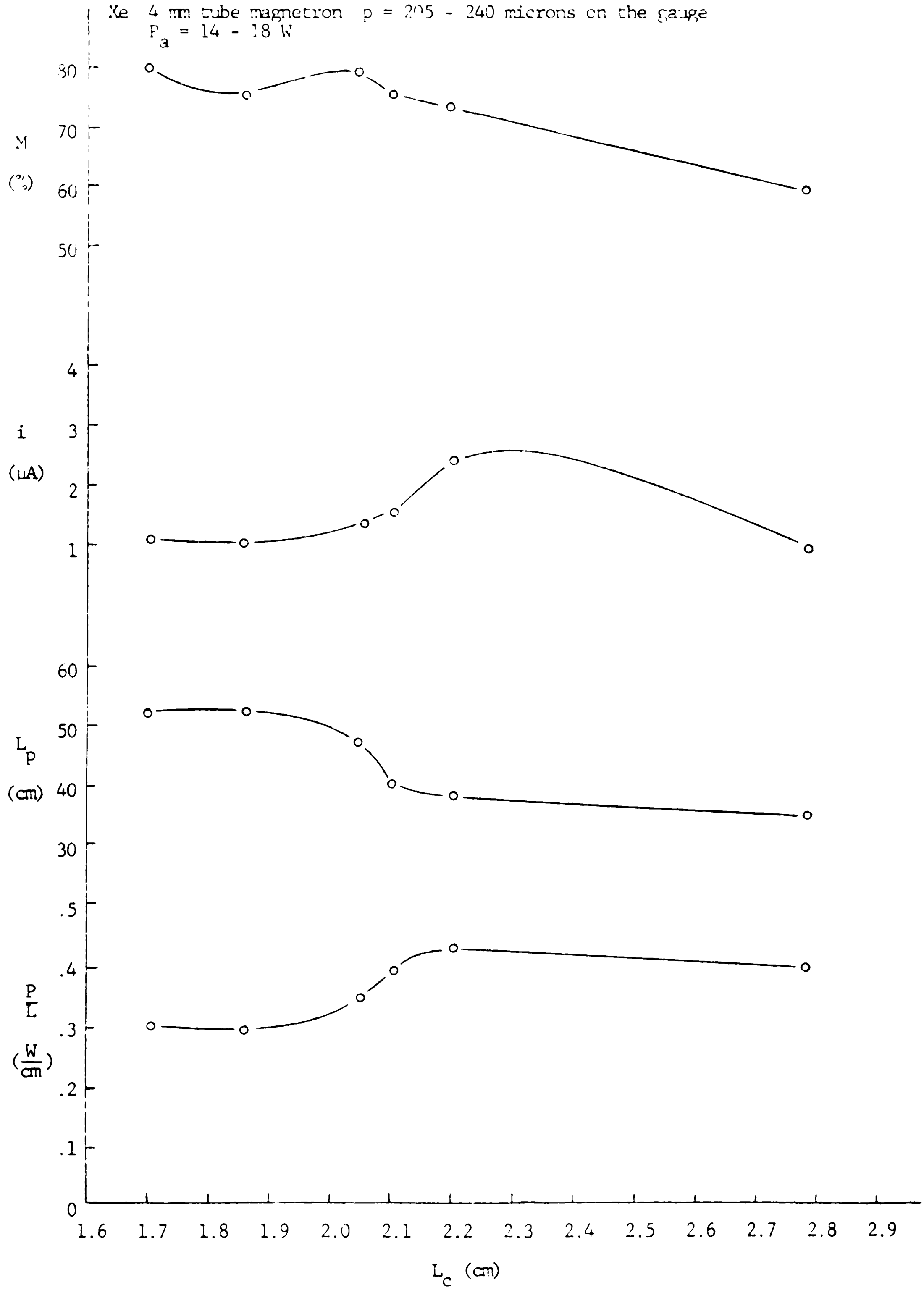

Figure 4.23 P/L vs. Cavity Length for Xe in the Coaxial Cavity

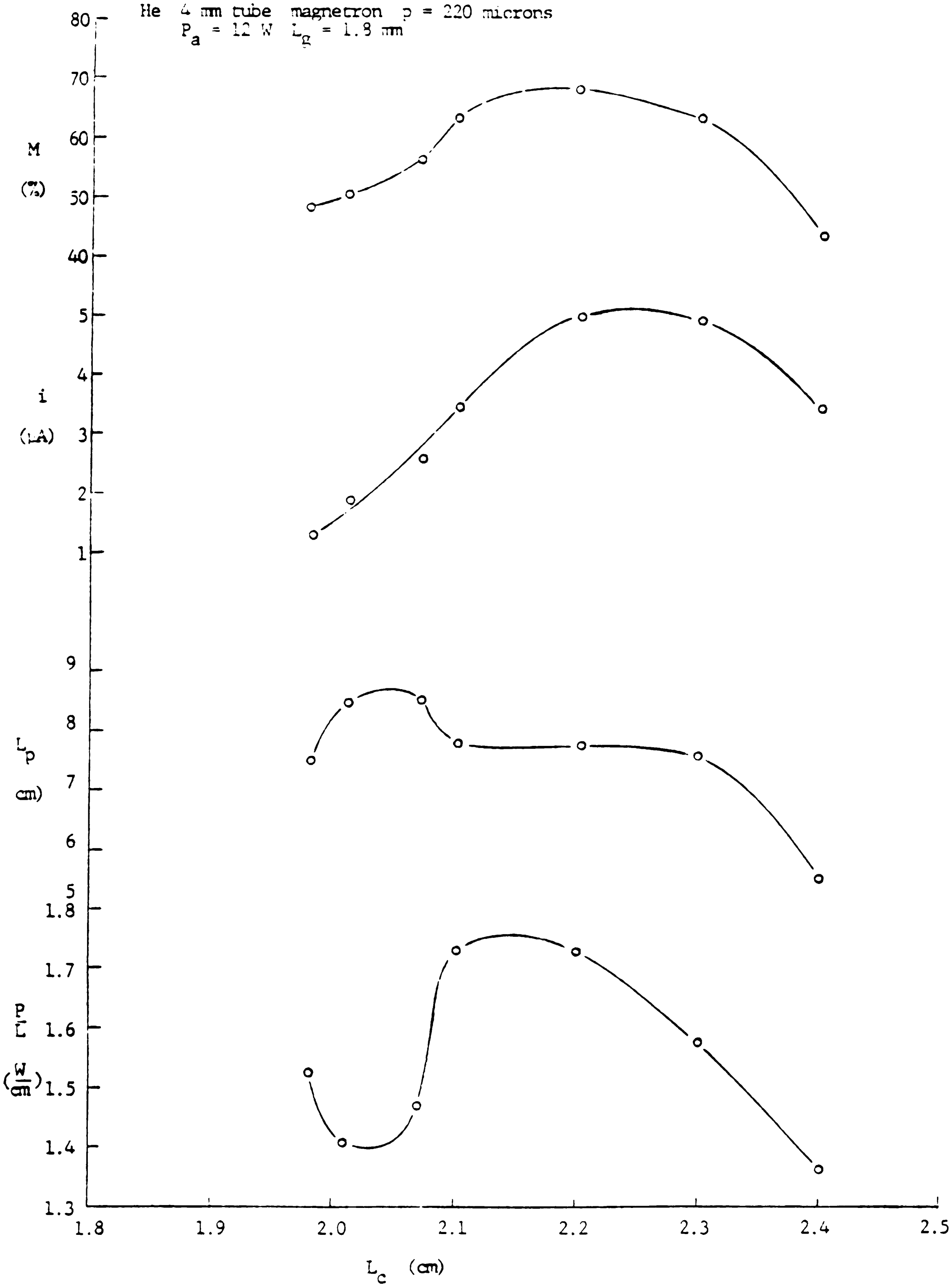

Figure 4.24 P/L vs. Cavity Length for He in the Coaxial Cavity

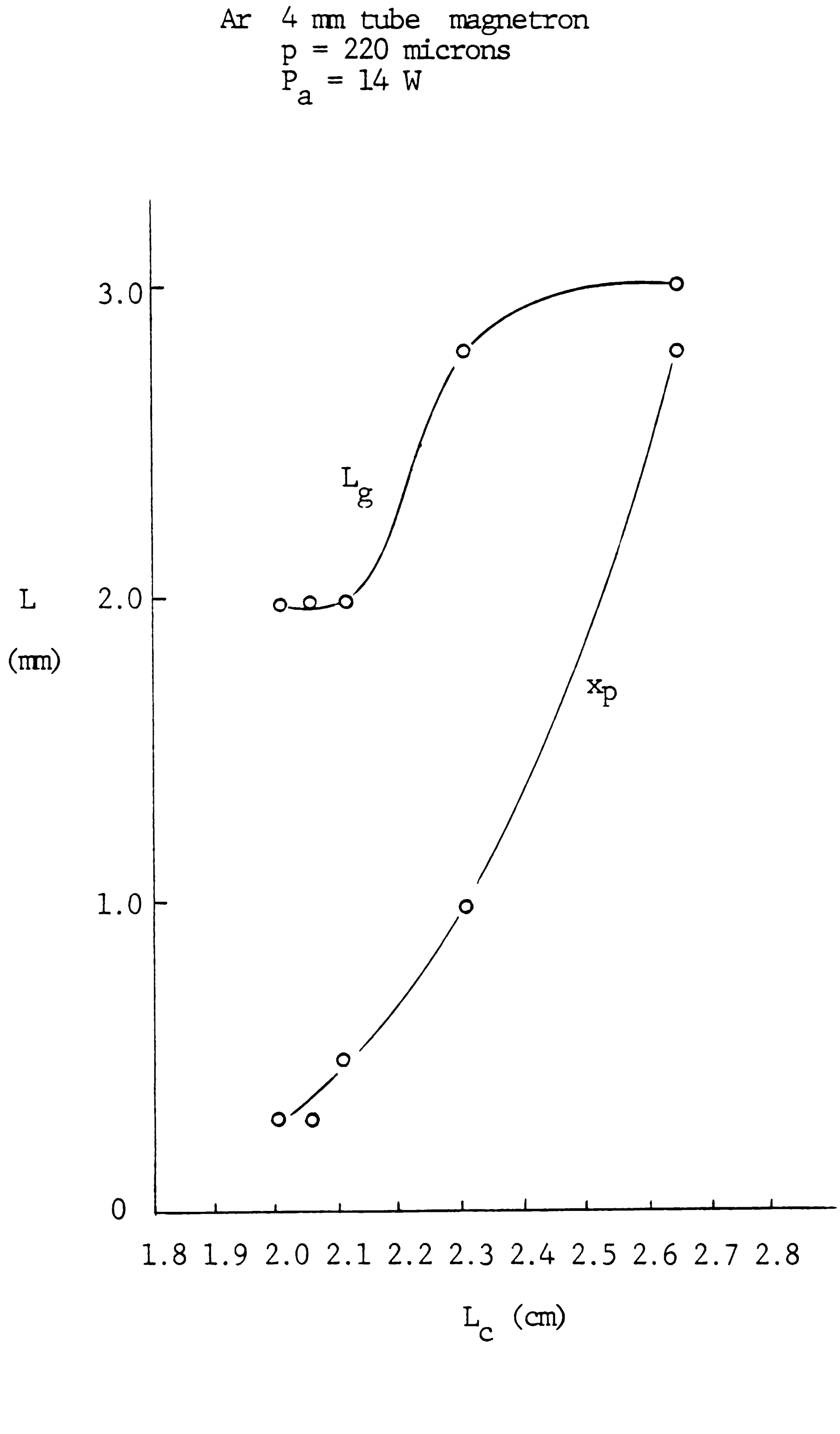

Figure 4.25 L_g, x_p vs. L_c for Best Power Match in the Coaxial Cavity

Figures 4.26 and 4.27 compare P/L vs. pressure curves for two orientations of the coupling probe. Since the probe was a circular loop, it could be oriented so that its magnetic field was radial or circumferential. The data were obtained by taking P/L vs. pressure curves as described in Section 4.2, that is, the cavity was adjusted for maximum power match and only the probe position, if anything, was adjusted as the pressure was varied. The curves labeled "radial H" were obtained by orienting the loop so that its plane was circumferential to the center conductor, causing the radiated magnetic field of the loop to be radially directed. The curves labeled "circumferential H" were obtained by orienting the loop so that its plane was radial, causing the radiated magnetic field to be circumferential around the center conductor.

Neglecting hysteresis effects, it appears that the radially directed magnetic field resulted in lower P/L, so all subsequent experiments were done with radially directed magnetic fields. However, the loop orientation yielding the lower P/L may mean that the plasma has a lower electron density than that produced by the other loop orientation with a higher P/L. Further investigation is needed.

A possibility exists that a loop size or shape can be determined that will optimize the coupling of energy into the plasma. The curves in Figure 4.28 compare a 5 mm by 7 mm rectangular loop with a 6 mm diameter circular loop, keeping the rest of the cavity geometry constant. After an experiment was performed, the cavity was disassembled and a new coupling loop was inserted. Then the cavity length and gap were reset to the previous values. In general, the circular probe gave a lower value of P/L than the rectangular probe. This is, however, a problem that could be studied in much more detail.

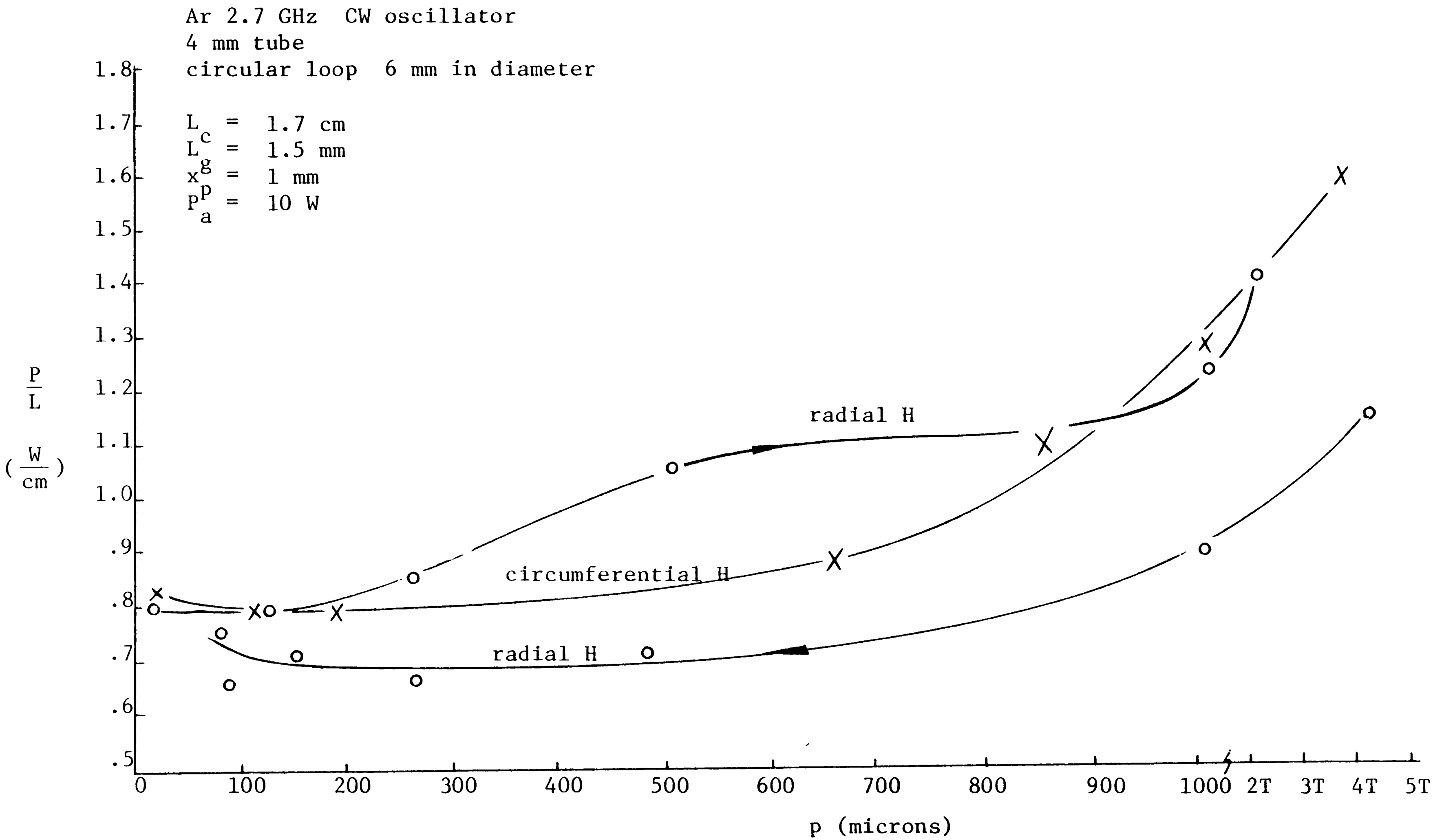

Figure 4.26 P/L vs. Pressure for Probes with Radial and Circumferential Fields in the Coaxial Cavity

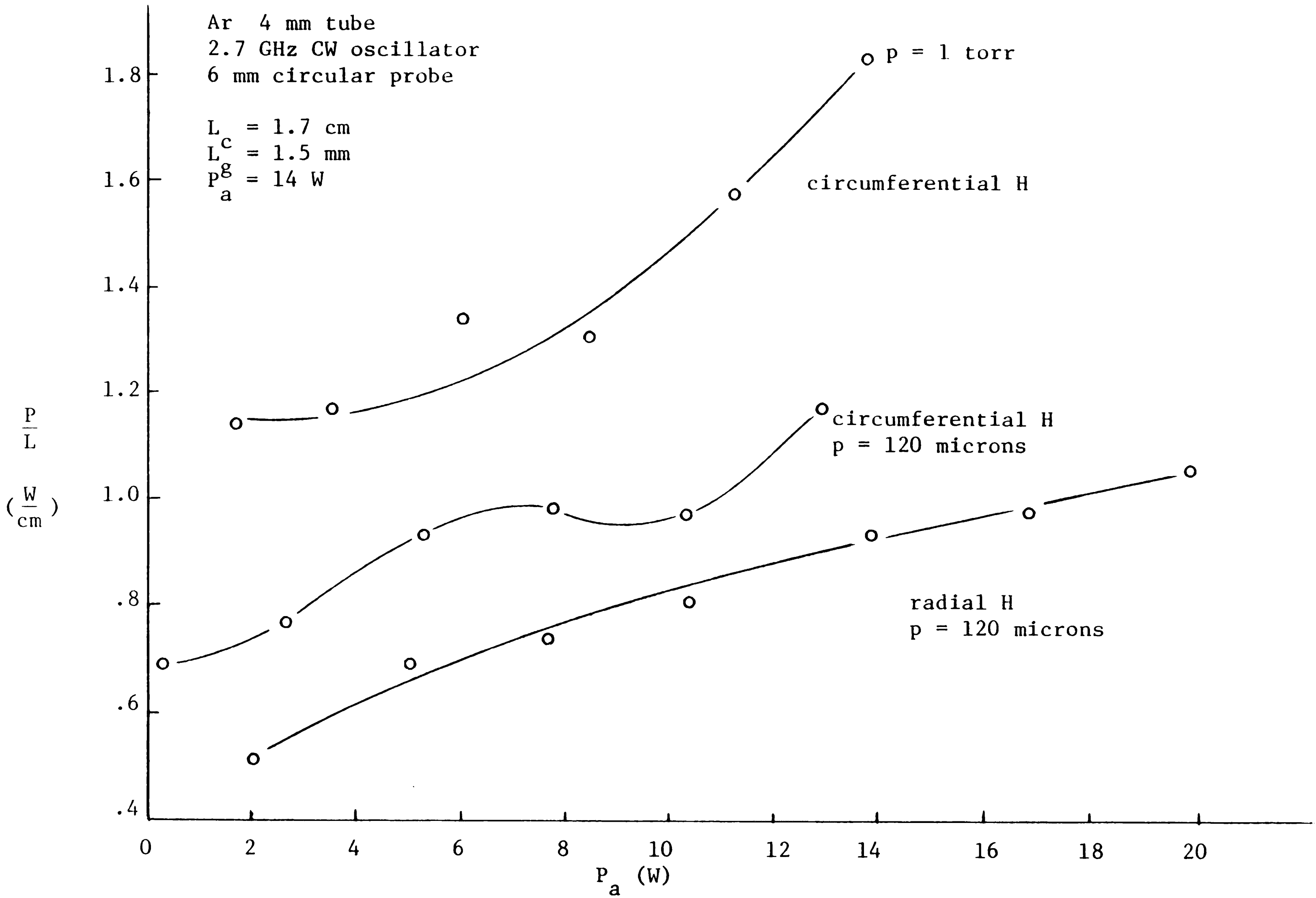

Figure 4.27 P/L vs. P_a for Circumferential and Radial H Fields in the Coaxial Cavity

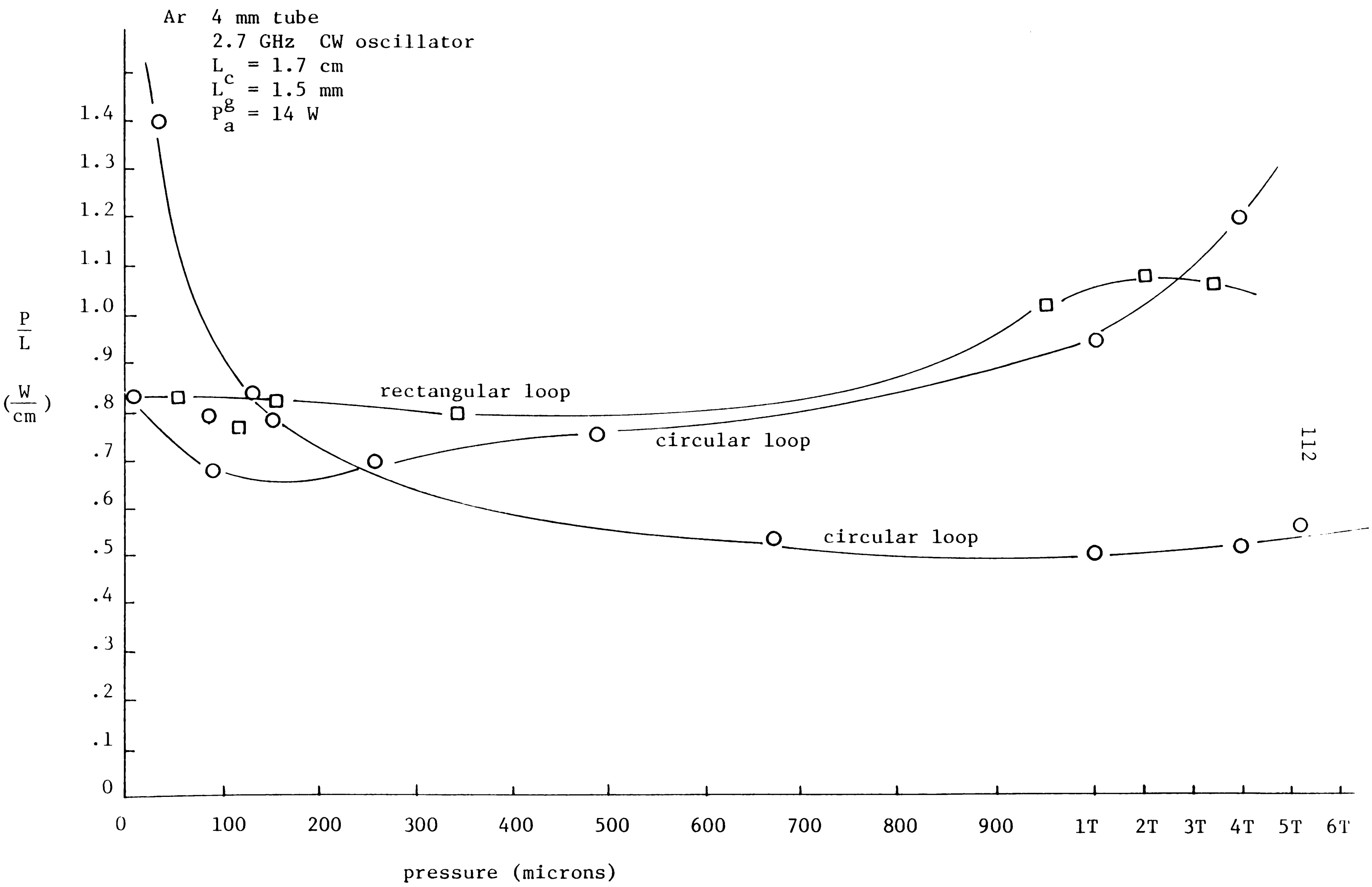

Figure 4.28 P/L vs. Pressure for Rectangular and Circular Loops in the Coaxial Cavity

In summary, examination of the experimental data shows that, for the frequency used, (1) there is a cavity length, gap and probe position at which the experimental discharge parameters can be maximized, though generally not simultaneously, (2) that all three are interrelated so that a change in one cavity parameter necessitates a change in the others to maintain optimum coupling of energy to the plasma (meaning a high power match), (3) that a circular loop appeared to provide better coupling than a rectangular loop of about the same area, and (4) that a radially directed field from the loop yielded lower P/L's than a circumferentially directed field. Finally, cavity geometry could be adjusted to produce a short, dense (bright) plasma or a longer, but less dense discharge, by operating the cavity in the appropriate regions for L_c (cavity length) and L_g (gap) as indicated by the curves.

4.8 P/L vs. Pressure: Cylindrical Cavity

While the studies done with the coaxial cavity provided a wealth of information, the cavity was limited to rf input powers of about 50 watts or less, because of arcing in the cavity or the microcoaxial input cable. Fortunately, a large cylindrical cavity was available in which experiments could be performed with incident rf power levels of up to 1200 watts (the maximum power output of the magnetron). This cavity was described in detail in Chapter 3. Experiments discussed in this section parallel those performed with the coaxial cavity with the same objective: to determine the variation of power match, plasma length, and P/L as functions of gas pressure.

The procedure used was similar to that of the coaxial cavity, except that there were fewer system variables. The quartz tube was evacuated and allowed to outgas, then the experimental gas was bled into the system, to a pressure of approximately 200 microns. Rf power was applied to the plasma-cavity system and the system was length tuned for minimum reflected power. The pressure was changed in small increments. If a pressure change resulted in a significant increase in reflected power, the cavity was retuned (length) before each reading. A Tesla coil was not needed for initiation of the discharge; breakdown occurred when the cavity length was properly adjusted.

In all of the curves to be presented in this section, the quartz tube was 10 mm in diameter (inner) and the excitation frequency was 2.45 GHz. The gases used were Ar and He. Absorbed power levels were approximately 125 watts and 385 watts for Ar and 100 watts and 210 watts for He.

The experimental curves for Ar are shown in Figures 4.29 and 4.30 for 125 watts and 385 watts, respectively. The power match and P/L were nearly constant over the entire range of 150 microns to 1.3 torr for "low" power and a range of 70 microns to 7 torr for the "high" power case. In both cases, the 113 cm quartz tube was entirely filled with the discharge.

He discharges did not fill the quartz tube and P/L exhibited a variation with pressure. The results are displayed in Figures 4.31 and 4.32. At an absorbed power of approximately 100 watts, power match increased from 60% to 97% as the pressure went from 225 microns to 750 microns. Discharges could not be sustained for pressures outside this region, at this power level. Plasma length decreased as the pressure increased and P/L appeared to be linear with pressure. At an absorbed power of about 220 watts, the discharge varied less with pressure than at 100 watts. Above 300 microns, the power match leveled off at 87%, plasma length

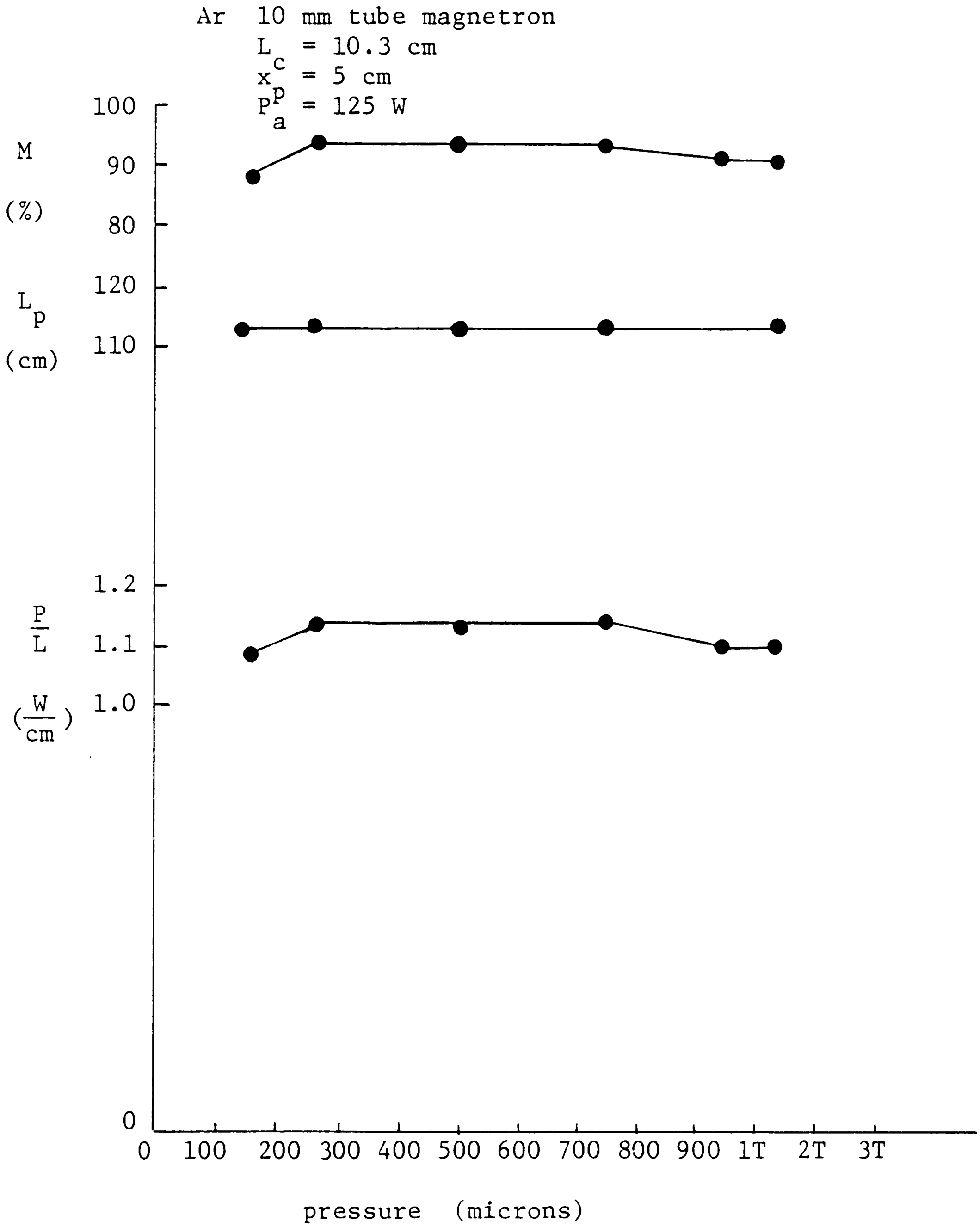

Figure 4.29 P/L vs. Pressure in the Cylindrical Cavity

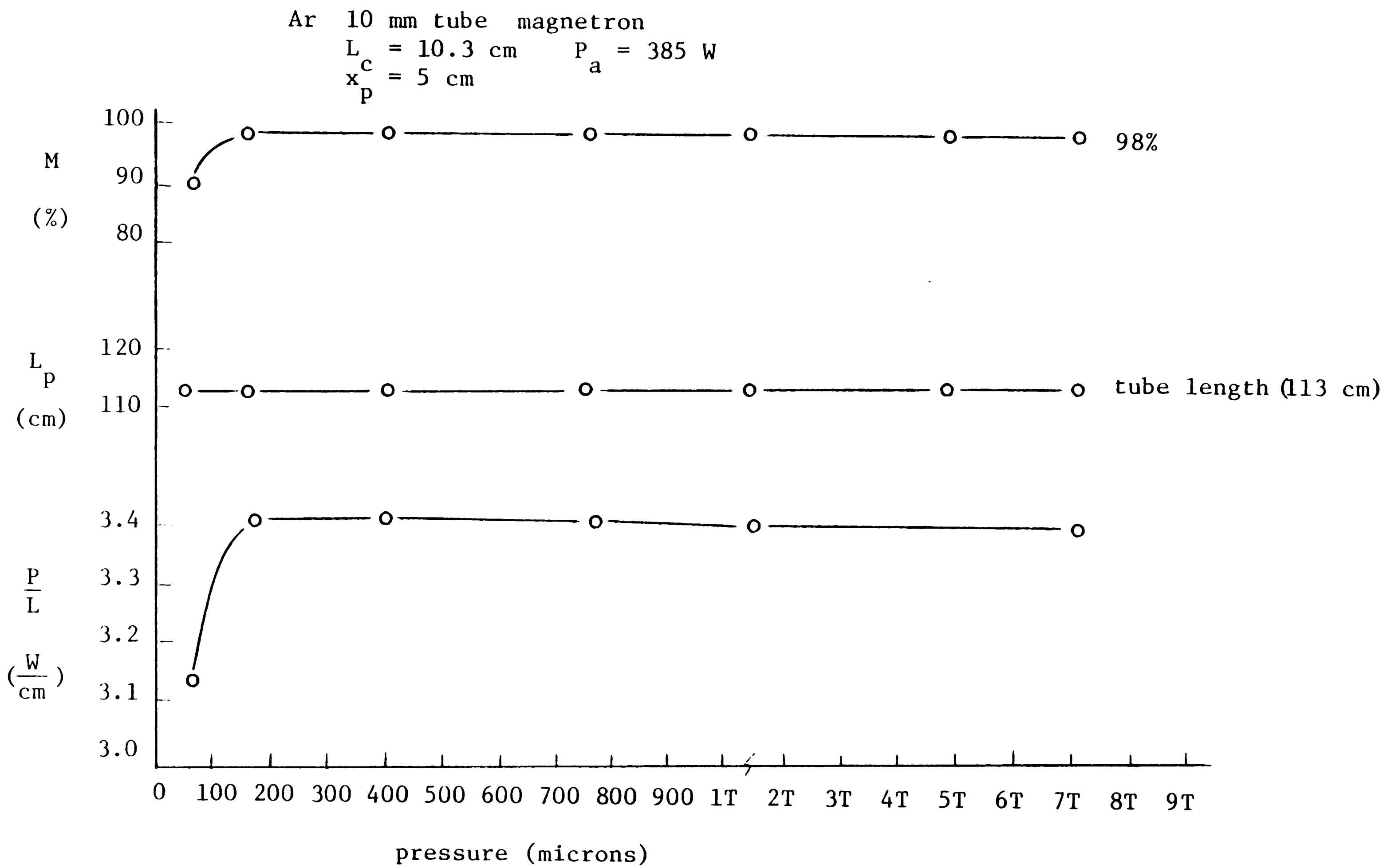

Figure 4.30 P/L vs. Pressure for Ar in the Cylindrical Cavity

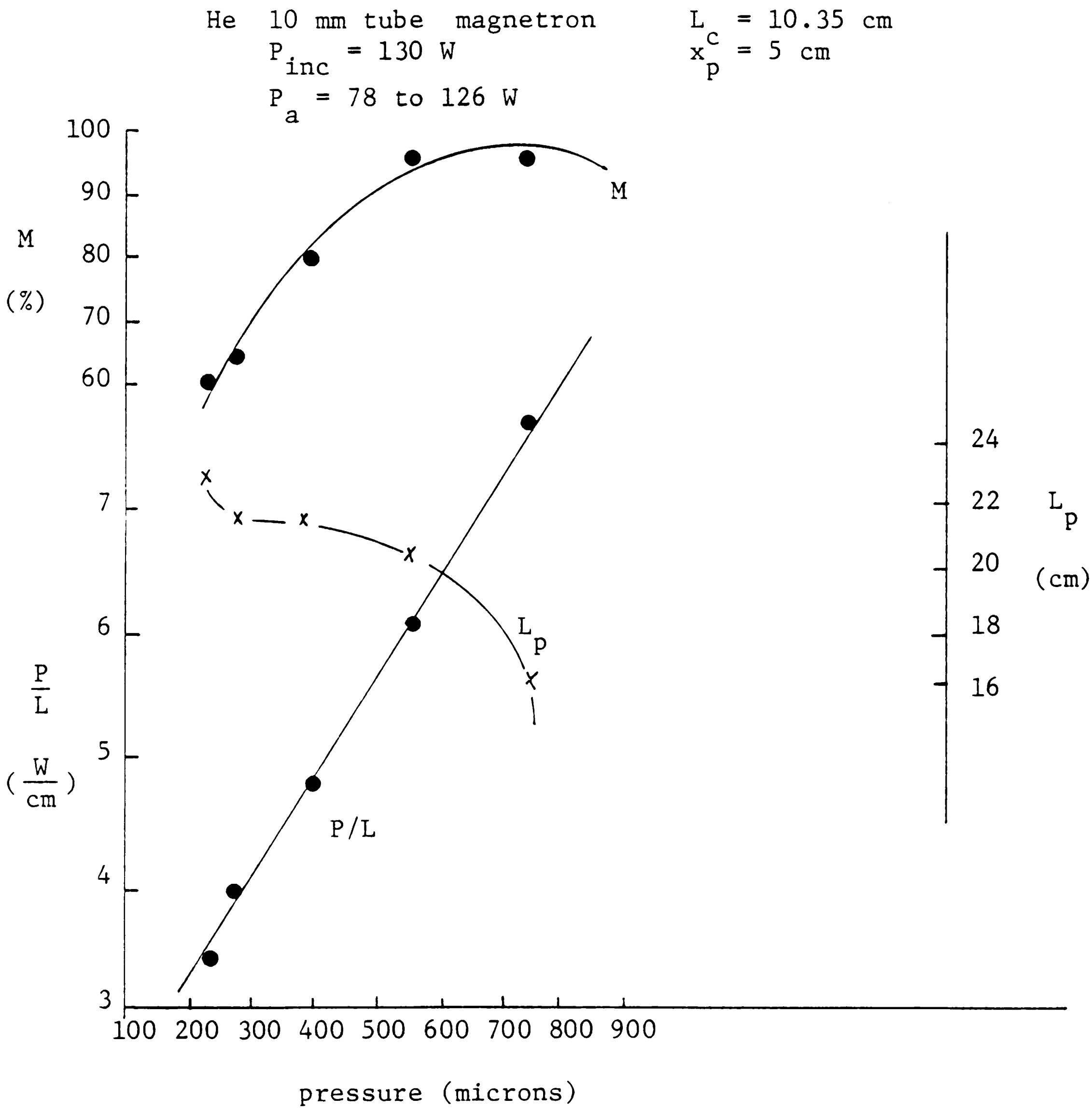

Figure 4.31 P/L vs. Pressure for He in the Cylindrical Cavity

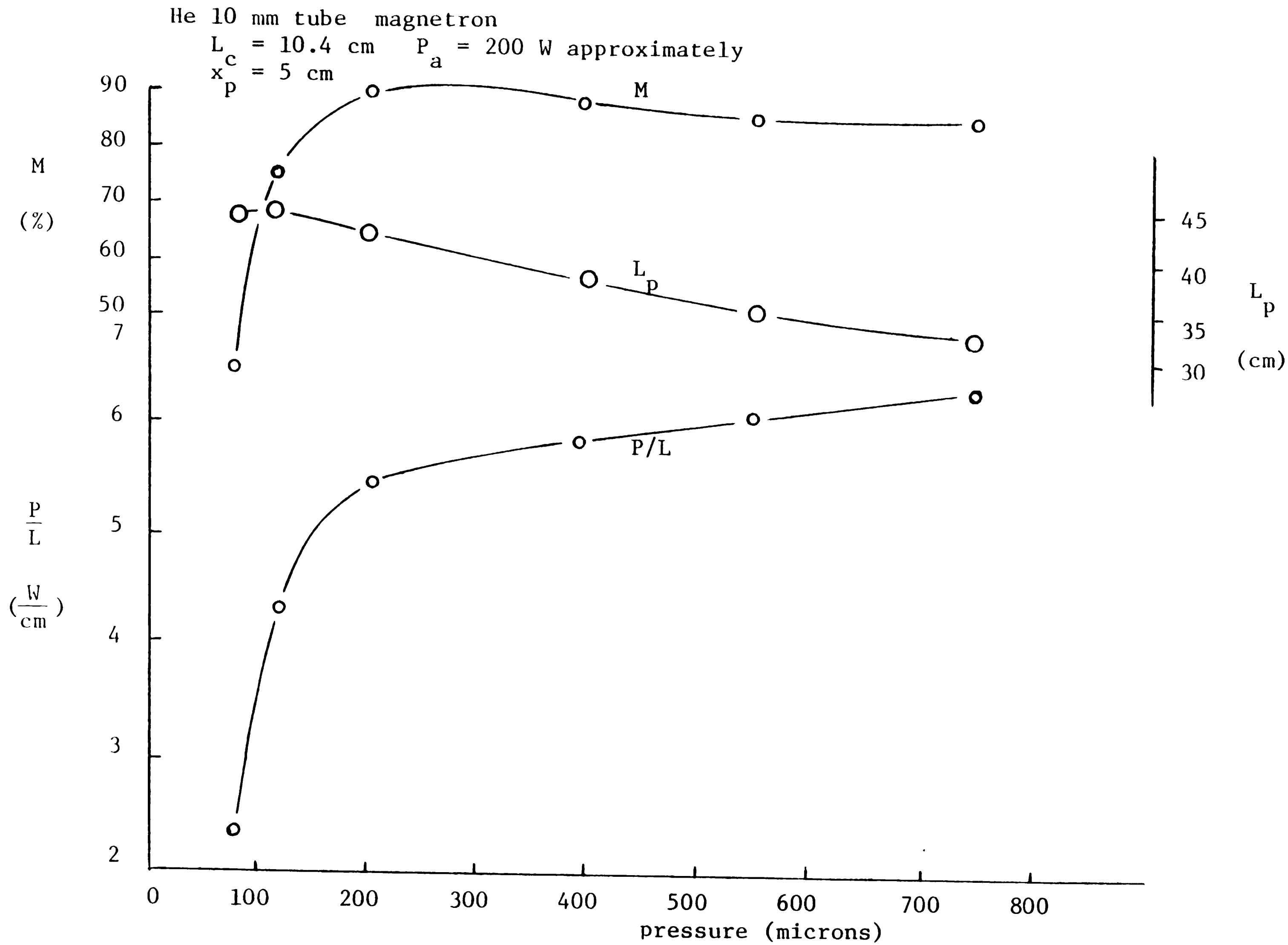

Figure 4.32 P/L vs. Pressure for He in the Cylindrical Cavity

gradually decreased from 45 to 34 cm and P/L began to "saturate" at 5 to 6 W/cm, as the pressure continued to increase.

4.9 P/L vs. Absorbed Power: Cylindrical Cavity

As with the coaxial cavity, experience showed that the absorbed power per unit length of discharge varied with the amount of absorbed power. In order to compare experimental results from one experiment to another, it is desirable to determine how the P/L depends on the power absorbed.

The method of creating the plasma was the same as that described in the previous section, with the length of the cavity adjusted for the best power match. In general, an increase in the incident power to the cavity did not affect the reflected power significantly. When it did, the length of the cavity was retuned to minimize this reflected power.

A 10 mm inner diameter tube was used with the magnetron as the power supply. Ar was used at a pressure of 225 microns, He pressure was 210 microns. The Ar discharge in the cylindrical microwave cavity generally had a linear P/L curve, as shown in Figure 4.33. This was an unavoidable result, since absorbed power levels of 100 watts would fill a 4 foot quartz tube. When the input power was increased, the plasma could not expand. Thus, P/L increased, since the power match was relatively constant at 90% or greater. This linearity is similar to that observed in the coaxial cavity, but the plasma did not generally fill the quartz tube for that cavity. The results of the same study performed with He as the experimental gas are shown in Figure 4.34. Power match became significant at about 100 watts, the increase in plasma length is almost linear and P/L varies as P_a^n, where n is less than unity.

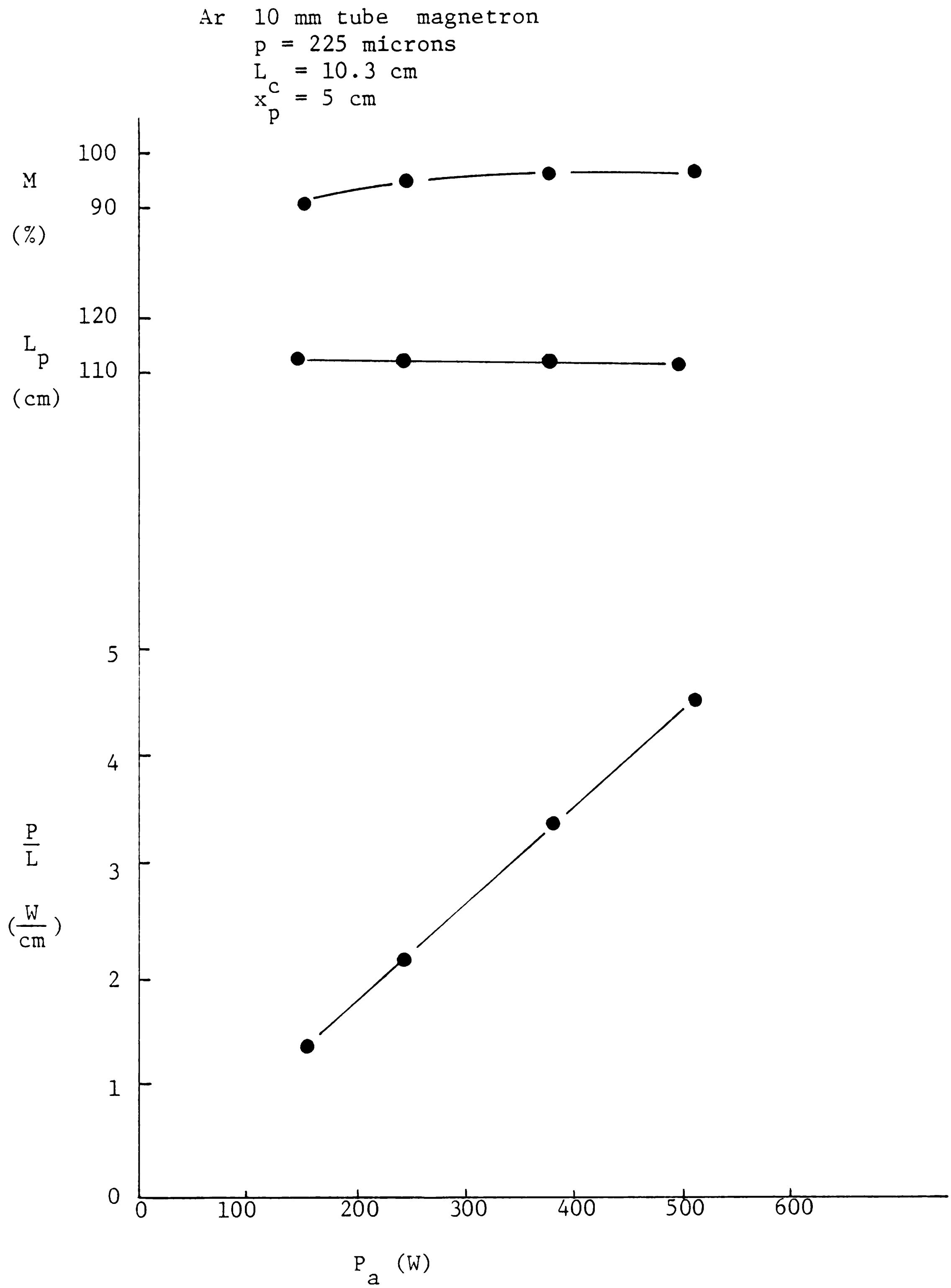

Figure 4.33 P/L vs. Absorbed Power for Ar in the Cylindrical Cavity

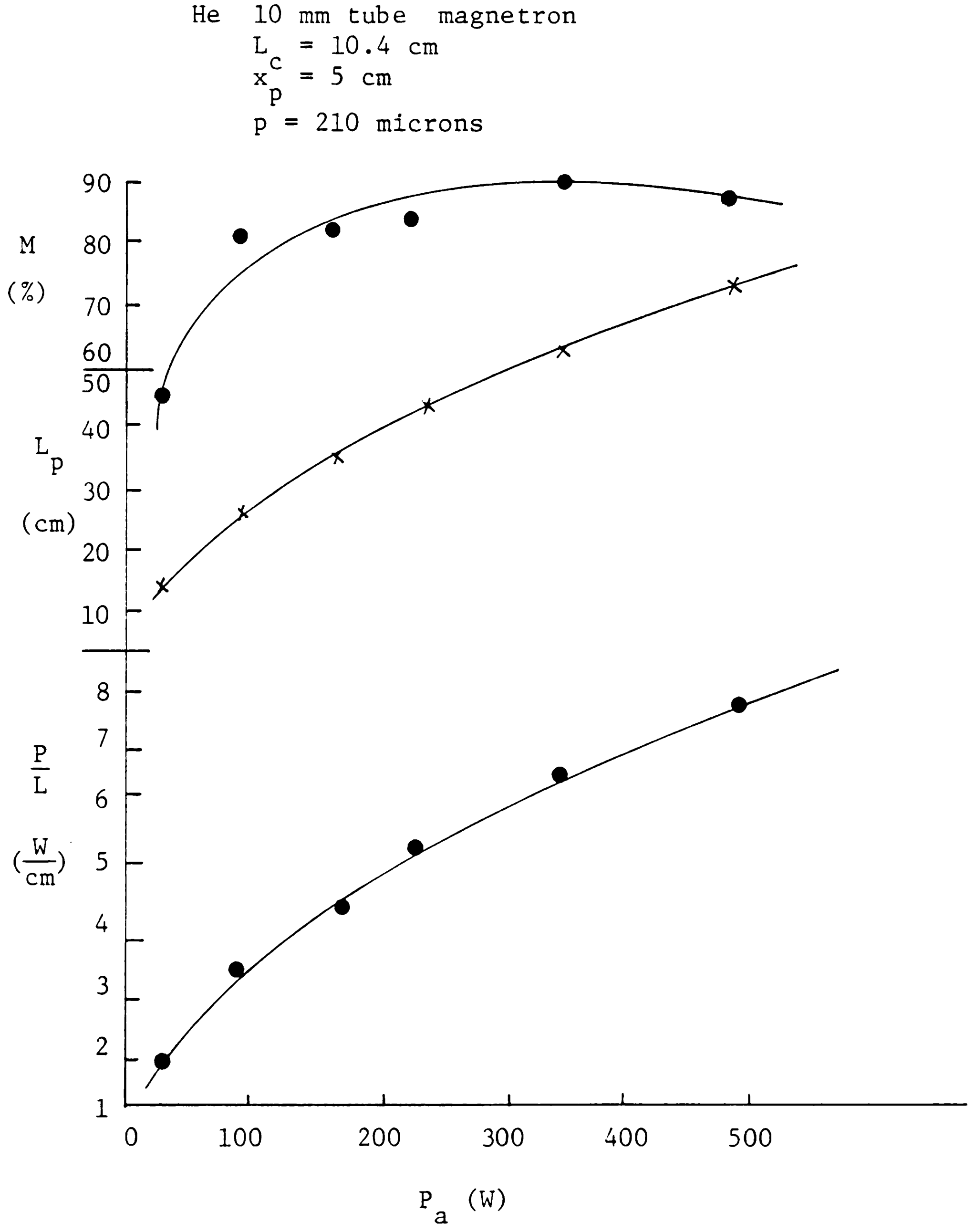

Figure 4.34 P/L vs. Absorbed Power for He in the Cylindrical Cavity

Because experiments were performed with two different cavities and one of the objectives of these studies was to create an efficient plasma source, a comparison was made between results from the coaxial cavity and those from the cylindrical cavity. See Figure 4.35. A 7 mm tube was used in both cavities. The experimental gas was Ar. In the coaxial cavity the pressure was 200 microns, while the pressure in the cylindrical cavity was 225 microns. The slope of the line for the cylindrical cavity is .008 cm^{-1} and that of the coaxial cavity is .0175, a little more than twice as large. Within their respective power ranges, the cylindrical cavity appears to couple energy more efficiently into the plasma surface wave, and can be used at much higher power levels than the coaxial cavity. However, if P/L is proportional to the plasma density for a given tube diameter, higher P/L may mean that the coaxial cavity may create a plasma with a higher density. Actual plasma density measurements should be made to study these effects further.

4.10 P/L and Power Density vs. Tube Diameter: Cylindrical Cavity

As with the coaxial cavity, it was decided to determine how the P/L and power density of the surface wave discharge depend on plasma density. Results reported in the literature are obtained with tubes of different sizes, and it is known that the tube diameter does affect the propagation of the surface waves along the tube. Thus, P/L, power density, plasma length and power match will be measured as functions of the tube diameter. The experimental curves will also show the corresponding data points of the curves from the coaxial cavity for comparison.

The data were obtained by running P/L vs. pressure and P/L vs. absorbed power curves for 7, 10 and 14 mm diameter tubes. The experimental

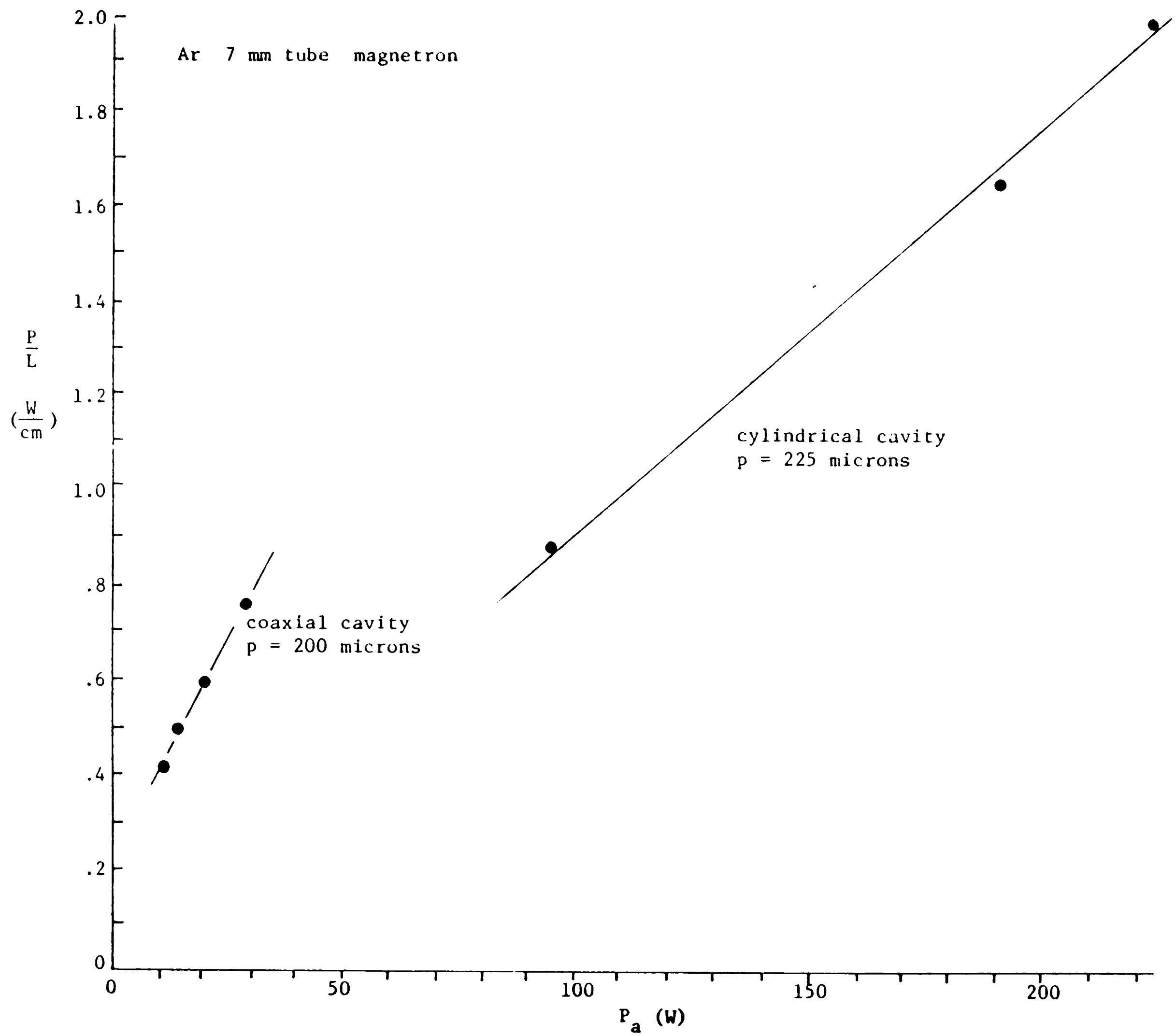

Figure 4.35 P/L vs. P_a for Ar in the Coaxial and Cylindrical Cavities

gases used were Ar and He. For each gas data for all three tubes were plotted on the same graph. For example, in the P/L vs. pressure curves, the points for all three tubes were plotted on the same set of axes. Since each tube had an absorbed power of about 200 watts, the values of P/L at 200 microns were read from the graphs and plotted on Figure 4.36, for Ar. The similar procedure was used to obtain the points in Figure 4.37 for He. Note that the 7 and 10 mm tubes were 113 cm long, while the 14 mm tube was only 110 mm long. This means that when all three tubes become filled with plasma at the same absorbed power, the P/L for the shorter tube will necessarily be higher than for the longer tube.

Looking at the first curve, for Ar, one can see that the power match decreased slightly as the tube diameter increased, using only the 200 watt curve. (This may be due to a coupling problem, i.e., it may be possible to couple more energy into the surface waves if the cavity geometry and tube position are adjusted properly.) All three tubes were completely filled with the Ar discharge. The power density decreased as the tube diameter increased, though it is considerably larger for the 7 mm tube than for the other two, which are nearly equal. Finally, the absorbed power per unit length is approximately constant. This is due to the fact that the tubes were filled with plasma and the absorbed power was the same for all three tubes. Aside from the power density being about twice as large for the 7 mm tube as for the other two, power match, plasma length, and P/L change very little with different tube diameters for tubes from 7 to 14 mm.

For purposes of comparison, points from the coaxial cavity are shown on this graph. They are the 2 mm, 4 mm, and 5 mm points, taken at a pressure of 200 microns and 20 watts of absorbed power. (These are from

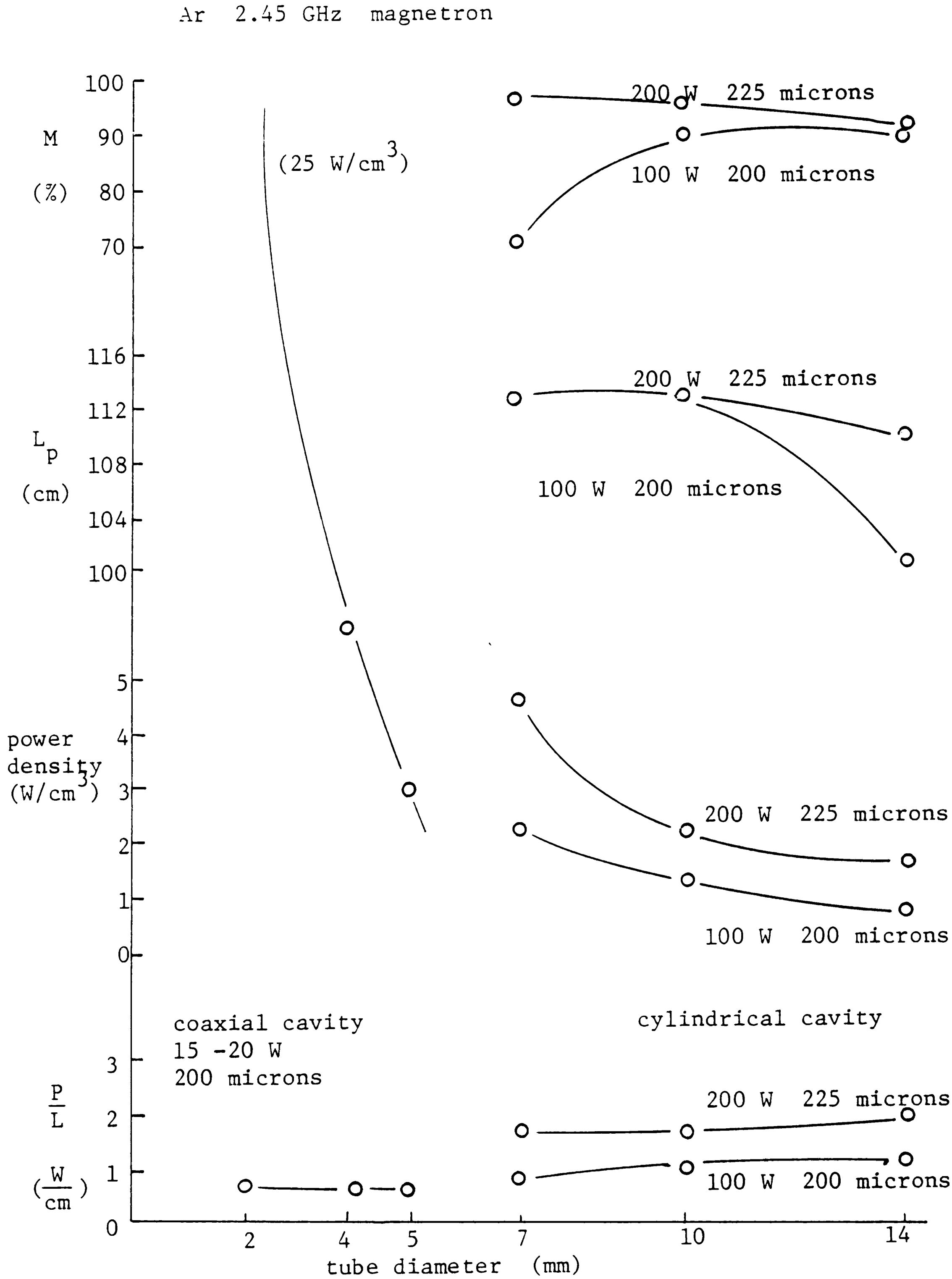

Figure 4.36 P/L vs. Tube Diameter for Cylindrical and Coaxial Cavities with Ar

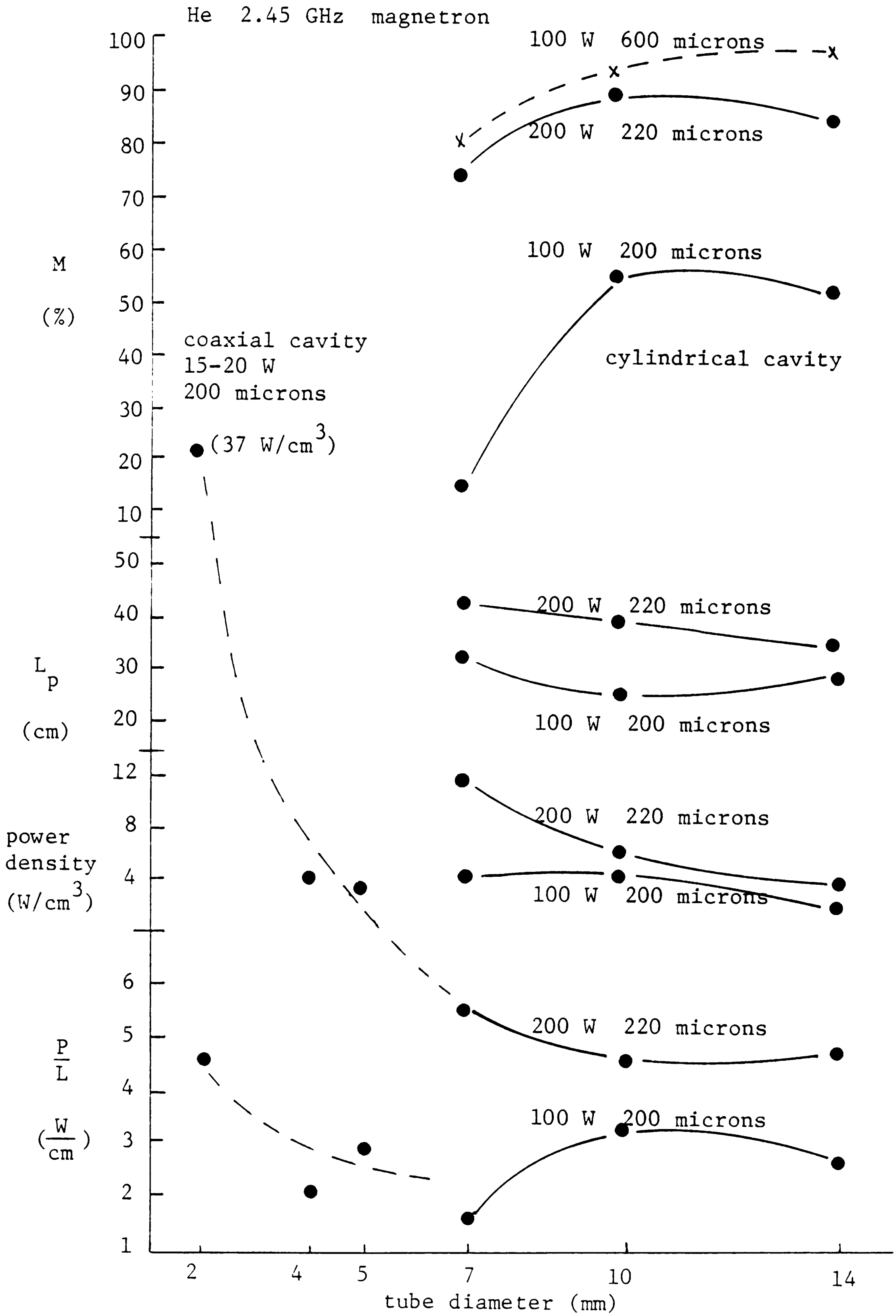

Figure 4.37 P/L vs. Tube Diameter for He in the Cylindrical and Coaxial Cavities

the Ar curve in Section 4.4.) P/L is a factor of 2 to 4 smaller for the tubes in the coaxial cavity, depending on the absorbed power, but the power density increases dramatically with smaller tube sizes, even though the absorbed power for the coaxial cavity was only about 1/10 of that in the cylindrical cavity.

The He curve, Figure 4.37, was also taken at 200 watts absorbed, and a pressure of 220 microns, which is similar to the Ar conditions. The power match was lowest for the 7 mm tube, and slightly higher for the 10 mm tube as compared to the 14 mm tube. Plasma length decreased almost linearly with increases in tube diameter. As with Ar, the power density is higher in the 7 mm tube and nearly equal in the 10 and 14 mm tubes. P/L was slightly lower in the 10 mm tube than in the 14 mm tube; the 7 mm tube had P/L about 30% higher than the others, for the 200 watt curve. The 200 watt curve is considered here because the power match is much higher than that for the 100 watt curve.

From the He curve of Section 4.4, data points were taken at 200 microns. The absorbed power was approximately 20 watts. These points are shown on Figure 4.37. P/L is approximately the same in the coaxial cavity (slightly higher in the 2 mm tube) as in the cylindrical cavity, but power densities are much higher for the smaller tubes.

Though the points are not shown on the experimental curves, power matches for the Ar and He discharges in the coaxial cavity were generally 80% or greater. Overall then, one could conclude that power match, plasma length and P/L depend on the tube diameter to some degree, and that the power density of the plasma in the tube is strongly dependent on the tube diameter. The comparison of P/L vs. tube diameter for the two cavities is open to question because of the large difference in absorbed powers.

4.11 Plasma Density Measurements from Standing Waves: Cylindrical Cavity

An important plasma parameter frequently discussed in the literature is the plasma electron density. Methods of measuring electron density have been known for many years and most involve the use of probes, microwave cavities or interferometers, or spectroscopic analysis based on the intensity of the light emitted from the discharge. The method described in this section is simple and requires only a meter stick and perhaps a photodiode circuit as described in Chapter 3. When standing waves can be observed in the discharge, plasma densities of a high power rf surface wave discharge can be measured.

Under a wide range of experimental conditions in the cylindrical cavity system, a standing wave pattern can be seen along the plasma tube. The tubes used in these experiments had metal flanges on the ends (for attachment to the rest of the vacuum system) that would reflect surface wave energy coming from the cavity and travelling along the plasma surface. As is well known, waves travelling in opposite directions interfere with each other. This interference manifested itself as a series of bright regions of several centimeters separated by regions of about 1 cm that were not as bright, similar to the nodes and antinodes of standing waves on a vibrating string.

If the distances between the "nodes" can be measured accurately (as with the variation of photodiode response along the tube) the wave length of the standing surface waves can be determined as twice the node-to-node distance. With the tube diameter, excitation frequency and a normalized dispersion diagram as presented in a paper by Zakrzewski (21), an approximate value of the plasma electron density can be calculated. The dispersion diagram is similar to the one discussed in Chapter 2 in relation to the Gould-Trivelpiece mode. An example is given in Figure 4.38, from Zakrzewski.

The variation of discharge light intensity as a photodiode was moved along the 7 mm tube is shown in Figure 4.39. In the calculation shown, distance was measured from antinode to antinode simply because there were four antinodes and only three nodes. The wave length was determined from the graph to be 9.4 cm (average). From the wave length, the propagation constant, k, can be determined. With the tube radius, a point on the horizontal axis of the dispersion diagram can be found. The appropriate point on the curve is then located, and ω/ω_p can be read from the graph, allowing one to determine the plasma frequency and thus, the plasma density. Experimental values of the wave length for the figure indicate that the plasma density is approximately 2×10^{12} cm^{-3}.

This experiment was repeated for five pressures and power levels to determine the variation of plasma density along the quartz tube, measured from the coupling probe inside the microwave cavity. See Figure 4.40. The density is found to vary spatially along the tube, but the highest values are near the end of the tube, adjacent to the metal flange, and in the region close to the bottom of the microwave cavity. Finally, the lower power, lower pressure plasma exhibits minimal spatial density variation, as compared to those at higher pressures and higher powers. This method should be investigated further by comparing these measurements with densities obtained from other methods, such as microwave cavity frequency shift, etc. Also, plasma density vs. absorbed power should be investigated.

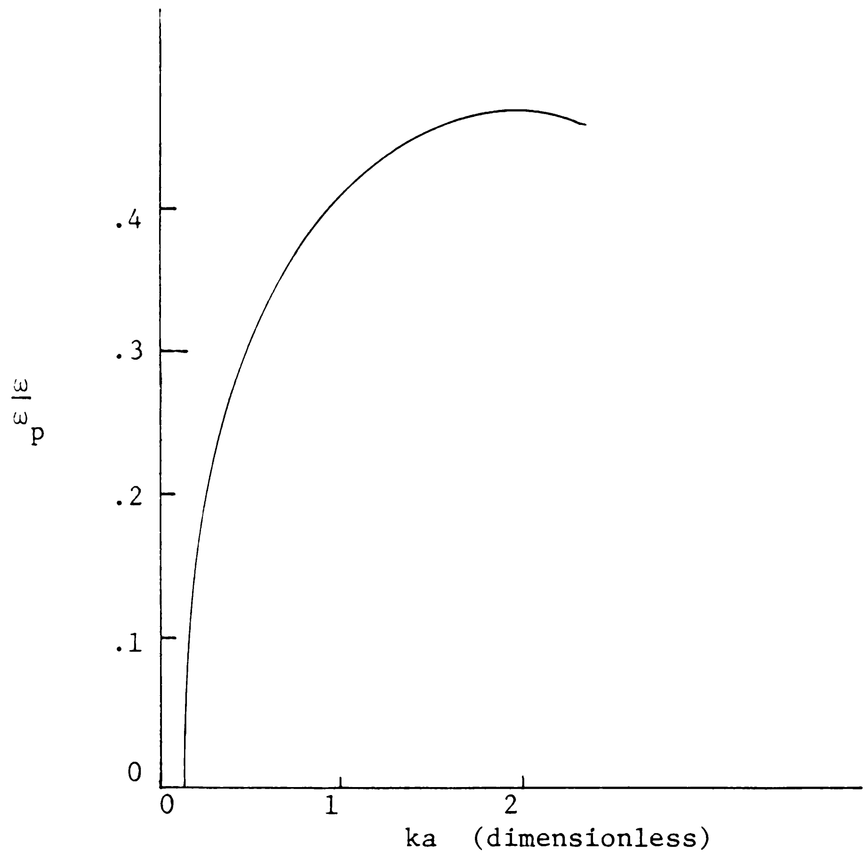

Figure 4.38 Normalized Dispersion Diagram for the Gould-Trivelpiece Surface Wave Mode

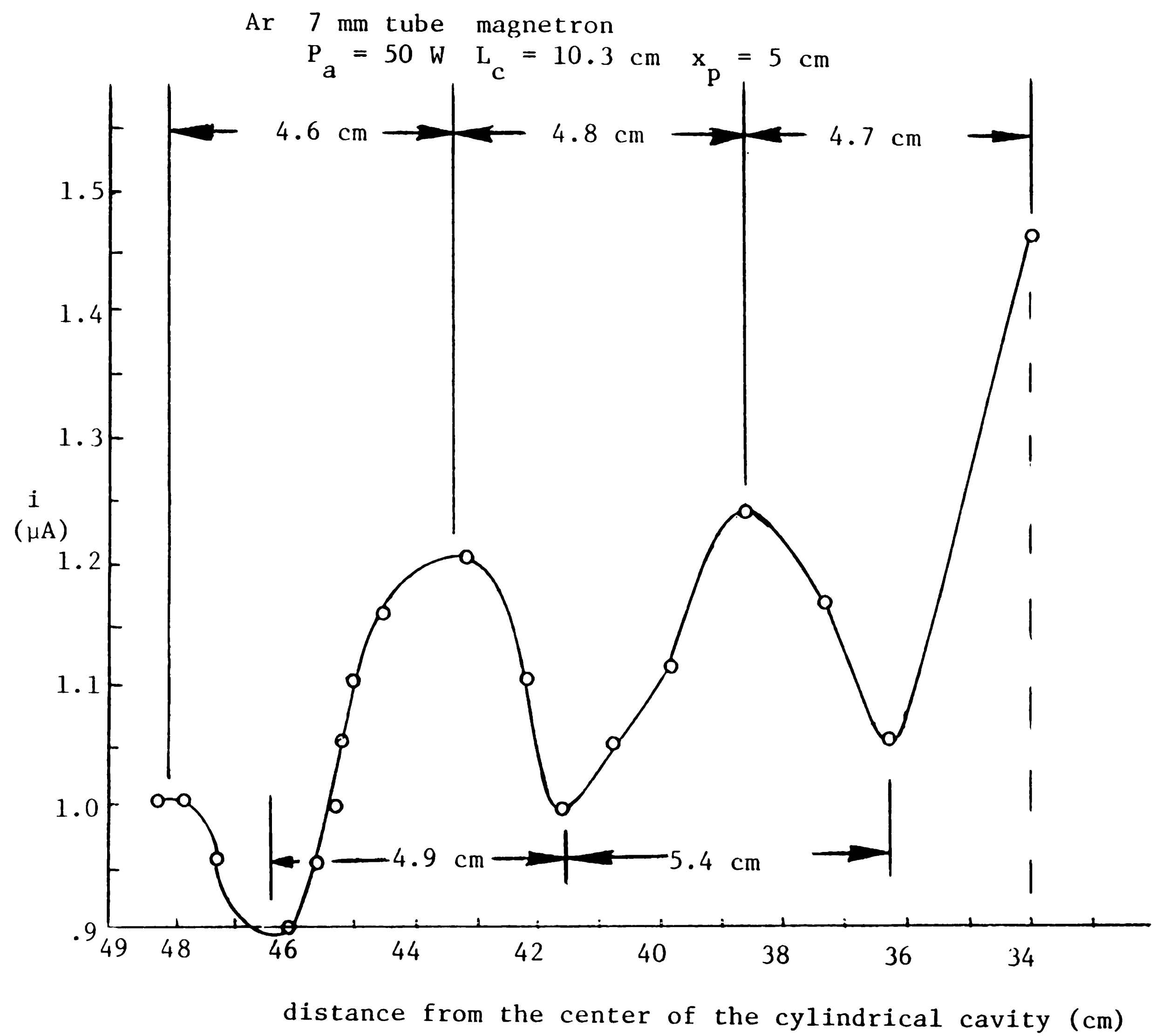

$a = .35$ cm

$k = 2\pi/\lambda = 2\pi/9.4$ cm

$ka = .234$

$\omega/\omega_p = .2 = f/f_p$

$f_p = f/.2 \simeq 10^4\sqrt{n}$

$n = (10^{-4}\ f/.2)^2$

$\simeq 2 \times 10^{12}\ cm^{-3}$

Figure 4.39 Variation of Light Intensity along the Plasma Tube

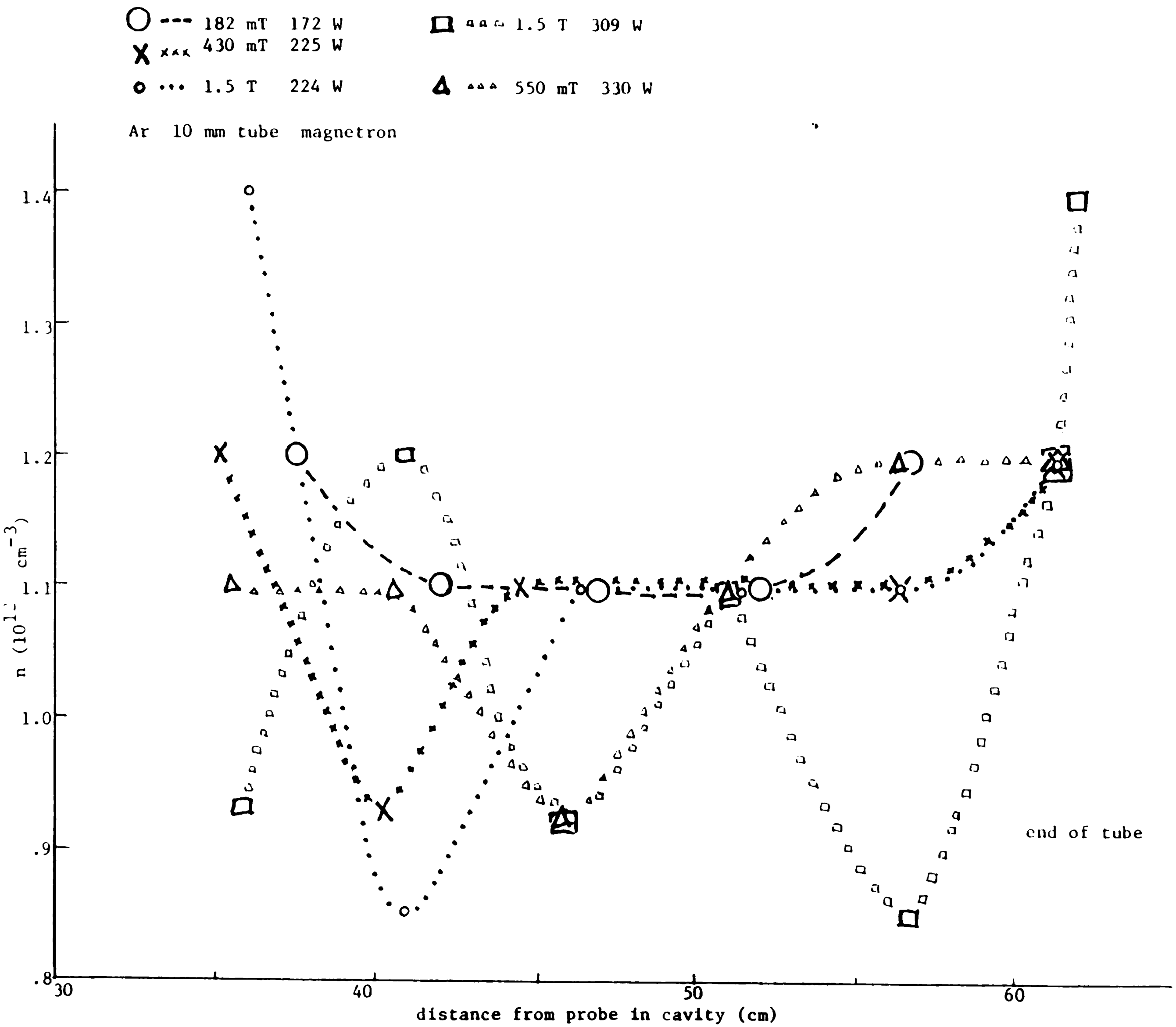

Figure 4.40 Spatial Variation of Electron Density Along the Plasma Tube in the Cylindrical Cavity

4.12 Optical Spectrum of an RF Argon Surface Wave Discharge in the Cylindrical Cavity

With any light source, the optical spectrum is of interest, especially if the possibility of discrete transitions exists for a glowing gas (as opposed to a continuous black body spectrum). Looking into the end of a discharge tube, an optical spectroscope was used with a diffraction grating of 600 lines/mm to measure the wave lengths of the lines of the Ar spectrum. The experimental arrangement is discussed in Chapter 3.

The tube that was used for this experiment was 113 cm long and had a 7 mm diameter. The wavelengths of the spectrum were determined when the gas was not flowing, the pressure was 285 microns and the absorbed power was 200 watts. Higher powers and flowing gases produced many spectral lines, none of which was particularly intense, though some were brighter than others. In addition, a continuous spectrum was superposed over the discrete lines. When the vacuum system was isolated from the pump so that there was no significant flow in the gas, this continuous background was absent, leaving only a few bright lines.

Ten or twelve very distinct lines could be observed. Only those in the blue end of the spectrum were of interest in this investigation, though wave lengths for an orange line and a red line are included in the table to indicate that lines from the entire visible spectrum were present. The observed wave lengths are shown in Table 4.1. These wave lengths were determined from the diffraction grating equation, $d\sin\theta = n\lambda$, where d is the grating spacing, θ is the angle at which the line is observed, n is the order of the line and is equal to unity for these readings, and λ is the wavelength of the light. λ and d have the same dimensions. A source of known wave length was used to determine d, when θ is measured. Then the source is changed and the wave lengths of its spectrum can be determined.

Table 4.1 Bright Lines in the Spectrum of an RF Argon Discharge

Color	Wave Length Right of Center	Wave Length Left of Center	Wave Length Average
Violet	4219.9	4238.7	4229.3
Violet	4290.2	4294.9	4292.6
Violet	4365.1	4369.8	4367.4*
Blue	4547.3	4552	4549.6*
Blue-Green	4896	4877.5	4886.8*
Orange	6108	6076.8	6092.6
Red	6654.7	6463.1	6558.9

The lines of most interest are the 4367 A, 4550 A, and 4887 A lines, marked with an asterisk. These correspond to observed lines of Ar^+ lasers (4370 A, 4550 A, and 4880 A). These three lines were also observed in flowing discharges at pressures of 100 to 250 torr approximately, with absorbed power levels of 400 or 500 watts. However, they were of the same intensity as about fifteen other lines.

The conclusion then, is that, by microwave excitation, lines corresponding to those observed in Ar^+ lasers are present in the discharge. The possibility of creating a laser excited by microwave energy exists if the optical cavity is properly designed, since the necessary optical transitions are present.

4.13 Two Cavity Excitation: Coaxial Cavities

Experiments with the coaxial cavity showed that the P/L of a discharge generally increased as the absorbed power increased. One of the objectives of the experiments was to find an efficient means of coupling energy into the surface waves, thus, the possibility of using two cavities was suggested. Both would be on the same quartz tube, but operating at lower powers. In other words, would two cavities at 20 watts each (on the same tube) yield lower values of P/L than one cavity at 40 watts. Or perhaps the absorbed power in two cavities would be the same as for one cavity, but the plasma would be longer.

The discharge was produced using the circuit shown in Figure 3.10. The method of operation was the same as in other coaxial cavity experiments: evacuate the tube, adjust the cavity geometry, bleed the gas into the tube at about 150 microns of pressure, and apply microwave power to the cavities. The cavities were then tuned individually (each had its own set of power meters) for minimum reflected power.

The results of the experiments indicate that P/L is about 30% lower for two cavities than for one cavity at a higher power. Figure 4.41 shows these results for Ar. The curves ranging from 10 to 35 watts of absorbed power correspond to the cavities when used individually, while the line going up to 65 watts was produced by passing the tube through both cavities, which were about 20 cm apart.

Helium was also used in the two cavity system. To get a single discharge the cavities had to be 5 to 10 cm apart. The values of P/L were lower than those obtained when the cavities were used separately, by about 25%. The discharge could not be made any longer when the cavities were separated by another centimeter or more. When the separation reached a certain point, the discharge would simply separate. Tuning one cavity to make the discharge longer would result in the discharge in the other cavity growing shorter, so that there was always a gap until the cavities were pushed together again. See Figure 4.42.

Ar 4 mm tube magnetron
C1, C2 done individually
C1 + C2 were both on the same tube

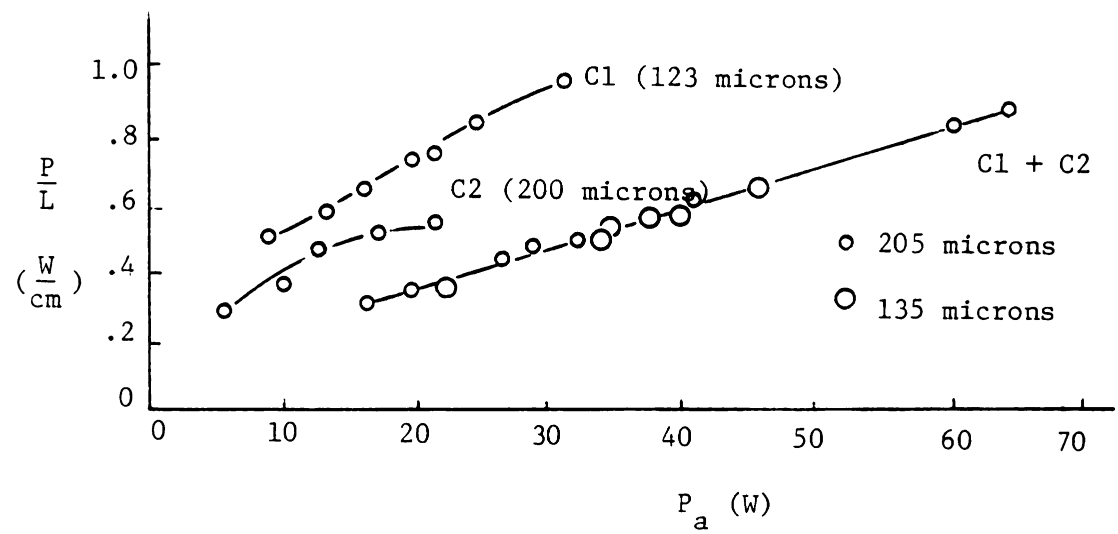

Figure 4.41 P/L vs. P_a for Doubly Excited Surface Wave Plasma Using Ar

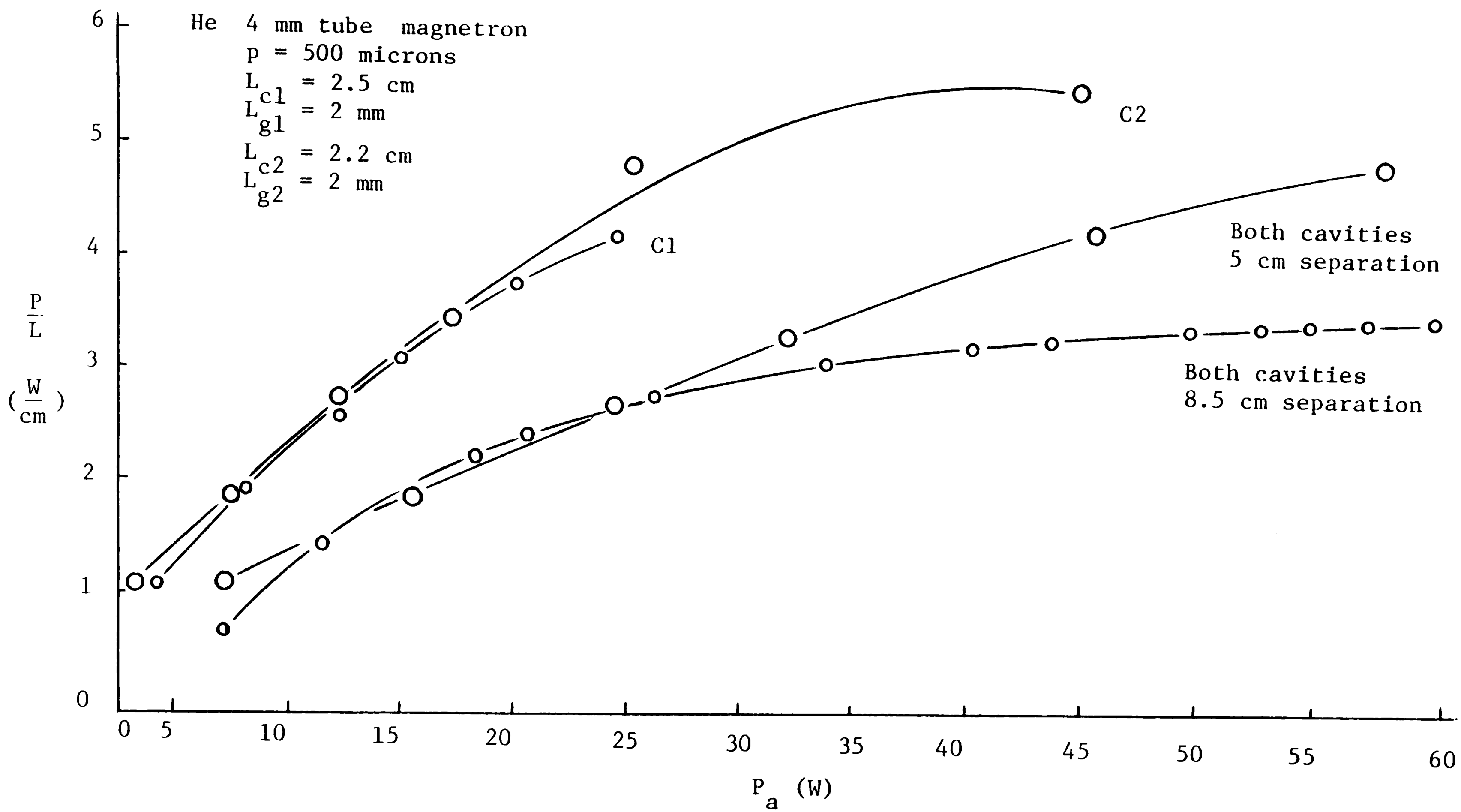

Figure 4.42 P/L vs. P_a for Doubly Excited Surface Wave Plasma using He

The effect produced by moving one of the cavities led to a quantitative investigation, which resulted in Figures 4.42 and 4.43. One can see that P/L decreased as the separation between cavities increased, even after the discharge had separated into two smaller discharges. (One might wonder what the effect of three cavities would be, or what value would be obtained for P/L for two cylindrical cavities on the same tube.)

During the course of moving the cavities relative to each other, a standing wave pattern, similar to the one already described, appeared in an Ar discharge. The wave length was measured to be about 9 cm, yielding a plasma density of approximately 6×10^{12} cm^{-3}, using the Gould-Trivelpiece normalized dispersion diagram.

The use of the dispersion diagram of Figure 4.38 does have a limitation. Values of ka between 0 and .1 are not allowed, while those from .1 to about .11 or .12 could yield ω/ω_p anywhere from 0 to .1, since the curve is almost vertical in this region. To allow a reasonable margin when using this diagram, ka should be around .2 or greater.

The standing wave effect was observed in P/L, total power absorbed for the two cavities, plasma length and power match when the distance between the cavities was changed by moving just one of them. These effects are shown in Figures 4.44 and 4.45. As the cavity separation increased, P/L, plasma length and total power absorbed would rise and fall at regular intervals, giving a wave length of approximately 10 cm. Changes in the power match for each cavity showed that the cavities interfered with each other in coupling. One cavity peaked while the other fell to a minimum. Such effects show that the cavities were definitely coupled to each other.

In conclusion, experiments have shown that two coupled cavities at

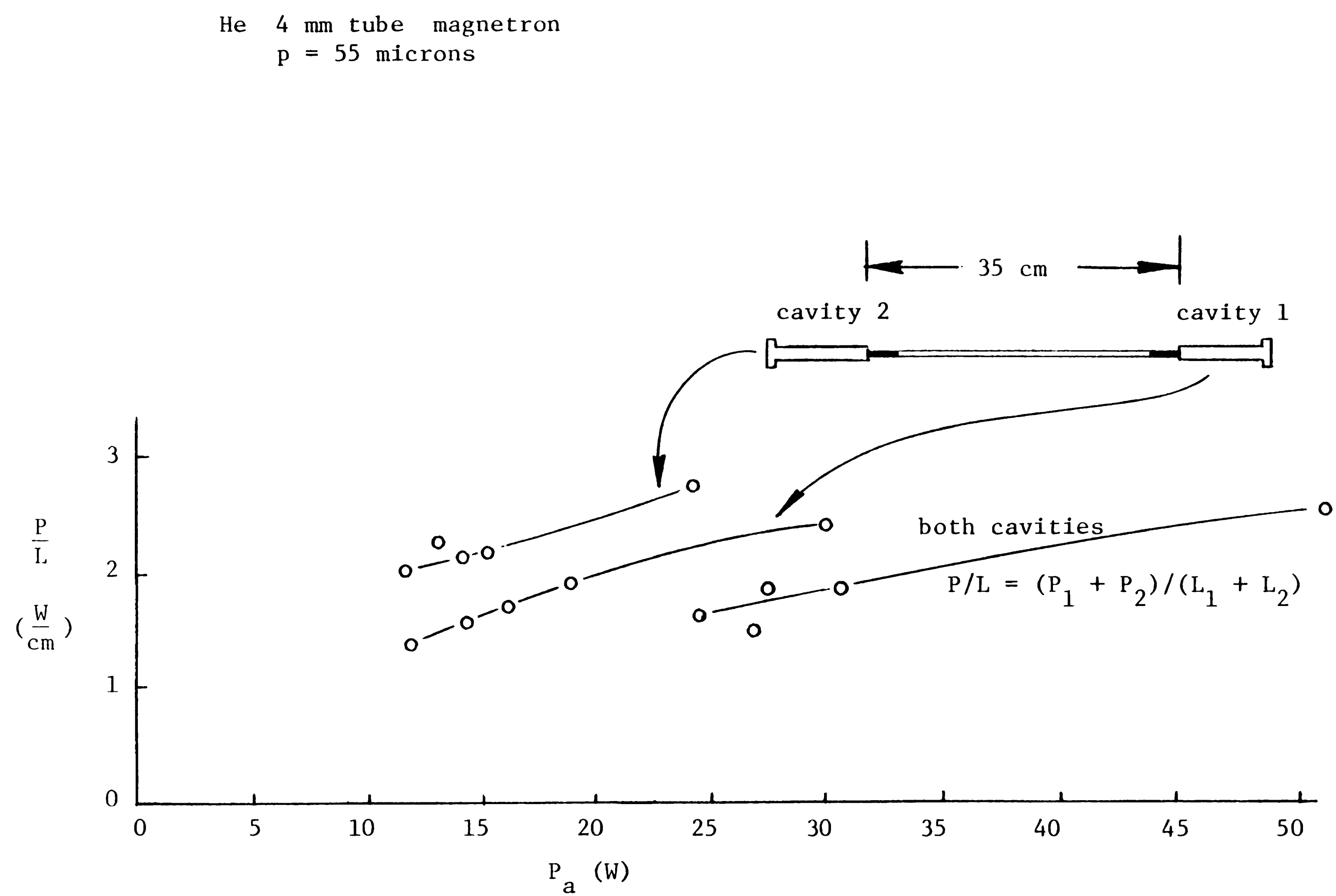

Figure 4. 43 P/L vs. P_a for Two He Plasmas in the Coaxial Cavities

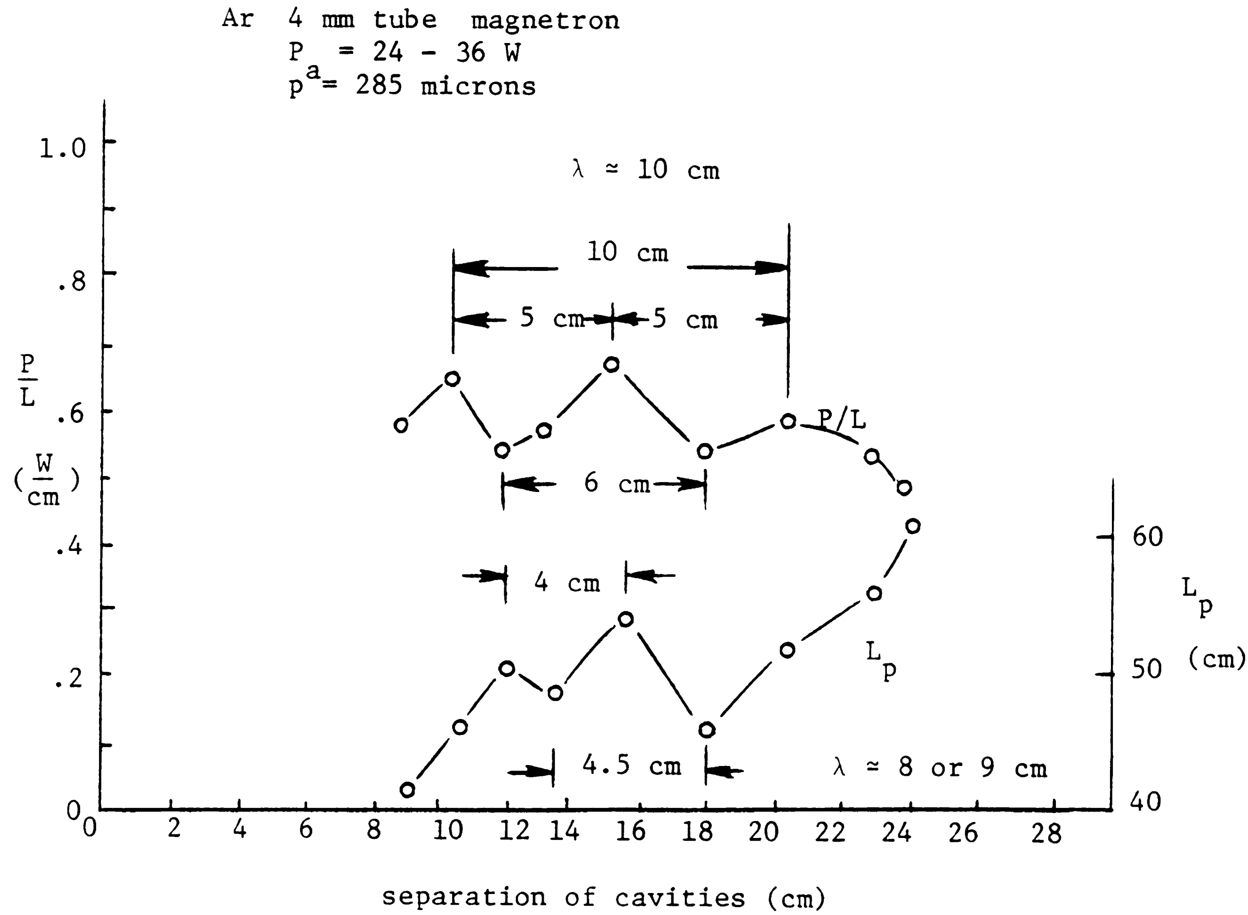

Figure 4.44 P/L and L_p for Ar as a Function of Cavity Separation for a Doubly Excited Surface Wave Plasma

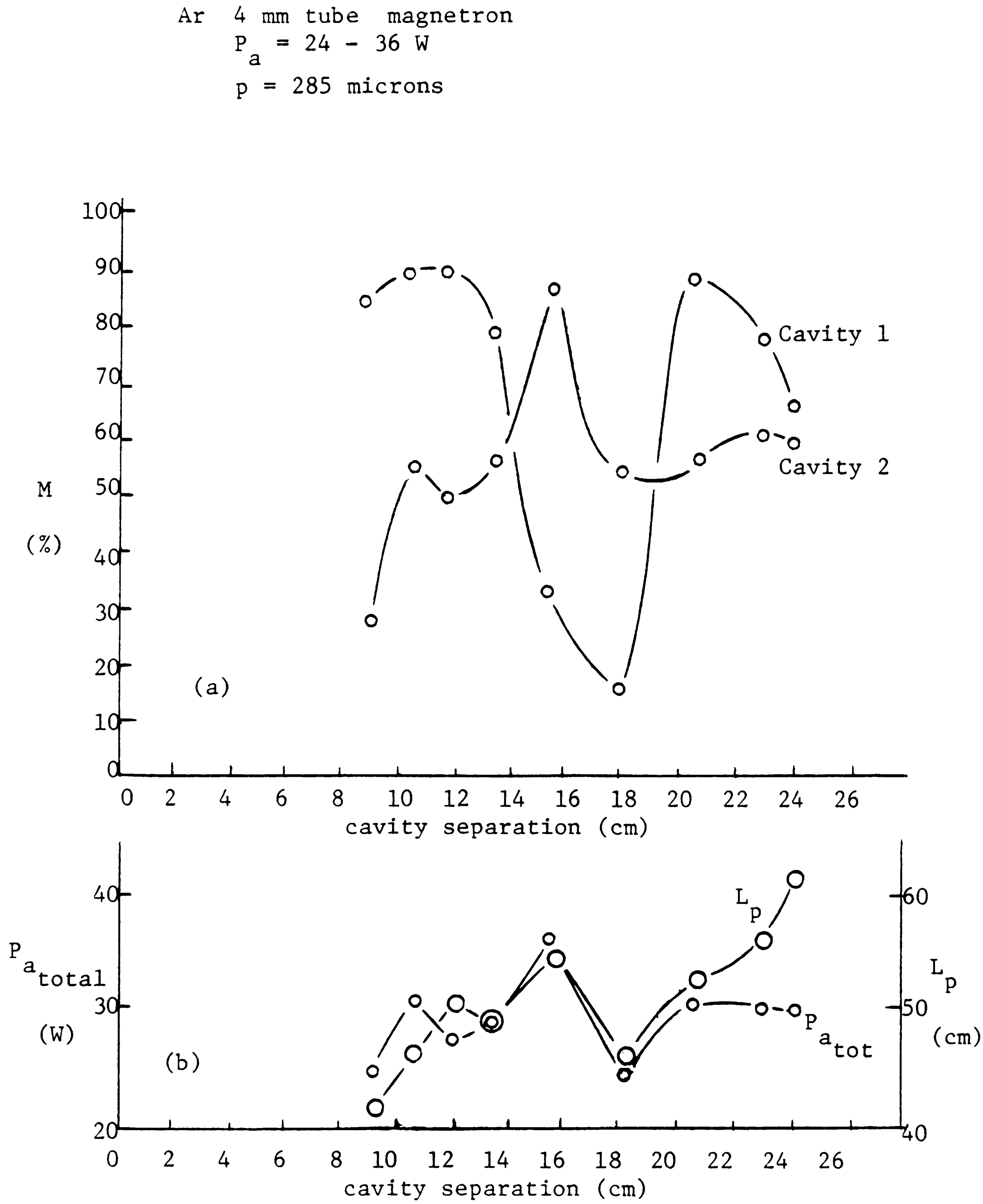

Figure 4.45 (a) P_a/P_i vs. Cavity Separation for Doubly Excited Ar Plasma
(b) $P_{a_{tot}}$ and L_p vs. Cavity Separation

low powers (1) can create a given length of plasma more efficiently than one cavity at the same total power (the plasma density may be less), (2) that standing waves existed along the doubly excited plasma column, demonstrating that the surface waves excited by each cavity interfere with each other, allowing the plasma density to be calculated, and (3) that, since the cavities were coupled on the same circuit, adjustments of one cavity affected the performance of the other cavity.

4.14 Suggested Experiments

As with most experimental work, questions arose which could not be answered at the time of their origination, due to time constraints or lack of facilities. For the benefit of others who may wish to continue this work, a list of experiments is provided. These experiments would have been performed if time had been available.

1. Spectroscopic determination of the wave lengths of the gases used, including quantitative measurements of line intensities, for both cavities.

2. Investigation of power coupling vs. loop sizes, primarily in the coaxial cavity, though loops can be used in the cylindrical cavity.

3. Investigation of energy coupling vs. loop shape, for both cavities.

4. Determination of the impedance of the coupling structure and its relation to cavity conditions.

5. Investigation of coupling vs. probe position in the cylindrical cavity, and for different cavity modes.

6. Comparison of electron density determination using diagnostic microwave cavities and with standing waves.

7. Determination of plasma electron density as a function of absorbed power.

8. If a discharge can be made to "lase" in the microwave cavity, the output, gain and efficiency could be measured as functions of gas pressure, tube diameter, absorbed power, probe position and cavity length. The nature of the coupling structure--stub or loop--could also be varied.

CHAPTER V

ANALYSIS AND CONCLUSIONS

5.1 Introduction

All of the experiments undertaken for this study were of an exploratory nature. To some degree they were an extension of studies to determine the absorption of microwave power by plasmas, but those discharges were generally confined to the excitation region of the coupling structure in which they were created. These experiments were designed specifically to excite surface waves along the discharge tube. The surface waves transmitted the energy required for the breakdown of the gas and sustained the plasma along the tube.

This chapter will discuss basic theory of steady state rf plasmas, including stability, and the electron density along a cylindrical plasma tube. The results of some of the more significant experiments discussed in Chapter 4 are explained. Results obtained with the coaxial cavity generally will not be distinguished from those of the cylindrical cavity, since the overall trends are similar. A dispersion diagram and previously developed theory will be used to account for the changes in P/L with variations in (1) gas pressure, (2) absorbed power, (3) tube diameter, (4) excitation frequency, and (5) ionization potential of the experimental gas. Implications of variation of the cavity geometry, observation of standing waves, and the observed lines of the rf Ar spectrum will be briefly discussed.

The chapter will conclude with suggestions for applications and a short review of the more important areas that warrant further investigation.

5.2 Basic Theory of RF Plasmas

This section will consider the power absorption and loss characteristics of the steady state rf plasma, the conditions necessary for stability, and the distribution of plasma electrons along the plasma column.

During the experiments, the incident and reflected rf power to the cavity-plasma system were measured. The absorbed power, P_a, was defined to be the difference between P_i and P_r. In reality, another term should be included:

$$P_i - P_r = P_c + P_a$$

The first term on the right side of the equation, P_c, represents the power lost to the rf couplers and cavity systems, though it could not be measured. Thus, when $P_i - P_r$ increases, the power absorbed by the plasma increases, but the losses in the coupling structure and cavity also increase. Doubling the difference between P_i and P_r, then, does not mean that the absorbed rf power is doubled.

The power absorbed by the plasma, P_a, has been shown to be

$$\begin{aligned} P_a &= \tfrac{1}{2} \text{ Re } \int_V \sigma \; |E|^2 \, dV \\ &= \tfrac{1}{2} \frac{e^2}{m\nu_e} \; \frac{\nu_e^2}{(\nu_e^2 + \omega^2)} \int_V n_e(r) E^2(r) dV \end{aligned}$$

where σ = plasma conductivity

$E(r)$ = the electric field within the plasma

e = the charge on the electron

m = the mass of the electron

ν_e = the effective electron-neutral collision frequency

ω = the excitation frequency of the source

$n_e(r)$ = the plasma electron density

and the integration $\int_V (\ldots) dV$ is over the plasma volume (24). The power absorbed by the plasma is a function of damping mechanisms within the plasma and the coupling of the internal and external electric fields of the plasma. As shown in Figure 5.1, the absorbed power in a cavity exhibits a resonance with the average plasma density.

Also shown on the figure is the power loss curve. The power loss, P_L, is given by (12)

$$P_L = \left(\omega_p^2 \frac{m}{e} \varepsilon_o \right) (\nu_i V_i + \beta T_e + \Sigma \nu_x V_x)$$

where

ω_p = the plasma electron frequency

m = the electron mass

e = the electron charge

ε_o = the permittivity of free space

ν_i = the ionization frequency of the plasma

V_i = the ionization energy of the gas

βT_e = a term representing the energy transported to the walls of the tube by electrons and ions

β = transport coefficient

T_e = electron temperature

ν_x = the excitation frequency of the gas

V_x = the excitation energy of the gas

Reproduced from (12)

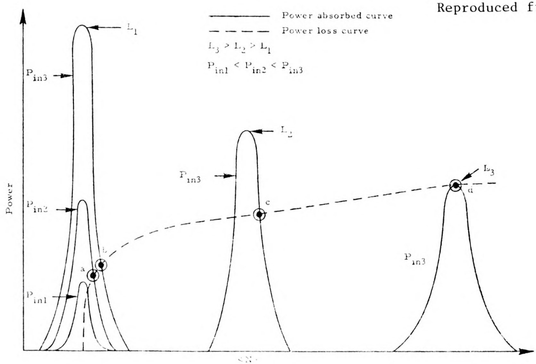

Figure 5.1 Power-loss and power-absorbed curves for three incident powers and three cavity lengths. Low-pressure model $\nu/\omega \ll 1$. Excitation frequency and background pressure are constant. $\langle N \rangle$ equals average plasma density.

From the equation, one can see that the primary loss mechanisms are (1) inelastic ionization collisions ($\nu_i V_i$), (2) excitation collisions ($\Sigma\nu_x V_x$), and (3) energy transported to the walls by electrons and ions. Energy transported out of the plasma by gas flow is not incorporated into the equation above, and would not be present when the plasma tube is isolated from the vacuum system, for there would be no significant flow of gas.

The steady state is characterized by

$$P_a = P_L$$

so that there is no net gain or loss of energy in the plasma. This condition corresponds to points on Figure 5.1 where the P_a and P_L curves intersect. Not all of the intersections, however, represent stable operating points. The power absorbed curve must have a negative slope or the slope of the power loss curve must be greater than that of the power absorbed curve. Otherwise the plasma is unstable. Consider the point c on the curve. If the electron density increases, moving to the right, the power loss is greater than the power absorbed by the plasma, so the density will decrease. If the density had decreased, moving to the left of point c, more power is absorbed by the plasma causing the density to increase, again moving back to point c. For the intersection on the other side of the curve, an increase in plasma density causes the absorbed power to increase over the losses, moving eventually to point c. A decrease in plasma density means that power loss would be greater than the power absorbed and the density would further decrease until the plasma was extinguished. Finally, at point d, the plasma is marginally stable, for regions to the right of point d. However, any cavity length longer than L_3 will have not an intersection between the two curves. The plasma-cavity system will drop out of resonance and the plasma will be extinguished. The cavity length must be reduced to approximately L_1 to reignite the plasma.

Two results from the paper by Zakrzewski, et al. (21), will also be used to explain the results reported in Chapter 4. As has already been mentioned, the surface wave generated plasma follows the normalized Gould-Trivelpiece dispersion relation. This is shown in Figure 3 of their paper (experimental points are close to the calculated curve). Secondly, the electron density is proportional to the light intensity of the plasma, which decreased with a slight downward curve as the detector was moved along the tube away from the cavity--Figure 5.2. This result will be extended by assumption, by plotting a hypothetical density vs. length curve, for a plasma that is symmetric about the source. The figure displays the density vs. length behavior of the surface wave discharge as the absorbed rf power is increase from P_1 to P_2 to P_3. As the absorbed power is increased, the plasma length grows but the average plasma density (proportional to P/L) increases only slowly. When the discharge tube is filled with plasma, so that the length is restricted, then the plasma density increases more rapidly.

5.3 Analysis of Experimental Results

The variation, or lack of it, of P/L with changes in pressure can be explained by considering the power absorbed by the plasma. From section 5.2 this can be written as

$$P_a = \frac{e^2}{2m\nu_e} \frac{\nu_e^2/\omega^2}{(1 + \nu_e^2/\omega^2)} \int_V n_e(r) E^2(r) dV$$

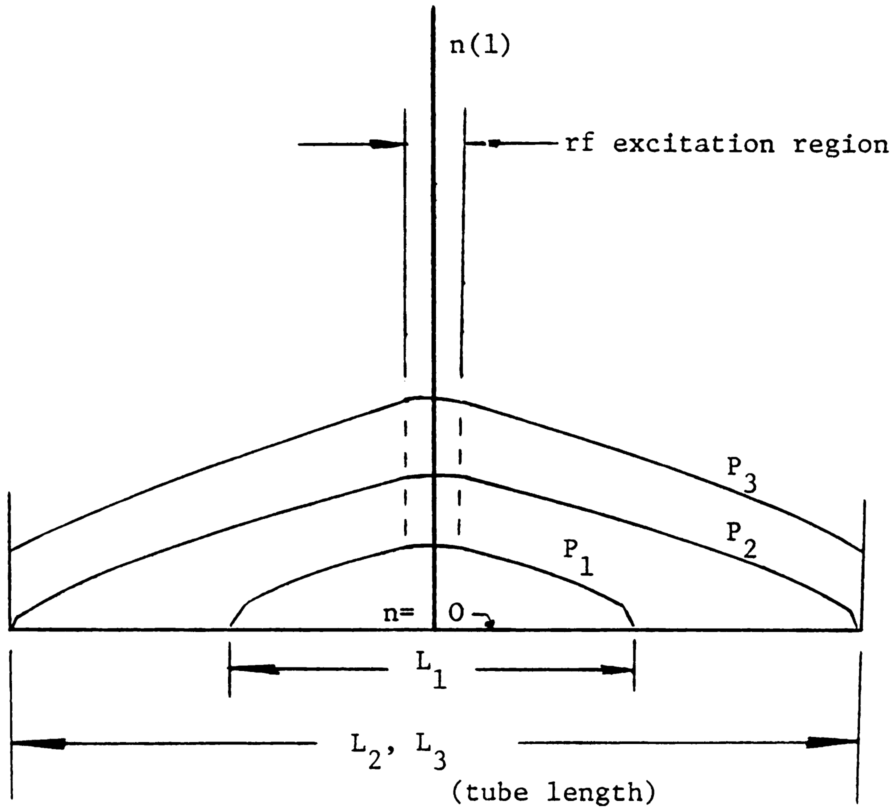

Figure 5.2 Assumed Variation of n(l) with P_a

With excitation frequency, tube radius, and cavity geometry held constant, it was observed that P/L remained nearly constant over a wide pressure range. This means that as the pressure decreases, and ν_e^2/ω^2 also decreases, nE^2 must increase since the absorbed power changed very little. In the pressure range for which ν_e^2/ω^2 is relatively constant, then nE^2 is also relatively constant. Thus the plasma adjusts itself so as to keep the absorbed power constant, over a pressure range of roughly 100 microns to 1 torr or greater. In addition, the power match exhibited little change, indicating that the plasma-cavity system impedance was relatively constant. See Figures, 4.1, 4.2, 4.3, 4.29, 4.30, and 4.32.

When the absorbed power was increased, keeping pressure, frequency, tube size and cavity geometry constant, P/L was observed to increase. As Figure 5.2 indicates, the average density will increase with absorbed power. The entire curve in Figure 5.2 may move up by equal amounts, or some regions may rise more than others. Whether the shape of the curve changes for higher absorbed power could be determined by finding the density as a function of position along the tube, for different levels of absorbed power. This would be a straightforward extension of the experiment performed by Zakrzewski, et al.

This same problem (P/L vs. P_a) can be viewed from the steady state theory. As the absorbed power increases, power losses must also increase. Recall $P_i - P_r = P_a + P_c$. P_a includes losses in the plasma (i.e., steady state implies $P_a = P_L$), and P_c, the losses in the rf coupling structure and cavity, could not be measured. One would expect the system losses to increase, which is probably the case since the cavity and transmission lines were observed to be warmer after a given period of operation at high power, as compared to low power operation.

Note that as the density increases, the skin depth of the plasma will decrease, as least for very low pressures. This means that the external electric field of the plasma is larger, increasing losses in the metallic conductors of the cavity and coupling structure.

A last point to be made on the P/L vs. P_a problem is that P/L in-increased linearly with absorbed power when the length of the plasma was restricted (Ar). The power match remained constant. This means that the area under the two upper curves in Figure 5.2 must increase approximately linearly as the absorbed power increases (though the shapes of the curves may change).

When the tube diameter was changed, keeping the pressure, frequency and absorbed power constant, and tuning the cavities, there appeared to be an optimum tube size for minimum P/L, and the power density within the plasma decreased as the tubes were made larger. The minimum value of P/L for a given tube indicates that there may be an rf coupling resonance between the cavity and the plasma column. For varying tube sizes, the power density is a better indicator of the plasma density. This appears to fall off as the inverse of the cross sectional area of the tube. This means that $\int nE^2 dV / \int dV$ is proportional to $1/\pi a^2$ (or 1/A). Thus, while P/L changes slightly with an increase in tube diameter, the power density (and maybe the plasma density) change is proportional to 1/A.

The curve that compared P/L in the coaxial and cylindrical cavities for a 7 mm tube, at different levels of absorbed power, showed P/L for the coaxial cavity to be larger. This is an indication that losses in the coaxial system may be higher than those in the cylindrical cavity, due to the small (coaxial) vs. large (cylindrical) rf excitation regions.

The increase in P/L with excitation frequency, keeping pressure, absorbed power and tube size constant, and tuning the cavity at each frequency, can be explained with the normalized dispersion diagram. Not only did the P/L decrease with frequency, but it appeared to level off to some minimal value, depending on which gas was used, and on the rf power level. This behavior can be explained in two ways. With the dispersion diagram and assuming a constant value of ka, one can see that as the excitation frequency is increased, the plasma frequency must also increase, and thus, P/L will increase. If ka is not kept constant, there is a maximum value of ω/ω_p, i.e., a minimum for the plasma frequency. This implies that there is a minimum value of plasma density and P/L for which the surface wave can propagate.

The other way to explain this problem is by using Figure 3 of reference (9). If the axes are rotated by 90° and the mirror image is taken to give a density (P/L) vs. frequency curve, it is obvious that the plasma density increases with frequency.

By varying the frequency, then, one can see that: (1) plasma density and P/L exhibit similar behavior, and they are both functions of f^n, where f is the source frequency and n is greater than unity, and (2) the approximate measurement of electron density indicates that the point of operation on the dispersion diagram was near the light line for the experiments reported herein.

Changing the cavity geometry, with all the other parameters kept constant, produced changes in P/L. The geometry could be changed to produce short, bright plasmas, and P/L increased. The increase in light intensity and P/L implies that the plasma density increased. The density term appears in the expression for power loss. Since this is equal to the absorbed power, the conclusion is that the E field (or nE^2) within the plasma increases when the change in cavity geometry results in higher P/L.

The power loss expression can be used to explain why P/L increased with the ionization potential of the gas:

$$P_L = \left(\frac{\omega_p^2 m\varepsilon_o}{e}\right)(\nu_i V_i + \beta T_e + \Sigma\nu_x V_x) = P_a \quad \text{(steady state)}.$$

If all the other factors were to remain (nearly) constant, the power absorbed or lost would depend linearly on the ionization potential of the gas. The ionization potentials of Kr and Xe are lower than that of Ar, and transport losses are slightly lower (due to the lower mobility of the heavier atoms). He and He-Ne not only have larger ionization potentials, but the transport losses would be larger because of the relatively higher mobility of these ions. Finally, O_2 has a low ionization potential (about 12 eV) and transport losses would be comparable to those of Ar, Kr, and Xe, but the dissociation ($O_2 \rightarrow 2O^+$) and excitation losses would be much larger because of the diatomic structure of the molecule.

When two cavities were used to excite the surface waves, it was found that P/L for two cavities was lower than P/L for one cavity at the same equivalent rf absorbed power. This indicates that the average density for two cavities is less than the average density for just one cavity. This problem is related to the P/L vs. P_a problem. Lower values of P_a yield lower densities, and lower cavity-plasma system losses. Thus, the operating point on the normalized dispersion diagram is higher for two cavities than for one cavity.

Measurements of the wave lengths of the Ar spectrum show that transitions are present which correspond to transitions found in Ar ion lasers. Generally, in the dc laser, the atoms are excited to higher states by single collisions with electrons. The excitation frequencies of the microwave sources are of the order of 10^9 Hz, while the optical frequencies of the emitted light are of the order of 10^{14}. The energy that the electrons can acquire from the oscillating field is proportional to the frequency of the electric field (of the source). Thus the electrons that ionize the gas must receive their energy through several electron-neutral collisions.

5.4 Implications and Applications

An experiment that was not mentioned in Chapter 4 that should be performed is the determination of electron density along the plasma column for different values of absorbed rf power. Of the experiments that were suggested, probably the most significant in terms of applications would be the comparison of electron density measurements using diagnostic cavities and with standing waves, and the development of the microwave discharge laser. Descriptions of a few microwave excited lasers have appeared in the literature, but the application of microwave power for this purpose is not widespread.

LIST OF REFERENCES

LIST OF REFERENCES

1. Fehsenfeld, F. C., Evenson, K. M., Broida, H. P., "Microwave Discharge Cavities Operating at 2450 MHz," Rev. Sci. Instr., Vol. 36, No. 3, p. 294, March 1965.

2. Dorman, F. H., McTaggart, F. K., "Absorption of Microwave Power by Plasmas," J. Microwave Power, Vol. 5, No. 1, p. 4, 1970.

3. Lee, Q. H., Asmussen, J., "Impedance Measurements of a Bounded Plasma in Resonance," Bull. Am. Phys. Soc., Vol. 15, p. 1469, 1970.

4. Fredericks, R. M., Asmussen, J., "An Experimental Study of a Resonantly Sustained Bounded Plasma Located Inside Microwave Cavities," Bull. Am. Phys. Soc., Vol. 15, p. 1469, 1970.

5. Maksimov, A. I., "Excitation and Ionization in a Helium Microwave Discharge," Sov. Phys.-Tech. Phys., Vol. 14, No. 11, p. 1500, May 1970.

6. Bossisio, R. G., Weissfloch, C. F., Wertheimer, M. R., "The Large Volume Microwave Plasma Generator (LMP™): A New Tool for Research and Industrial Processing," J. Microwave Power, Vol. 7, No. 4, p. 325, 1972.

7. Lee, Q. H., Colestock, P. L., Asmussen, J., "An Experimental Study of Cold Plasma and Temperature Resonances at High RF Power," G-AP International Symposium, Ohio State University, Columbus, Ohio, p. 68, 1970.

8. Unpublished experimental results.

9. Fredericks, R. M., Asmussen, J., "Excitation of a Warm Plasma, Rotationally Symmetric Resonances in a Short-Gap Cavity," Proc. IEEE, Vol. 59, No. 2, p. 315, Feb. 1971.

10. Fredericks, R. M., Asmussen, J., "Retuning and Hysteresis Effects of a RF Plasma in a Variable Size Microwave Cavity," J. Appl. Phys., Vol. 42, No. 9, p. 3647, Aug. 1971.

11. Fredericks, R. M., Asmussen, J., "High-Density Resonantly-Sustained Plasma in a Variable-Length Cylindrical Cavity," Appl. Phys. Lett., Vol. 19, No. 12, p. 508, 15 Dec., 1971.

12. Asmussen, J., Mallavarpu, R., Hamann, J. R., Park, H. C., "The Design of a Microwave Plasma Cavity," Proc. IEEE, Vol. 62, No. 1, p. 109, Jan. 1974.

13. Asmussen, J., Hawley, M. C., Mallavarpu, R., Mertz, S., "Behavior of a Bounded Plasma Inside a Microwave Cavity at High and Low Pressures," Proc. Second Topical Conference on RF Plasma Heating, Texas Tech. University, Lubbock, TX, C4, 1 (1974)

14. Mallavarpu, R., Asmussen, J., Hawley, M. C., "Behavior of a Microwave Cavity Discharge Over a Wide Range of Pressures and Flow Rates," IEEE Trans. Plasma Science, Vol. PS-6, No. 4, p. 341, Dec. 1978.

15. Vandenplas, P. E., Electron Waves and Resonances in Bounded Plasmas, (John Wiley & Sons, LTD, New York, 1968).

16. Messiaen, A. M., Vandenplas, P. E., "Bounded, Resonantly Sustained High-Frequency Plasmas in a Magnetic Field and Densities High Above Critical Density," Phys. of Fluids, Vol. 12, No. 11, p. 2406, Nov. 1969.

17. Moisan, M., Beaudry, C., Leprince, P., "A New HF Device for the Production of Long Plasma Columns at a High Electron Density," Phys. Lett., Vol. 50A, No. 2, p. 125, 18 Nov. 1974.

18. Moisan, M., Beaudry, C., Leprince, P., "A Small Microwave Source for Long Column Production Without Magnetic Field," IEEE Trans. Plasma Science, Vol. PS-3, No. 2, p. 55, June 1975.

19. Moisan, M., et al., "New RF Plasma Sources Using Surface Wave Propagation: Characteristics and Applications," source unknown.

20. Moisan, M., Ricard, A., "Density of Metastable Atoms in an Argon Plasma Produced by an RF Surface Wave," Can. J. Phys., Vol. 55, p. 1010, 1977.

21. Zakrzewski, Z., Moisan, M., Claude, V. M. M., Beaudry, C., Leprince, P., "Attenuation of a Surface Wave in an Unmagnetized R.F. Plasma Column," Plasma Physics, Vol. 19, p. 77, 1977.

22. Krall, N. A., Trivelpiece, A. W., Principles of Plasma Physics, (McGraw-Hill, Inc., New York, 1973), pp. 173-77.

23. Trivelpiece, A. W., Gould, R. W., "Space Charge Waves in Cylindrical Plasma Columns," J. Appl. Phys., Vol. 30, No. 11, p. 1784, Nov. 1959.

24. Mallavarpu, R., "An Investigation of the Electromagnetic Behavior of a Microwave Plasma Source Over a Wide Range of Pressures and Flow Rates," Ph. D. Thesis, Michigan State University, 1976.

[redacted]